

ADVANCED TECHNIQUES BASED ON
MATHEMATICAL MORPHOLOGY FOR THE ANALYSIS
OF REMOTE SENSING IMAGES

GREINING FJARKÖNNUNARMYNDI MEÐ FRAMSÆKNUM
FORMFRÆÐI AÐFERÐUM

MAURO DALLA MURA



PhD in Information and Communication Technologies -
Telecommunications Area

Department of Information Engineering and Computer Science

UNIVERSITY OF TRENTO

Advisor: Lorenzo Bruzzone

PhD in Electrical and Computer Engineering
Faculty of Electrical and Computer Engineering

UNIVERSITY OF ICELAND

Advisor: Jón Atli Benediktsson

April 2011

THESIS COMMITTEE

Prof. JÓN ATLI BENEDIKTSSON	Chair, Advisor
Prof. LORENZO BRUZZONE	Advisor
Prof. PHILIPPE SALEMBIER	Member
Prof. PAOLO GAMBA	Member

Mauro Dalla Mura: *Advanced Techniques based on Mathematical Morphology for the Analysis of Remote Sensing Images*, PhD in Information and Communication Technologies - Telecommunications Area, *Greining fjarkönnunarmynda með framsæknum formfræðiaðferðum*, PhD in Electrical and Computer Engineering, © April 2011, ISBN 978-9979-9935-7-5

When work, commitment, and pleasure all become one and you reach
that deep well where passion lives, nothing is impossible.

— Francois de la Rochefoucauld

Yesterday is history, tomorrow is a mystery, but today is a gift.
That is why it is called the “present”.

— Kung Fu Panda

Dedicated to the memory of my father,

Bruno Dalla Mura

1944 – 2003

ABSTRACT

Remote sensing optical images of very high geometrical resolution can provide a precise and detailed representation of the surveyed scene. Thus, the spatial information contained in these images is fundamental for any application requiring the analysis of the image. However, modeling the spatial information is not a trivial task. We addressed this problem by using operators defined in the mathematical morphology framework in order to extract spatial features from the image. In this thesis novel techniques based on mathematical morphology are presented and investigated for the analysis of remote sensing optical images addressing different applications.

Attribute Profiles (APs) are proposed as a novel generalization based on attribute filters of the Morphological Profile operator. Attribute filters are connected operators which can process an image by removing flat zones according to a given criterion. They are flexible operators since they can transform an image according to many different attributes (e.g., geometrical, textural and spectral).

Furthermore, Extended Attribute Profiles (EAPs), a generalization of APs, are presented for the analysis of hyperspectral images. The EAPs are employed for including spatial features in the thematic classification of hyperspectral images.

Two techniques dealing with EAPs and dimensionality reduction transformations are proposed and applied in image classification. In greater detail, one of the techniques is based on Independent Component Analysis and the other one deals with feature extraction techniques. Moreover, a technique based on APs for extracting features for the detection of buildings in a scene is investigated.

Approaches that process an image by considering both bright and dark components of a scene are investigated. In particular, the effect of applying attribute filters in an alternating sequential setting is investigated. Furthermore, the concept of Self-Dual Attribute Profile (SDAP) is introduced. SDAPs are APs built on an inclusion tree instead of a min- and max-tree, providing an operator that performs a multilevel filtering of both the bright and dark components of an image.

Techniques developed for applications different from image classification are also considered. In greater detail, a general approach for image simplification based on attribute filters is proposed. Finally, two change detection techniques are developed.

The experimental analysis performed with the novel techniques devel-

oped in this thesis demonstrates an improvement in terms of accuracies in different fields of application when compared to other state of the art methods.

Key words: Remote sensing, mathematical morphology, image processing, pattern recognition, classification, image simplification, building extraction, change detection, very high resolution images, hyperspectral images, urban scenes, attribute filters, connected operators, multi-level analysis.

Fjarkönnunarmyndir með mjög mikla greiniehæfni geta veitt nákvæmar og ítarlegar upplýsingar um yfirborð jarðar. Þær staðbundnu upplýsingar sem er að finna í þessum myndum eru mjög mikilvægar fyrir margs konar greiningu á myndunum. Hins vegar er líkanagerð fyrir staðbundnu myndupplýsingarnar ekki einfalt verkefni. Í þessari doktorsritgerð er fengist við þetta vandamál með því að nota virkja sem skilgreindir eru með stærðfræðilegri formfræði (e. Mathematical Morphology).

Í ritgerðinni eru settar fram nýjar aðferðir sem byggja á stærðfræðilegri formfræði fyrir greiningu mismunandi gerða fjarkönnunarmynda. Grundvallaraðferðin í ritgerðinni er auðkennaprófilar (e. Attribute Profiles, APs) sem er nýstárleg útvíkkun á formfræðilegum prófílum (e. Morphological Profiles), en APs notast við auðkennasiur í stað hefðbundinna formfræðilegra sía. Auðkennasiur eru samtengdir myndvirkjar sem meðhöndla myndir með því að fjarlægja „flötásvæði (svæði með sama grágildi) samkvæmt tiltekinni viðmiðun. Þær eru sveigjanlegir virkjar þar sem þeir geta breytt mynd með notkun margra mismunandi auðkenna (sem byggja t.d. á rúmfræði, áferð og rófupplýsingum).

Í ritgerðinni eru einnig settir fram útvíkkaðir auðkennaprófilar (e. Extended Attribute Profiles EAPs)), en þeir eru útvíkkun á APs, og eru notaðir til að fá fram upplýsingar um rúmfræðileg einkenni við greiningu mynda með mikilli rófupplausn. Tvær aðferðir eru notaðar með EAPs í flokkun og víddafækkun, þ.e. óháð þáttagreining (e. Independent Component Analysis, ICA) og útdráttur einkenna (e. Feature extraction). Til viðbótar er þróuð tækni sem byggir á APs til útdráttar einkenna fyrir greiningu á byggingum í þéttbýli.

Aðferðir sem vinna bæði bjarta og dimma hluti í myndunum samtímis eru rannsakaðar. Í þessu sambandi er hugmyndin um Self-Dual Attribute Profile (SDAP) kynnt. Jafnframt er sett fram almenn aðferð til einföldunar mynda með APs. Að lokum eru tvær aðferðir til skynjunar á breytingum þróaðar.

Aðferðirnar sem þróaðar hafa verið í rannsókninni er beitt í flokkun margs konar fjarkönnunarmynda. Flokkunarnákvæmnin er almennt betri en með þeim bestu aðferðum sem hingað til hefur verið beitt við flokkun þessara fjarkönnunarmynda.

Lykilorð: Fjarkönnun, stærðfræðileg formfræði, myndvinnsla, mynstur-
greining, flokkun, einföldun myndefnis, greining bygginga, skunjun
á breytingum, mjög mikil greinihæfni, myndir með mikla rófupp-
lausn, myndir úr þéttbýli, auðkennasíur, samtengdir virkjar, margstiga
greining.

PUBLICATIONS

BOOK CHAPTER

- [A1] M. Dalla Mura, J. Benediktsson, J. Chanussot, and L. Bruzzone, *Optical Remote Sensing - Advances in Signal Processing and Exploitation Techniques*. Springer Verlag, 2011, ch. The Evolution of the Morphological Profile: from Panchromatic to Hyperspectral Images.

INTERNATIONAL JOURNALS

- [B1] M. Dalla Mura, A. Villa, J. A. Benediktsson, J. Chanussot, and L. Bruzzone, "Classification of hyperspectral images by using extended morphological attribute profiles and independent component analysis," *IEEE Geoscience and Remote Sensing Letters*, vol. 8, no. 3, pp. 541–545, 2010.
- [B2] M. Dalla Mura, J. A. Benediktsson, B. Waske, and L. Bruzzone, "Extended profiles with morphological attribute filters for the analysis of hyperspectral data," *International Journal of Remote Sensing*, vol. 31, no. 22, pp. 5975–5991, Nov. 2010.
- [B3] —, "Morphological attribute profiles for the analysis of very high resolution images," *IEEE Transactions on Geoscience and Remote Sensing*, vol. 48, no. 10, pp. 3747–3762, Oct. 2010.
- [B4] M. Dalla Mura, J. A. Benediktsson, F. Bovolo, and L. Bruzzone, "An unsupervised technique based on morphological filters for change detection in very high resolution images," *IEEE Geoscience and Remote Sensing Letters*, vol. 5, no. 3, pp. 433–437, July 2008.

INTERNATIONAL CONFERENCES

- [C1] J. A. Benediktsson, L. Bruzzone, J. Chanussot, M. Dalla Mura, P. Salembier, and S. Valero, "Hierarchical analysis of remote sensing data: Morphological attributes profiles and binary partition trees," in *Proc. of 10th Int. Symp. on Mathematical Morphology (ISMM 2011)*, P. Soille, G. K. Ouzounis, and M. Pesaresi, Eds., Intra, Lake Maggiore, Italy, 6th–8th July 2011, invited paper.

- [C2] M. Dalla Mura, J. A. Benediktsson, and L. Bruzzone, "Self-dual attribute profiles for the analysis of remote sensing images," in *Proc. of 10th Int. Symp. on Mathematical Morphology (ISMM 2011)*, P. Soille, G. K. Ouzounis, and M. Pesaresi, Eds., Intra, Lake Maggiore, Italy, 6th-8th July 2011.
- [C3] —, "A general approach to the spatial simplification of remote sensing images based on morphological connected filters," in *2011 IEEE International Geoscience and Remote Sensing Symposium (IGARSS)*, 2011, accepted.
- [C4] S. Peeters, P. R. Marpu, J. A. Benediktsson, and M. Dalla Mura, "Classification using extended morphological profiles based on different feature extraction techniques," in *2011 IEEE International Geoscience and Remote Sensing Symposium (IGARSS)*, 2011, submitted.
- [C5] M. Pedernana, P. R. Marpu, M. Dalla Mura, J. A. Benediktsson, and L. Bruzzone, "Fusion of hyperspectral and lidar data using morphological profiles," in *Image and Signal Processing for Remote Sensing XVII - SPIE Proceeding*, 2011, submitted.
- [C6] M. Dalla Mura, J. A. Benediktsson, and L. Bruzzone, "Alternating sequential filters with morphological attribute operators for the analysis of remote sensing images," in *Image and Signal Processing for Remote Sensing XVI - SPIE Proceeding*, vol. 7830. Toulouse, France: SPIE Publications, Bellingham, WA, 2010, pp. 783 006–1–783 006–8.
- [C7] M. Dalla Mura, J. A. Benediktsson, and L. Bruzzone, "Classification of remote sensing images with attribute profiles and extended attribute profiles," in *32nd Symposium on Remote Sensing for Environmental Sciences (RESES 2010)*, Shikanoshima, Fukuoka, Japan, 29 - 31 August 2010, pp. 7–17, invited paper.
- [C8] N. Falco, M. Dalla Mura, F. Bovolo, J. A. Benediktsson, and L. Bruzzone, "Study on the capabilities of morphological attribute profiles in change detection on VHR images," in *Image and Signal Processing for Remote Sensing XVI - Proceedings of SPIE*, vol. 7830. Toulouse, France: SPIE, Bellingham, WA, 2010, pp. 783 016–1–783 016–10.
- [C9] M. Dalla Mura, J. Benediktsson, and L. Bruzzone, "Classification of hyperspectral images with extended attribute profiles and feature extraction techniques," in *2010 IEEE International Geoscience and Remote Sensing Symposium (IGARSS)*, 2010, pp. 76–79.

- [C10] M. Dalla Mura, A. Villa, J. A. Benediktsson, J. Chanussot, and L. Bruzzone, "Classification of hyperspectral images by using morphological attribute filters and independent component analysis," in *Proc. 2nd Workshop on Hyperspectral Image and Signal Processing: Evolution in Remote Sensing*, Reykjavik, Iceland, 14–16 June 2010.
- [C11] M. Dalla Mura, J. A. Benediktsson, and L. Bruzzone, "Modeling structural information for building extraction with morphological attribute filters," in *Image and Signal Processing for Remote Sensing XV - SPIE Proceeding*, vol. 7477. Berlin, Germany: SPIE, Bellingham, WA, 2009, pp. 747 703–1–747 703–9.
- [C12] M. Dalla Mura, J. A. Benediktsson, B. Waske, and L. Bruzzone, "Morphological attribute filters for the analysis of very high resolution remote sensing images," in *Proc. IEEE International Geoscience and Remote Sensing Symposium 2009, IGARSS '09*, vol. 3, July 2009, pp. III–97 –III–100.
- [C13] G. H. Halldorsson, R. A. Karlsson, S. H. Hardarson, M. Dalla Mura, T. Eysteinnsson, J. M. Beach, E. Stefansson, and J. A. Benediktsson, "Automatic retinal oximetry," in *Proceedings of the 6th International Workshop on Information Optics (WIO'07)*, vol. 949, Reykjavik, Iceland, 25–30 June 2007, pp. 200–209.
- [C14] M. Dalla Mura, J. A. Benediktsson, L. Bruzzone, and F. Bovolo, "A novel technique based on morphological filters for change detection in optical remote sensing images," in *Proceedings of the 6th International Workshop on Information Optics (WIO'07)*, vol. 949, Reykjavik, Iceland, 25–30 June 2007, pp. 75–82.

ACKNOWLEDGMENTS

My deepest gratitude goes to my advisors Lorenzo and Jón. My reaching is also due to their insightful advice, their many last-minute corrections and their flexibility in coping with the necessities due to the growth of my family. Over almost four years, a solid professional relationship, not to mention a friendship has been built up. And this has further enriched the experience.

Moving down the rank of the professional hierarchical tree, I would like to thank the RSLab, in particular the lasting members (listed in alphabetical order): Adamo, Begüm, Claudio, Francesca, Luca, Michele, Silvia (a special thank you to her for having shared a desk with me for these three years) and Patra. We have been in each other's company on a three-days-per-week basis.

Concerning my stays at 64.139N, 021.953W, Iceland (an awesome country!), I must mention Alberto, Giulia, Hildur, Nicola and Gísli, Róbert from Oxymap. A particular thanks goes to Alberto for having paid me several outstanding rúsínur-included dinners. Thanks also to Hjörtur and the italo-icelandic community of Laugardalslaug (Ester, Leone and Roberto) for their company during my stays. How could I forget Sundhöll, Laugardalslaug and Vesturbæjarlaug (my favorite!) for the many happy hours spent there.

I also wish to thank prof. Philippe Salembier and prof. Paolo Gamba (for providing the data sets of Pavia) for being part of the committee.

Now that the academic acknowledgments are over, I thank Alberto (l'Albe), for the mid-day routine: pizza and discussions on a lot of low-level technical stuff. Thanks also to Nicola (il Nico), the abstract discussions on the multivariate analysis of the fMRI data have accompanied me on many return trips to Verona.

I also take this opportunity to mention my friends: Giana, Davide, Cic, Iulbi, Claudio and the crew of the swimming pool of Fumane, for having shared the few moments of spare time available to me.

Thanks go to my mother Carla and my sister Marta (and Alessandro) especially for their considerable help with the kids. The work on innumerable occasions has been helped by this.

Last in this list but first for importance, I want to thank my family-team: Francesca, Alessandro and Massimo. Without whom I would have done much more, but every thing would be much less significant.

Mauro
Verona, April 2011

CONTENTS

I INTRODUCTION AND BACKGROUND	1
1 THESIS OVERVIEW	2
1.1 The Remote Sensing Imaging System	2
1.2 Towards the Interpretation of the Scene	3
1.3 Modeling the Spatial Information	5
1.4 Image Analysis based on Mathematical Morphology .	8
1.5 Objectives and Novel Contributions of the Thesis . . .	9
1.6 Thesis Organization	10
2 FUNDAMENTALS	13
2.1 Fundamental Properties	13
2.2 Opening and Closing by Reconstruction	14
2.3 Attribute Filters	16
2.4 Representations of an Image as a Tree	20
2.5 Attribute Filters based on Tree Representations	24
3 RELATED WORKS: MORPHOLOGICAL PROFILES	25
3.1 Introduction	25
3.2 Morphological Profiles	26
3.2.1 Morphological Profiles and Differential Mor- phological Profiles	26
3.2.2 Experimental Analysis and Discussion	27
3.3 Extended Morphological Profiles	30
3.3.1 Extended Morphological Profile	30
3.3.2 Experimental Analysis and Discussion	31
3.4 Conclusion	33
II PROPOSED TECHNIQUES FOR IMAGE CLASSIFICATION AND OBJECT EXTRACTION	35
4 ATTRIBUTE PROFILES	36
4.1 Introduction	36
4.2 Limitations of Morphological Profiles	37
4.3 Definition of Attribute Profiles	38
4.4 Analysis of the complexity	41
4.5 Experimental Results	43
4.5.1 Data set Description	43
4.5.2 Results	45
4.6 Conclusion	54
5 EXTENDED ATTRIBUTE PROFILES	56
5.1 Introduction	56

5.2	Morphological Operators for Multi-tone Images . . .	57
5.3	Extended Profiles with Attribute Filters	58
5.4	Experimental Results	61
5.4.1	Data set Description	61
5.4.2	Experimental Set Up	62
5.4.3	Results with Extended Profiles	63
5.4.4	Results with a Reduced Number of PCs . . .	64
5.5	Conclusion	64
6	EXTENDED ATTRIBUTE PROFILES AND DIMENSIONALITY REDUCTION	75
6.1	Classification with EAPs and ICA	75
6.1.1	Introduction	75
6.1.2	Independent Component Analysis	76
6.1.3	Approaches to Deal with Multiple EAPs . . .	77
6.1.4	Experimental Results	77
6.1.5	Conclusion	81
6.2	Classification with EAPs and Feature Extraction . . .	82
6.2.1	Introduction	82
6.2.2	Feature Extraction Techniques	83
6.2.3	Experimental Results	84
6.2.4	Conclusion	86
7	DUAL TECHNIQUES	88
7.1	Alternating Sequential Attribute Filters	88
7.1.1	Introduction	88
7.1.2	Definition of ASAF	90
7.1.3	Implementation of ASAF based on Min- and Max-tree	92
7.1.4	Experimental Results	93
7.1.5	Conclusion	94
7.2	Self-Dual Attribute Profiles	96
7.2.1	Introduction	96
7.2.2	Definition of Self-dual Attribute Profiles . . .	97
7.2.3	Experimental Results	98
7.2.4	Conclusion	101
8	ATTRIBUTE PROFILES FOR BUILDING EXTRACTION	104
8.1	Introduction	104
8.2	Attributes for Building Extraction	105
8.3	Filtering by Optimization based on GAs	106
8.3.1	Genetic Algorithms	106
8.3.2	Parameters Tuning with Genetic Algorithms .	107
8.4	Experimental Results	108
8.4.1	Data set Description	108
8.4.2	Experimental Set up	109

8.4.3	Results	111
8.5	Conclusion	113
III PROPOSED TECHNIQUES FOR IMAGE SIMPLIFICATION AND		
	CHANGE DETECTION	115
9	A GENERAL APPROACH TO IMAGE SIMPLIFICATION	116
9.1	Introduction	116
9.2	Proposed General Approach	117
9.2.1	Selection of the Filter Parameters	117
9.2.2	Filtering	119
9.2.3	Discussion	120
9.3	Experimental Results	120
9.4	Conclusion	122
10	CHANGE DETECTION TECHNIQUES	124
10.1	Introduction on Change Detection	124
10.2	Technique based on Morphological Connected Filters	126
10.2.1	Introduction	126
10.2.2	Proposed Change-Detection Technique Based on Morphological Filters and Change Vector Analysis	127
10.2.3	Experimental Results	131
10.2.4	Conclusion	135
10.3	Change Detection Technique based on APs	135
10.3.1	Introduction	135
10.3.2	Proposed Change Detection Technique Based on Morphological Attribute Profiles	136
10.3.3	Experimental Results	140
10.3.4	Conclusion	141
11	CONCLUSION	146
	BIBLIOGRAPHY	151

LIST OF FIGURES

Figure 2.1	Example of opening by reconstruction	17
Figure 2.2	Example of binary attribute thinnings.	19
Figure 2.3	Example of max-tree.	22
Figure 3.1	Example of Morphological Profile	27
Figure 3.2	Panchromatic images.	28
Figure 3.3	Example of extended morphological profile. . .	30
Figure 3.4	ROSI-03 Hyperspectral images of Pavia.	31
Figure 4.1	Examples of differential profiles.	41
Figure 4.2	Trento Data set 1.	43
Figure 4.3	Trento Data set 2.	44
Figure 4.4	Extracts of differential profiles.	47
Figure 4.5	Classification maps for data set 1.	52
Figure 4.6	Classification maps for data set 2.	53
Figure 5.1	Architecture for computing an Extended Attribute Profile.	59
Figure 5.2	Examples of EAPs.	60
Figure 5.3	Architecture for computing an Extended Multi-Attribute Profile.	61
Figure 5.4	Centre and University data sets.	66
Figure 5.5	Centre data set. Classification maps.	67
Figure 5.6	University data set. Classification maps	68
Figure 5.7	Centre data set. Details of the classification maps.	69
Figure 5.8	University data set. Details of the classification maps.	71
Figure 6.1	Proposed approaches for dealing with multiple EAPs.	78
Figure 6.2	ROSI Pavia University data set. Classification maps.	82
Figure 6.3	University data set. Classification maps.	84
Figure 6.4	Flow chart.	85
Figure 7.1	Example of Alternating Sequential Filters.	90
Figure 7.2	Borgo Valsugana data set.	93
Figure 7.3	ASAF with increasing attributes and order preserving relation.	95

Figure 7.4	ASAF with non-increasing attributes and order preserving relation.	95
Figure 7.5	ASAF with non-increasing attributes and order reversing relation.	96
Figure 7.6	Examples of filtering with area close, area open and grain filter.	99
Figure 7.7	GeoEye-1 Borgo Valsugana data set.	101
Figure 8.1	General architecture of the proposed technique.	108
Figure 8.2	Trento data set.	109
Figure 8.3	Trento data set. Classification maps.	110
Figure 9.1	Flowchart of the proposed general approach. . .	118
Figure 9.2	Bam data set. Simplification of the scene.	122
Figure 9.3	Bam data set. Objects enhancement.	123
Figure 10.1	General scheme of the proposed technique. . . .	127
Figure 10.2	Trento data set.	132
Figure 10.3	Trento data set. Change-detection maps.	134
Figure 10.4	General scheme of the proposed technique. . . .	137
Figure 10.5	Bam data set. Reliable levels maps.	139
Figure 10.6	Bam data set.	140
Figure 10.7	Bam data set. Example of unchanged region. . .	142
Figure 10.8	Bam data set. Example of changed region. . . .	143
Figure 10.9	Bam data set. Examples of DAPs.	144
Figure 10.10	Bam data set. Change indicator maps.	145
Figure 10.11	Bam data set. Change detection maps.	145

LIST OF TABLES

Table 4.1	Number of samples per class for the training and test set for the two data sets.	45
Table 4.2	Errors obtained by classifying the panchromatic image along with morphological/attribute profiles for data set 1.	50
Table 4.3	Errors obtained by classifying the panchromatic image along with morphological/attribute profiles for data set 2.	50
Table 4.4	Class specific Producer Accuracy and User Accuracy obtained for data set 1.	51

Table 4.5	Class specific Producer Accuracy and User Accuracy obtained for data set 2.	51
Table 5.1	Number of samples per class for the train and test sets for the Centre and University data sets.	70
Table 5.2	Variance and Cumulative Variance in percentage explained by each principal component for Centre and University data sets.	70
Table 5.3	Centre data set: Overall Accuracy (OA), Average Accuracy (AA) and Kappa value.	70
Table 5.4	University data set: Overall Accuracy (OA), Average Accuracy (AA) and Kappa value.	71
Table 5.5	Centre data set: Class specific Producer Accuracy (PA) and User Accuracy (UA) of the obtained results. The best accuracies obtained are marked in bold.	72
Table 5.6	University data set: Class specific Producer Accuracy (PA) and User Accuracy (UA) of the obtained results. The best accuracies obtained are marked in bold.	73
Table 5.7	Centre data set: Classification accuracies obtained by considering a reduced number of PCs.	74
Table 5.8	University data set: Classification accuracies obtained by considering a reduced number of PCs.	74
Table 6.1	University data set. Classification accuracies.	80
Table 6.2	Centre data set. Classification accuracies.	81
Table 6.3	Overall Accuracies obtained without any FE technique.	86
Table 6.4	Overall Accuracies obtained with the FE techniques.	87
Table 7.1	GeoEye-1 Borgo Valsugana data set. Classification accuracies	103
Table 8.1	Trento data set. Training and test sets.	109
Table 8.2	Trento data set. Classification accuracies with maximum likelihood classifier.	111
Table 8.3	Trento data set. Classification accuracies with random forest classifier.	112
Table 10.1	Change-detection errors.	133

Part I

INTRODUCTION AND BACKGROUND

THESIS OVERVIEW

Abstract. In this chapter, we give an introduction to this dissertation. In particular, we briefly present the context in which this work has been developed by providing an overview of the problem of the modeling of the spatial information for the analysis of remote sensing images. The main objectives and the novel contributions of this thesis are then presented. Finally, the organization of this document is reported.

1.1 THE REMOTE SENSING IMAGING SYSTEM

Remote sensing passive imaging sensors detect the electromagnetic energy radiated and reflected by the Earth surface. The energy that reaches the sensor from the surface comes from an emitting source (in the visible spectrum, mainly the sun), propagates through the Earth's atmosphere and the transmitted component of the incident energy hits the surface. The surface interacts with the incident electromagnetic wave by absorbing, scattering and reflecting it. The scattered and reflected components propagate back through the atmosphere (again with absorption) reaching the sensor. The radiance measured by the sensor is split into different spectral components for collecting the signal in only some bands of the electromagnetic spectrum (according to the type of sensor) and then is focused by the optics of the imaging system and modulated in electrical current for being finally detected and stored. The imaging system is defined by a characteristic impulse response. For more details on the imaging process please refer to [1, 2, 3, 4, 5, 6, 7, 8]. In real imaging sensor, the energy emitted by a punctual source is imaged as a disk by the detector since the energy is spread over a finite patch in the focal plane. This effect due to the optics and the finite size of electronic detectors (e.g., cells of the CCD sensor) placed on the focal plane defines the spatial resolution of the sensor (capacity of the sensor in distinguish two spatially adjacent points on the ground) [1]. Thus, the electromagnetic energy measured

Part of this chapter is going to appear in:

J. A. Benediktsson, L. Bruzzone, J. Chanussot, M. Dalla Mura, P. Salembier, and S. Valero, "Hierarchical analysis of remote sensing data: Morphological attributes profiles and binary partition trees," in *Proc. of 10th Int. Symp. on Mathematical Morphology (ISMM 2011)*, P. Soille, G. K. Ouzounis, and M. Pesaresi, Eds., Intra, Lake Maggiore, Italy, 6th-8th July 2011, invited paper.

is quantized both in the spectral and spatial domain by the acquisition process. Spatially, the sensed scene is imaged in a set of cells (pixels) distributed in a regular rectangular grid (due to the geometry of the CCD sensor). The portion of the ground surface enclosed in the beam with width given by the angular aperture of the imaging sensor is referred as Ground-projected Field Of View (GFOV) and can be roughly seen as the sensor footprint on the ground [6, 9]. The spacing between pixels on the ground is named the Ground-projected Sample Interval (GSI) and is usually designed to equal the Ground-projected Instantaneous Field of View (GIFOV). However, the representation of the GIFOV as square footprint is inadequate because the reflected energy measured corresponds to the integration energies across a surface which almost never matches a square pattern (since the point spread function of the sensor is bell shaped) [10].

It is clear that the potential of the remote sensing imagery strongly depends on how much in details of the sensed reality can be described. The capability of the imaging sensor in representing the scene can be assessed in terms of spatial, spectral and radiometric resolution. With particular attention to the spatial domain, the spatial resolution indicates the smallest distance between two objects that can be distinguished by the sensor [11]. When the size of the objects on the surveyed landscape (e.g., buildings, trees, roads) is close to the geometrical resolution of the sensor, the objects are represented in the image as a single or few adjacent pixels. In this scenario, the digital numbers of neighboring pixels show a relatively low correlation. Due to the possible presence of different land cover types in the footprint of each pixel on the ground, the digital number associated to the pixel can be thought as obtained by merging the reflectance response of the different materials, leading to the so called “mixed pixel”. Moreover, the spectral response correspondent to a pixel can be also affected by the radiation components scattered from or reflected by surrounding land covers of the area investigated [12]. When the spatial resolution of the sensor increases, the objects on the ground are represented in the image as regions of spatially connected pixels. This mixing phenomenon can be reduced with the increased resolution but cannot be completely canceled. In fact, it can be still found on pixels representing the boundaries between objects with different characteristics of reflectivity [6]. This effect is referred as the “boundary effect” in [13].

1.2 TOWARDS THE INTERPRETATION OF THE SCENE

Focusing the attention on the image analysis, Schowengerdt [6, Ch. 1, p. 7–8] dichotomizes the analysis of remote sensing imagery in *data-*

centered and *image-centered* approaches. The former approach performs an analysis of the sensed images driven by the data. Tasks such as the measure of the spectral absorption, the estimation of fractional abundances of surface materials or of parameters as the soil moisture, biomass etc. are included in this type of analysis. The latter approach refers to the interpretation of the scene by exploiting the spatial relationships among features on the ground. The extraction of the information from the scene can be done by an experienced user through photointerpretation or by a computer aided system (“quantitative analysis” in [5]). The image analysis performed by a computer try to mimic the activity of the photointerpreter and thus, has to be driven by some opportunely coded knowledge.

The interpretation of a natural scene, when is performed by a human, seems an intuitive and quite straightforward process due to the innate facility for humans in extracting information from visual shapes, forms, and textures [14]. Nevertheless, the process of interpreting the scene is actually made up by several different and complex steps. For example, the interpretation of an entire scene can be done by splitting and analyzing the image in different parts separately. Afterwards, objects can be recognized according to their characteristics (e.g., spectral, spatial and relational) which are matched with templates derived by preexistent knowledge (i.e., known by the interpreter). The semantic of the structures in the image is exploited for increasing the understanding of the scene. During the analysis, a set of expert rules is built up performing the interpretation image.

Computer-based techniques for image analysis basically aims at modeling the human interpretation process. Due to its complexity, this task is still an open issue. For this reason, most of the practical interpretations of the scene are based on the human analysis [3]. However, the ever increasing amount of data acquired by the satellites and the availability of aerial and satellite images from archives make a “manual” approach to the analysis completely inadequate for a full exploitation of the information. Thus, the need of an automated analysis is clearly a demand.

In practical situations, the access and exploitation of the information extracted by Earth Observation (EO) data for applications such as resource inventory and management, urban planning, land records for taxation and ownership control, facilities management, marketing and retail planning, vehicle routing and scheduling [15] is performed through Geographical Information Systems (GIS) [5]. Methodologies belonging to the fields of image processing, information extraction, pattern recognition and machine learning make possible the increase in the level of abstraction from the numerical value of a pixel to the rep-

resentation of the geospatial objects that model the real-world entities, needed for linking remote sensing data and GIS. However, a complete and automatic integration of remote sensing data and GIS has still to be achieved since many issues are still open [16, 15]. For example, in [17] it is evidenced the constant need of further developments in spatially-based image analysis methods. Striving for an information interchange between remote sensing and GIS, it is fundamental to work towards an object oriented analysis for bridging between geospatial concepts in GIS and the synergy between image-objects and their radiometric characteristics and analyses in remote sensing data [18]. In this perspective, in [18] the importance of the Object-Based Image Analysis (OBIA) is clearly pointed out. Working at the object level permits to extract from the overwhelming amount of details of the scene only the informative components through the representation of the scene in a simplified way enhancing the content and increasing the understanding. Moreover, a representation of the scene through object entities can fully exploit the advances in artificial intelligence such as fuzzy logic classification, rule-based classification from the expert systems domain, and neural nets, which model the human ways of thinking [19]. Different techniques have been presented for accomplish this goal: image classification, segmentation, texture analysis, pattern matching, object recognition, etc.

Since the analysis carried out by the computer emulates the human perception, the guiding principle for the definition of the transition from the image domain to the object representation domain is given by concepts from spatial thinking and more in general by cognitive psychology [18]. In this perspective, the ultimate benchmark of the automated image analysis is human perception [18].

1.3 MODELING THE SPATIAL INFORMATION

With the constant increase in geometrical resolution of Earth Observation sensors faced in the last decades, the *spatial information* provides a ever increasing contribute to the understanding of the remote sensing imagery, since it characterizes the sensed landscape in a complementary way with respect to the spectral signatures of the land covers. In the past, the processing of low resolution images was mainly performed with pixel-based approaches due to their direct application to the image. Such set of approaches only takes into account the spectral signature of the pixels but not any spatial measure or characteristic extracted by the image. Although, the results produced can be satisfactory for low resolutions, since a low correlation is experienced between neighboring pixels, the performances of such approaches

drastically reduce when applied to VHR images. This effect is not only related to non considering any spatial measure but also because with a finer geometrical resolution, the within-class variability of an object in the image increases. In a classification task, the increased spectral covariance produced by a greater variability within a class reduces the overall class spectral separability [13].

Although an approach based only on the spectral values can be applied straightforwardly to the image since each pixel can be considered separately to the others, the extraction and exploitation of the spatial information is a complex and multifaced task.

Furthermore, when dealing with VHR images, the interpretation of the scene can largely benefit from the analysis of the spatial domain. In addition, the reach of a fine spatial resolution usually is obtained at the detriment of the spectral resolution. In fact, in general most VHR sensors can acquire one or few spectral bands. In this scenario, the inclusion of information belonging to the spatial domain is compulsory for obtaining consistent results in the analysis of the image. Spatial information can be coded as relations between neighboring pixels, patterns in the spatial domain (e.g., texture), spatial characteristics of regions (e.g., geometrical, morphological, textural measures), structural relations in objects, relational links between entities in the scene, etc. In general, we can refer to spatial information as the knowledge on the scene that can be derived by characteristics extracted from the spatial domain.

Recently, Daya Sagar and Serra [20] underlined how the retrieval and characterization of the spatial information is a current challenge for geoscience scientists. Due to the wide range of features related to the spatial domain, there are several ways of characterizing this information source. From a general survey of techniques modeling the spatial information in remote sensing, one can notice that there are different approaches for extracting the spatial information and correspondent ways (with different levels of abstraction) for including the extracted information in the processing chain aiming at the understanding of the image.

Roughly, it is possible to group the techniques in three approaches (ordered increasingly according to the level of semantic introduced in the representation of the scene) ranging from the pixel- to region- and to object-level. With the term "region" we refer to a set of spatially connected pixels with similar characteristics (e.g., intensity, spectral signature, texture) which are different from surrounding ones [21]. The term "object" can be roughly intended as a region with a semantic information. More formally, in [18, p.98] object is referred to a discrete spatial entity that has many permanent properties which endow it

with an enduring identity and which differ in some way or another from the properties of its surroundings. The three macro-groups in which we have clustered the different techniques are the following:

1. *Pixel-level.* At this level the spatial information that can be modeled is mainly related to the spatial context of the pixels. The characterization of the spatial content is done by exploiting the correlation among the spectral signature of pixels included by a subset of the spatial domain (e.g., a window). The correlation shown by neighboring pixels is both due to the acquisition of significant portions of energy from adjacent pixels by the imaging sensors and to the presence of the same land cover on regions large compared with the size of a pixel [5, Ch. 8],[22, Ch. 6]. The investigation of the neighborhood of each pixel can be done in different ways. The dependent spatial variations of the neighboring pixels have been modeled in a stochastic framework as a realization of a spatial random field (SRF) [23], e.g., with Markov Random Fields (MRFs) [24, 25, 26, 27, 28, 29, 30, 31, 32, 33, 34, 35, 36, 37] and Conditional Random Fields (CRFs) [38, 39, 40, 41]. In [42, 43, 44, 45, 46, 47, 48, 49, 50, 51] the contextual relations between pixels were exploited for a robust analysis of the scene in an image classification task.

The characterization of the spatial context can be done also by computing some measures on the pixels included in a local window. Such operation is actually a filtering. According to the transformation performed on the neighborhood of each pixel (i.e., the type of measures computed) it is possible to extract features such as, texture, shape, size, etc.

The spatial context was investigated by considering the correlation of couples of pixels at a fixed distance and direction in the Gray Level Cooccurrence Matrix (GLCM) [52] or in semivariograms [53]. The textural information has also been characterized by Gabor filters and wavelets [54, 55, 56], as well as many other techniques.

The application of a sequence of filters in a multiscale architecture has proven to be useful for performing a multiscale decomposition of the image [57, 58]. The multiresolution decomposition attempts to mimic human perception in identifying objects of different shape and structure on different scales.

The characteristics of the (homogeneous) region in which each pixel is included were extracted by spatial features such as the length and width of lines centered at each pixel spanning the homogeneous area [59, 60, 61], the Pixel Shape Index (PSI) [62].

Measures computed from straight lines extracted in from the scene were also used in [63].

2. *Region-level.* At this level, the scene is partitioned in regions (i.e., segmentation) permitting to extract spatial features that can describe the structures in the scene [17, Ch. 5]. The segmentation can be exploited in different ways. For example can increase the robustness of analysis by considering the segments as the fundamental spatial entities (i.e., increasing the robustness of the analysis w.r.t. pixel-based approaches) [64, 65, 66, 67, 68, 69]. The segmentation can also increase the understanding of the scene by considering textural, spatial and spectral features extracted from the segments [70, 71].

Different segmentation techniques can be used for performing the segmentation (e.g., watershed [17], morphological filters [72], mean-shift [73], etc.).

In many cases a single segmentation of the scene is not sufficient for a consistent representation of the objects in the scene. Thus, hierarchical approaches can overcome this limitation [74, Ch.2], [71, 64].

3. *Object-level.* This is the highest level of abstraction with semantic included in the analysis giving information on the thematic of the regions. Thus, from this representation of the scene it is possible to perform an analysis on the relations between objects leading to the deepest understanding of the scene (obviously, if the extraction of the objects is consistent) [19, 18, 75, 76, 77, 14, 78, 79].

Obviously, by increasing the level of abstraction in the analysis it is possible to extract and exploit more spatial information. However, the increase in the abstraction strongly requires the application of proper techniques in order to guarantee the consistency of the results.

1.4 IMAGE ANALYSIS BASED ON MATHEMATICAL MORPHOLOGY

In the context of the modeling of the spatial information, Mathematical Morphology (MM) [80, 81, 82, 83] holds a fundamental role since it provides a set of powerful tools for analyzing the spatial domain.

In 2002, Soille and Pesaresi [84] identified as the main applications in the context of remote sensing image analysis that could be addressed by MM: i) image filtering; ii) image segmentation and iii) image

measurements. Thus, MM tools permit to enrich the image analysis by including spatial information mainly at pixel- and region-level, according to the analysis carried out in the previous section. In fact, many MM operators are defined as neighborhood transformations of the image [82]. Thus, the spatial context is "natively" considered when applying such operators. Moreover, MM techniques have been proven to be effective when applied to tasks such as image classification, object recognition and extraction, segmentation, etc.

In ten years of developments from the general survey of [84], we have witnessed to the appearance of many techniques involving MM for the analysis of remote sensing images strengthening the mutual connection between remote sensing and MM [85]. Focusing the attention to very high resolution (VHR) images, we highlight the consolidation of the role of *connected operators* [86, 87] as efficient filters for achieving a simplification of the image obtained by only merging flat zones (i.e., avoiding the detriment of the geometrical features of the regions unaffected by the transformation). Connected operators have been proven to be suitable to handle the characteristics of VHR images since they are capable to perform an image transformation that can selectively suppress uninteresting details and maintaining unaffected structures that are relevant for the analysis. Connected operators have gained popularity in the remote sensing community also due to the successful diffusion of Morphological Profiles (MPs) [72]. MPs are a multiscale decomposition of a grayscale image in a stack of filtered images obtained by transforming the input scene with a sequence of opening and closing by reconstruction filters (i.e., connected operators) based on structuring elements (SEs) with fixed shape and increasing size. The application of the MP and its extension are reviewed in details in Ch. 3 in a review of the relevant works employing multilevel approaches in the application of connected filters.

1.5 OBJECTIVES AND NOVEL CONTRIBUTIONS OF THE THESIS

The work presented in this thesis is aimed at investigating and defining novel techniques based on mathematical morphology for the analysis of remote sensing images. In particular, this study is devoted to the definition and in depth evaluation of the use of connected operators in a multilevel architecture for different remote sensing applications. State of the art techniques based on the application of connected operators in a multilevel approach (e.g., MP) have already proven to be effective for the analysis of the scene (see Ch. 3 for a review). Nevertheless, several limitations exist (e.g., on the capabilities of modeling the spatial information, efficiency in the computation, etc. see Ch. 4).

The work presented in this dissertation attempts to overcoming those limitations.

The novel contributions of this thesis are as follows.

1. *Pioneering the use of attribute filters and tree-based image representation structures in remote sensing [88].*
To the best of our knowledge, morphological attribute filters [89] and the hierarchical tree representations of the image with max-tree [90] were not yet used in the remote sensing field before our work of [88].
2. *Definition of Attribute Profiles [91].*
The Attribute Profile (AP) concept is based on the application of attribute filters in a multilevel architecture. It generalizes the definition of the MP leading to an efficient structure with an increased capability in modeling the spatial information.
3. *Definition of Extended Attribute Profiles [92].*
The Extended Attribute Profiles (EAPs) extends the concept of Attribute Profiles to the analysis of hyperspectral images.
4. *Investigation of dual techniques [93, 94].*
In some applications a simultaneous processing of both dark and bright structures in the scene is desirable. Thus, we have investigated two approaches based on dual connected operators for the processing of VHR images.
5. *Definition of a general approach to the spatial simplification of VHR images [95].*
Image simplification is a key operation leading to the understanding of the scene. We proposed a general approach to the simplification of the scene driven by the type of available information on the scene according to different operative scenarios.
6. *Application of multilevel techniques based on connected filters to different tasks.*
The proposed techniques were successfully considered and tuned for remote sensing applications such as thematic classification of the scene [96, 97, 98, 92, 91, 88, 94], image simplification [95], change detection [99, 100] and object recognition [101].

1.6 THESIS ORGANIZATION

This dissertation is organized in three parts and eleven chapters.

Part 1 aims at giving both an introduction to the problem addressed by our research and a description on the context in which the work has been developed.

Chapter 2 presents some fundamental concepts of mathematical morphology on which the proposed technique are based.

Chapter 3 recalls the concept of morphological profile and its extension to the hyperspectral domain as related work.

Moreover, a survey of significant techniques appeared in the literature based on the morphological profiles is also presented.

Part 2 collects the contributions of this work for the image classification and object extraction tasks.

Chapter 4 introduces the concept of attribute profile as generalization of the morphological profile based on attribute filters. The results of the experimental analysis carried out on a panchromatic image are reported.

Chapter 5 presents extended attribute profiles the extension of the AP for hyperspectral images. The experiments performed on two hyperspectral images are shown.

Chapter 6 reviews two techniques dealing with EAPs. One technique performs the computation of the EAP on the features extracted by an independent component analysis. The second technique addresses the problem of dimensionality reduction by applying different feature extraction techniques.

Chapter 7 deals with dual techniques. In this chapter, the application of attribute filters in an alternating sequential setting (leading to a quasi self-dual operator) is presented. Moreover, self-dual attribute profiles are introduced as self-dual version of the APs.

Chapter 8 describes a technique based on AP for the extraction of features suitable for the detection of the buildings in the scene. The AP are computed by optimizing the selection of the parameters of the filters.

Part 3 presents techniques addressing applications such as, image simplification and change detection.

Chapter 9 reports a general approach aiming at performing a simplification of the image in different ways driven by the information available on the scene.

Chapter 10 presents two change detection techniques. One technique is based on CVA and connected operators. In the second technique APs are used for gathering information on the changes occurred on the morphological characteristics of the objects.

Finally, in the last chapter, concluding remarks on the proposed techniques are given. Furthermore, future research developments are discussed.

Abstract. In this chapter fundamental concepts on connected operators are presented. In particular, the definition of opening and closing by reconstruction and attribute filters is recalled and the representation of the image as a hierarchical trees of regions is reviewed.

2.1 FUNDAMENTAL PROPERTIES

Let us consider a grayscale 2D image f with discrete single tone pixel values. Then, the image f can be defined as a mapping from E , the image domain (which is a subset of \mathbb{Z}^2) into \mathbb{Z} . A morphological *neighborhood transformation* transforms a pixel p of the image f according to a function ψ and a neighborhood $N(p)$ of p (set of pixels connected to p according to a connectivity rule). This can be formulated as $[\psi(f)](p) = \psi[N(p)]$ [82]. Obviously, the output of the transform depends on the function ψ considered and on how the neighborhood N is defined. Usually, the set that defines the neighborhood in such transformations is known as a *structuring element* (SE) and it is defined by a certain shape and a center. The shape is usually a discrete representation of continuous shapes (e.g., lines, rectangles, circles, etc.) on the domain lattice. The center identifies the pixel on which the SE is superposed when probing the image.

We recall below the definitions of some fundamental properties of morphological image transformations that will be useful in the following discussion.

- *Idempotence.* A transformation ψ is idempotent if the output of the transformation is independent of the number of times it is applied to the image: i.e., $\psi(\psi(f)) = \psi(f)$.

Parts of this chapter were published in:

M. Dalla Mura, J. Benediktsson, J. Chanussot, and L. Bruzzone, *Optical Remote Sensing - Advances in Signal Processing and Exploitation Techniques*. S. Prasad, L. M. Bruce, J. Chanussot Eds. Springer Verlag, 2011, ch. The Evolution of the Morphological Profile: from Panchromatic to Hyperspectral Images.

M. Dalla Mura, J. A. Benediktsson, and L. Bruzzone, "Classification of remote sensing images with attribute profiles and extended attribute profiles," in *32nd Symposium on Remote Sensing for Environmental Sciences (RESES 2010)*, Shikanoshima, Fukuoka, Japan, 29 - 31 August 2010, pp. 7–17, invited paper.

- *Increasingness.* A transformation is said to be increasing if and only if it keeps the ordering relation between images, i.e., $f \leq g \Leftrightarrow \psi(f) \leq \psi(g) \forall f, g$. The notation $f \leq g$ means that $f(p) \leq g(p)$ for each pixel p in the definition domain of the images.
- *Extensivity and Anti-extensivity.* A transformation ψ is extensive if, for each pixel, the transformation output is greater or equal to the original image, i.e., $f \leq \psi(f)$. The correspondent property is anti-extensivity and is satisfied when $f \geq \psi(f)$ for all the pixels in the image.
- *Absorption property.* The absorption property is fulfilled when two transformations, defined by different parameters i, j , are applied to the image, and the following relation is verified:

$$\psi_i \psi_j = \psi_j \psi_i = \psi_{\max(i,j)}.$$

Another fundamental concept is that of the so-called *connected component*. In a grayscale image a connected component (also called a “flat zone”) is defined as a set of connected iso-intensity pixels. Two pixels are connected according to a connectivity rule. Common connectivity rules are the 4- and 8-connected, where a pixel is said to be adjacent to four or eight of its neighboring pixels, respectively. The connectivity can be extended by more general criteria defining a connectivity class [102].

2.2 OPENING AND CLOSING BY RECONSTRUCTION

The two fundamental neighborhood transformations in mathematical morphology are *erosion* and *dilation*. Most morphological operations are based on a selected combination of erosion and dilation. Erosion and dilation are denoted by ε_B and δ_B , where B refers to the structuring element used in the operation. The erosion or dilation operators transform an input image by giving as output for each pixel p the *infimum* (\wedge) or *supremum* (\vee) of the intensity values of the set of pixels included by the SE when it is centered on p , respectively. It is important to note that infimum and the supremum are the minimum and maximum of an ordered set, respectively. The definition of the erosion and dilation transformation for a grayscale discrete image f is given below.

$$\varepsilon_B(f) = \bigwedge_{b \in B} f_{-b}, \quad (2.1)$$

$$\delta_B(f) = \bigvee_{b \in B} f_{-b}. \quad (2.2)$$

The sequential composition of erosion and dilation leads to the definition of the morphological *opening* and *closing* transformations. Morphological opening of an image f by a structuring element B is defined as the erosion of f by B followed by the dilation of the eroded output by \check{B} , the reflected structuring element with respect to B :

$$\gamma_B(f) = \delta_{\check{B}}[\varepsilon_B(f)]. \quad (2.3)$$

In contrast, a morphological closing of an image f by a structuring element B is defined as the dilation of f by B followed by the erosion of the dilated output by the reflected structuring element \check{B} :

$$\phi_B(f) = \varepsilon_{\check{B}}[\delta_B(f)]. \quad (2.4)$$

While the output of an erosion would have an effect on all the brighter structures independent of the size, an opening flattens bright objects that are smaller than the size of the structuring element and, because of dilation, mostly preserves the bright large areas. Similar conclusion can be drawn for darker structures when a closing is performed. The terms brighter and darker are considered with respect to the surroundings gray tones. The morphological opening and closing operators usually lead to severe effects on the image especially when the SE is large with respect to the size of the structures in the image. Moreover, with these operators, the geometrical characteristics of the structures can be distorted or completely lost. This is obviously an undesirable effect when information on the objects of interest have to be retrieved after the filtering.

Morphological operators based on the *geodesic reconstruction* can effectively process the image by overcoming this issue. This is achieved by either completely removing or preserving the connected components in the image according to their interaction with the SE of the transformation. In greater detail, if a component in the image is larger than the SE then it will be unaffected, otherwise it will be merged to a brighter or darker adjacent region depending upon whether a closing or opening is respectively applied.

An opening by reconstruction is performed in two separated phases and can be formally defined as:

$$\gamma_R^{(i)}(f) = R_f^\delta[\varepsilon^{(i)}(f)]. \quad (2.5)$$

The first transformation, $\varepsilon^i(f)$, is an erosion of the image f with an SE of size i , which defines the size of the opening. This aims at creating the so called marker image for the reconstruction operation. The second phase performs a reconstruction by dilation, $R_f^\delta(\cdot)$, of the marker image taking as reference mask f . This operation is an

iterative procedure that applies geodesic dilation (which is defined as the infimum of the elementary dilation and the mask image) on the marker image until idempotence ($\delta_f^{(n)} = \delta_f^{(n+1)}$):

$$R_f^\delta(\cdot) = \delta_f^{(n)}(\cdot) = \underbrace{\delta_f^{(1)} \cdot \delta_f^{(1)} \dots \delta_f^{(1)}}_{n \text{ times}}(\cdot). \quad (2.6)$$

The reconstruction phase permits to fully retrieve all those structures that are not completely suppressed by the erosion and it potentially needs several iterations before reaching stability.

By duality, a closing by reconstruction is defined as the reconstruction by erosion of f from the dilation of f using a structuring element of size n :

$$\phi_R^{(i)}(f) = R_f^\varepsilon[\delta^{(i)}(f)]. \quad (2.7)$$

It is important to note that the result obtained with operators by reconstruction is less dependent on the shape of the selected structuring element than in the case of morphological opening or closing. Operators by reconstruction are also less severe than the corresponding morphological ones, which can be explained by analyzing the ordering relations between the operators:

$$\gamma \leq \gamma_R \leq f \leq \phi_R \leq \phi. \quad (2.8)$$

An example of the iterative process of an opening by reconstruction operation according to (2.5) is presented in Figure 2.1. It worths noting that the compact regions that were not completely erased by the erosion are fully retrieved in a single iteration of the reconstruction process. Conversely, the reconstruction of the elongated region needs 27 iterations. Thus, the presence of large regions with complex shapes strongly affects in terms of complexity the analysis, since they require a significant number of iterations for reconstructing the entire region and each iteration of the reconstruction process performs a processing of the whole image. However, more efficient algorithms for performing the reconstruction exists which permit to reduce of an order of magnitude the complexity of this transformation [103].

2.3 ATTRIBUTE FILTERS

Morphological attribute filters are morphological transformations that process an image according to a criterion. A generic criterion T can be defined as a mapping of the set S of values considered by T to the

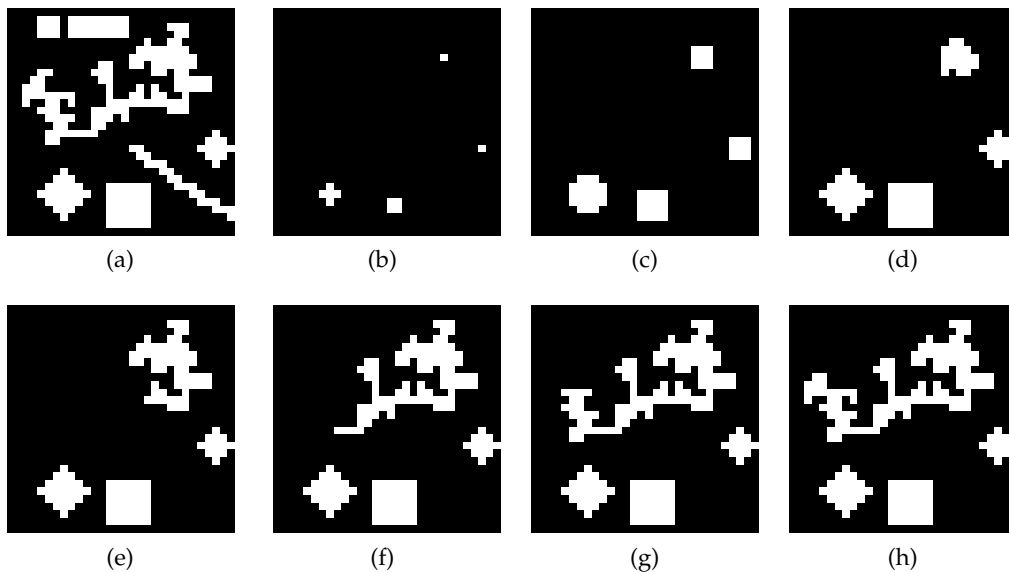


Figure 2.1: Example of opening by reconstruction. (a) Original binary 30×30 pixels image (F); (b) Morphological erosion of (a) with B a disk of diameter 5 pixels as SE ($\varepsilon_B(f)$); (c) Reconstruction by dilation, iteration 1; (d) Reconstruction by dilation, iteration 2; (e) Reconstruction by dilation, iteration 10; (f) Reconstruction by dilation, iteration 20; (g) Reconstruction by dilation, iteration 25; (h) Reconstruction by dilation, iteration 27 ($\Rightarrow \gamma_R(f)$).

couple of Booleans $\{false, true\}$. The criterion is evaluated on each connected component of the image. If the criterion is verified, then the component is preserved. If it is not verified, the component is removed. The criteria are usually related to the question whether the value of an attribute α of the component C fulfills a predefined condition, e.g., $T(C) = \alpha(C) \geq \lambda$, with $\{\alpha(C), \lambda\} \in \mathbb{R}$ or \mathbb{Z} for scalar attributes, where the attributes can actually be any measure computable on the image regions. This leads to great flexibility in the behavior of attribute filters, which consequently improves their capability in modeling the spatial information with respect to operators based on fixed SEs. For example, the attributes considered can be purely geometric (e.g., area, length of the perimeter, image moments, shape factors), textural (e.g., range, standard deviation, entropy), etc.

Since attribute filters can only transform an image by merging its connected components, these filters belong to the family of connected filters [89]. Actually, morphological attribute filters are connected filters and the morphological operators by reconstruction are included in their definition [89].

A very important property of the criterion considered in the transformation is *increasingness*. A criterion is said to be increasing when, if it is verified for a connected component, then it will be also true for all the components nested in it. This property leads to have for example $T(C_j) = \text{true}$ when also $T(C_i) = \text{true}$ for any $C_j \subseteq C_i$. Examples of increasing criteria involve increasing attributes (e.g., area, volume, size of the bounding box, etc.) and an inequality relation (e.g., \geq). In contrast, non increasing attributes, such as scale invariant measures (e.g., homogeneity, shape descriptors, orientation, etc.), lead to non increasing criteria.

In the following the definition of attribute filters will be recalled for binary and grayscale images. Attribute openings for binary images consider an increasing criterion T . According to [89], they are obtained by computing a trivial opening, Γ^T , on the output of a connected opening, Γ_F , applied to all the connected components of a binary image F . Given a pixel p in the image domain and a connected component C , the connected opening is computed as:

$$\Gamma_F(p) = \begin{cases} C & \text{if } p \in C; \\ \emptyset & \text{otherwise.} \end{cases} \quad (2.9)$$

The trivial opening keeps the regions for which the increasing criterion T holds. This can be expressed as:

$$\Gamma_T(C) = \begin{cases} C & \text{if } T = \text{true}; \\ \emptyset & \text{otherwise.} \end{cases} \quad (2.10)$$

Attribute opening is then given by:

$$\Gamma^T(f) = \bigcup_{p \in F} \Gamma_T(\Gamma_F(p)). \quad (2.11)$$

If the criterion considered is increasing, the resulting transformation is increasing, idempotent and anti-extensive (i.e., it is an opening). In contrast, if the increasingness property is not fulfilled by the criterion, the filter remains idempotent and anti-extensive but not increasing anymore. For this reason, the transformation based on a non-increasing criterion is not an opening, but a *thinning*.

Analogous considerations can be made for the dual transformation by considering the background regions instead of the foreground ones. If the criterion is increasing, the transformation is actually a *closing* otherwise it is a *thickening*.

An example of binary attribute thinnings is shown in Figure 2.2. From the filtered images it is possible to notice how the elongated objects can be isolated from the other compact objects by using the

moment of inertia attribute (Fig. 2.2c), whereas when considering the area as attribute only one of the two elongated objects is kept (Fig. 2.2b). This simple example proves how complementary information is extracted by considering different attributes.

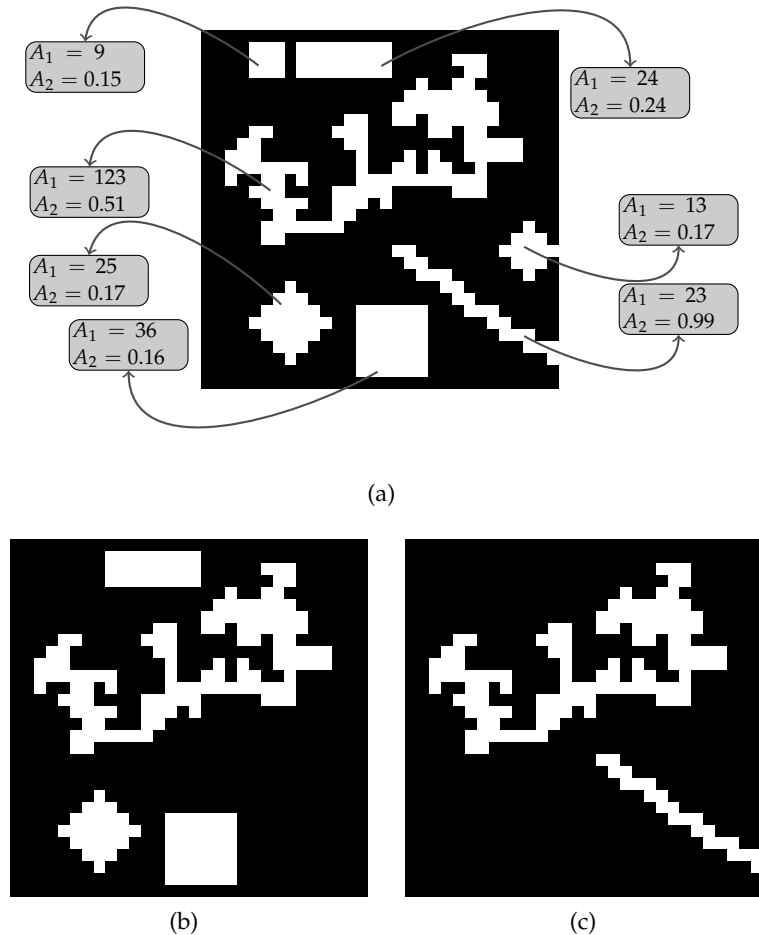


Figure 2.2: Example of binary attribute thinnings. (a) Original 30×30 pixels binary image showing the values of the attributes A_1 (area) and A_2 (moment of inertia) for each region in the image; (b) Binary attribute opening with predicate $T = A_1 \geq 50$; and (c) Binary attribute thinning with predicate $T = A_2 \geq 0.5$.

The extension of the operators from binary to gray-scale images is straightforward when the criterion is increasing because of the principle of threshold superposition [104]. Since a grayscale image can be expressed as the sum of all its binary thresholds, then the output

image of these filterings is the sum of all the filtered input threshold images, i.e.,

$$\gamma^T(f) = \sum_{k=0}^K \Gamma^T(F_k) \quad (2.12)$$

with F_a the binary threshold image f at graylevel $k \in [0, K]$ the destination domain of the grayscale values. Equation (2.12) can also be expressed as:

$$\gamma^T(f)(p) = \max\{k : \Gamma^T(F_k)(p) = 1\} \quad p \in E. \quad (2.13)$$

When the attribute criteria are not increasing, the extension to numerical functions is not straightforward anymore. For example, let us consider a numerical function f and a binary criterion T that acts on the binary sections F_k of f at successive thresholds $k_1 < k_2 < k_3$. We may have $F_{k_2} = \emptyset$, whereas $F_k \neq \emptyset$ for $k = \{k_1, k_3\}$. Thus, the results of the transformation applied to successive sections of the image do not decrease as k increases. Therefore, they cannot be considered as the stack of sections of a function. The simplest way to force the decreasingness of the sequence is to replace the image F_k by the union of all the binary thresholds from the top section, i.e., by $F'_k = \cup\{F_i(f), i \geq k\}$. This leads to the following definition of grayscale attribute thinning with a non increasing criterion \tilde{T} :

$$\gamma_{max}^{\tilde{T}}(f)(p) = \max\{k : \Gamma^{\tilde{T}}(F'_k)(p) = 1\}. \quad (2.14)$$

This solution leads the grayscale attribute thinning (see (2.13)), which is referred to as *max rule* in [90]. However, other arbitrary filtering strategies can be implemented in order to achieve different output effects when extending the binary thinning and thickening to numerical images [90, 105]. For example, Urbach *et al.* found that the so-called *subtractive rule* is particular suitable when considering shape descriptors as attributes [105]:

$$\gamma_{sub}^{\tilde{T}}(f)(p) = \sum_{k=0}^K \Gamma^{\tilde{T}}(F_k)(p). \quad (2.15)$$

If the criterion is increasing, then (2.14) and (2.15) are equal to (2.13). Similar conclusions can be drawn for attribute closing and thickening.

2.4 REPRESENTATIONS OF AN IMAGE AS A TREE

Let us consider a discrete 2D image f that is a map from the discrete image domain $E \subseteq \mathbb{Z}^2$ to \mathbb{Z} . Since the codomain of f is ordered, the

image can be fully represented by its *upper* or *lower level sets*, which are defined as

$$\begin{aligned} [f \geq \lambda] &= \{x \in E, f(x) \geq \lambda\} \\ [f < \lambda] &= \{x \in E, f(x) < \lambda\}, \end{aligned} \quad (2.16)$$

with $\lambda \in \mathbb{Z}$. Thus, upper and lower level sets are composed by binary images obtained by thresholding the input image at all the values mapped by the function f . The connected components extracted by the binarization of the input image related to the upper or lower level sets can be grouped in the sets:

$$\mathcal{U}(f) = \{X : X \in \mathcal{CC}([f \geq \lambda]), \lambda \in \mathbb{Z}\} \quad (2.17)$$

$$\mathcal{L}(f) = \{X : X \in \mathcal{CC}([f < \lambda]), \lambda \in \mathbb{Z}\} \quad (2.18)$$

with $\mathcal{CC}(f)$ the connected components of the generic image f . If we consider f as a function of the height (coded by the values of the codomain), the upper (lower) level sets are obtained by slicing the topographic relief at different heights and projecting the points with greater (lower) values than the thresholding height to the plane at the given height. By varying the height of the plane, it can be seen how connected components (i.e., regions of isolevel) can merge, enlarge, shrink, split, appear or disappear according to the morphology of the elevation surface. Among the connected components extracted by either the upper or lower level sets (belonging to $\mathcal{U}(f)$ or $\mathcal{L}(f)$ respectively) there is an inclusion relationship [106]. In greater details, any two components $A, B \in \mathcal{U}(f)$ are either nested ($A \subseteq B$ or $B \subseteq A$) or disjoint ($A \cap B = \emptyset$). Analogous considerations can be done for $\mathcal{L}(f)$. Due to the inclusion relations between the flat zones in the image, it is possible to associate a node of a tree to each connected component and represent the image as a hierarchical structure. The hierarchical tree representing the components in $\mathcal{U}(f)$ ($\mathcal{L}(f)$) and their inclusion relations is called *max-tree* (*min-tree*) [90]. In the max-tree representation, the root node is the entire image domain at the lowest grayscale value while the leaves of the tree are the regional maxima. An example of max-tree is reported in Fig. 2.3. By duality, the min-tree can be obtained by generating the max-tree on the complement of the image and shows as root the whole image at the highest grayscale value and as leaves the regional minima. Both min- and max-trees are equivalent representations of the image. However, not all the components present in $\mathcal{U}(f)$ are also present in $\mathcal{L}(f)$ and vice versa. For example, the top of two peaks (i.e., regional maxima) in the image having the same height, will be represented in the upper level set as two distinct components while in the lower level set they will belong to the same component. A self-dual representation of the connected

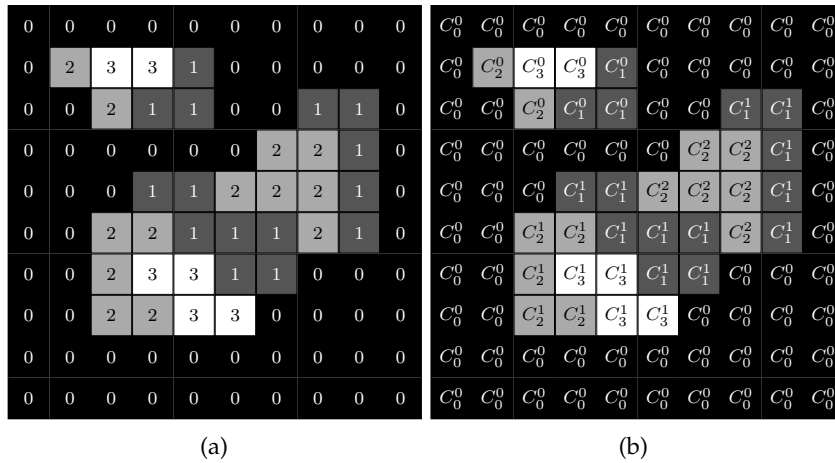


Figure 2.3: Example of max-tree. (a) Gray-scale image with intensities ranging from 0 to 3; (b) Image in (a) with its connected components labelled; and (c) Max-tree of (a). This shows the relations between the nodes associated to the connected components in (b).

components of an image called *inclusion tree* (or *tree of shapes*) exists for continuous images [107]. When dealing with discrete images (as in this work) different discrete connectivity rules have to be associated to minima and maxima regions (e.g., 8- and 4-connectivity for the definition of the upper and lower level sets, respectively [106]) leading to a quasi self-dual representation of the image. If only one type of connectivity was used for computing the inclusion tree, inconsistent results would be obtained since the notion of hole is not properly defined. We believe that the fact that the inclusion tree is not completely self-dual does not affect the results for practical applications. For example, even connected operators applied in an alternating sequence (providing a quasi self-dual effect biased by which operator starts first in the sequence) proved to be suitable for obtaining a simplification of the

image [93]. The inclusion tree is also a complete representation of the input image (i.e., it is possible to fully retrieve the image from the tree). The inclusion relations between flat regions represented in this tree structure is given by the *saturation* of the connected components. The saturation is an operator that fills the *holes* of a component. With holes of a connected component A are intended all those regions that belong to the background of A but which are not connected to its border. A saturated region (i.e., component with its holes filled) is also called a *shape*. Thus, according to the operator of saturation, a component A can be considered as included in B (regardless their relative graylevel difference) if $A \subseteq B$ in $\mathcal{U}(f)$ or $\mathcal{L}(f)$. The construction of the tree can be performed by an efficient algorithm called Fast Level Set Transform (FLST) that starts from considering the regional extrema (leaves of the tree) and progressively saturates the components until only a single flat region (the root of the tree) is obtained [107]. The progressive saturation of the components explains the inclusion relations on which the tree is constructed. The inclusion tree is a more general representation of the image with respect the max- and min-trees since comprehends both the $\mathcal{U}(f)$ and $\mathcal{L}(f)$ sets.

Another representation of the image as hierarchical tree of isolevel regions is given by *binary partition trees* (BPTs) [108]. Since BPTs contain those connected components considered more interesting according to the criterion involved during the tree creation (e.g., homogeneity, size, contrast, etc.) they can enhance certain features (according to the criterion used) more than a min- max- or inclusion tree. Connected operators can be efficiently computed on the trees generated from the image [109]. The representation of the image as max-tree is useful for performing anti-extensive connected operators (e.g., thinning). By duality, extensive connected operators (e.g., thickening) can be computed on the min-tree. Self-dual connected operators can be obtained by considering an inclusion tree. Moreover, since the inclusion tree stores both the components of the upper and lower level sets, one can perform an anti-extensive or extensive transformation by only considering the regions of the upper or lower level set, respectively. Since connected operators modify an image only by merging its flat zones, the filtering is performed on the hierarchical tree as a pruning. In general, the tree is pruned by evaluating a binary predicate T on the nodes and removing those that do not fulfill it. The predicate usually compares an attribute $attr$ computed on the pixels belonging to a connected component C (corresponding to a node in the tree) and a given threshold value taken as reference λ : e.g., $T = attr(C) \geq \lambda$. The attributes can be any measure computable on the regions (e.g., area, volume, entropy, etc.).

If we consider a filtering done according to an increasing predicate (i.e., for the connected components A and B holds that if $T(A) = true$ then $T(B) = true$ with $B \subseteq A$) the connected operator obtained will also be increasing and the pruning can be performed by removing entire branches (constituted by a node and all its descendants) from the tree. If the predicate is non-increasing, then different filtering rules can be applied in order to determine which nodes have to be removed since the evaluated criterion could be fulfilled for certain nodes but not for their descendants [109].

2.5 ATTRIBUTE FILTERS BASED ON TREE REPRESENTATIONS

Attribute filters computed on gray-level images according to the definitions given in Sec. 2.3 are not efficient in terms of implementation. However, it is possible to take advantage of the hierarchical representations of the image as trees (e.g., max-tree).

The computation of the attribute filters on the max-tree structure is composed by three steps which are detailed in the following.

- i) *Max-tree creation.* This step aims at generating the tree from the image by identifying the connected components in the image and by modeling the hierarchical representations between nested nodes. This phase of the process is computationally most demanding.
- ii) *Evaluation of the criterion.* After the creation of the tree, the criterion is evaluated by comparing the attribute extracted from each node and the threshold value (λ) which is considered as reference and defines the degree of filtering. Then, the tree is pruned by removing those nodes that do not fulfill the criterion. If the criterion is non increasing, different filtering rules can be implemented as reported above (see (2.14), (2.15)). They correspond to different strategies in pruning the tree [90, 105].
- iii) *Image restitution.* The final step is the conversion of the pruned tree back to an image.

Since the max-tree is constructed by growing the tree from the lowest grayscale value to the maximum one, this structure is suitable for transformations such as opening and thinning. On the contrary, for operators of closing and thickening, the min-tree is considered. A min-tree is the representation of the image dual with respect to max-tree and can be simply computed as the max-tree of the complement of the input image.

RELATED WORKS: TECHNIQUES BASED ON MORPHOLOGICAL PROFILES

Abstract. This chapter aims at recalling the concepts of Morphological Profile and Extended Morphological Profile and their theoretical definitions. Moreover, an overview of the many significant contributions that have appeared in the literature since the definition of the MP is also reported.

3.1 INTRODUCTION

Morphological Profiles (MPs) are an effective tool for extracting spatial features from the image in order to describe the objects in the scene [72]. A MP performs a multiscale decomposition of an image based on a simplification of the scene through the suppression of progressively larger details. The MP is defined on the morphological operators of opening and closing by reconstruction (morphological operators particularly suitable for the analysis of high geometrical resolution images [82]) and it was firstly applied in 2001 on panchromatic images [72]. From its presentation, the MP was used in an increasing number of applicative domains. Remarkably, the MP definition has been generalized from the analysis of a single band image (e.g., panchromatic) to hyperspectral images made up of hundreds of spectral channels and has become one of the state of the art techniques for the analysis of such images [110].

In this chapter, we present an overview of the concepts of MP and of its extension suitable for the analysis of hyperspectral images, *extended morphological profile* (EMP). Furthermore, we give an overview of the different techniques involving the MP that have appeared in the literature allowing the reader to follow the evolution of the MP over this last decade.

This chapter were published in:

M. Dalla Mura, J. Benediktsson, J. Chanussot, and L. Bruzzone, *Optical Remote Sensing - Advances in Signal Processing and Exploitation Techniques*. S. Prasad, L. M. Bruce, J. Chanussot Eds. Springer Verlag, 2011, ch. The Evolution of the Morphological Profile: from Panchromatic to Hyperspectral Images.

3.2 MORPHOLOGICAL PROFILES FOR THE ANALYSIS OF PANCHROMATIC IMAGES

3.2.1 Morphological Profiles and Differential Morphological Profiles

In general, for real applications it is unlikely that filtering of an image with a single opening and closing by reconstruction completely models the spatial information in a complex scene. This behavior might limit the capability of the image analysis. A common procedure is to filter an image with a sequence of many different SEs in order to extract more information on the scene. Granulometries and anti-granulometries are examples of this approach. A granulometry is obtained by the application of a series of opening with SEs of increasing sizes and fixed shape. An anti-granulometry is generated analogously by closing operators. By analyzing the result of a granulometry one is able to gather information on the size distribution of those objects brighter than the surrounding background. Thus, we can refer to this procedure as a multi-scale analysis. When performing such an analysis with operators based on the geodesic reconstruction, the progressive simplification of the image does not come at the detriment of the geometry of those objects that are not canceled from the image.

The *morphological profiles* are based on these ideas. Morphological profiles were introduced by Pesaresi and Benediktsson in [72] and defined as a concatenation of an anti-granulometry followed by a granulometry performed by closing and opening by reconstruction transformations, respectively. The anti-granulometry is referred as closing profile Π_ϕ and the granulometry as opening profile Π_γ . The morphological opening profile of an image f is an array of n openings performed on the original image using a SE of size λ , and it is defined as

$$\Pi_\gamma(f) = \{\Pi_{\gamma_\lambda}(f) : \Pi_{\gamma_\lambda}(f) = \gamma_R^\lambda(f)\} \quad \lambda = 0, 1, \dots, n. \quad (3.1)$$

Thus by duality, the morphological closing profile composed by n levels can be denoted by

$$\Pi_\phi(f) = \{\Pi_{\phi_\lambda}(f) : \Pi_{\phi_\lambda}(f) = \phi_R^\lambda(f)\} \quad \lambda = 0, 1, \dots, n. \quad (3.2)$$

Therefore, both the opening and closing profiles are generated by opening and closing by reconstruction operators with the image f taken as mask and with SEs of fixed shape and size increasing on the n levels. When a closing profile and an opening profile, both of size n , are joined a morphological profile is obtained. The MP is of size $2n - 1$, because when $\lambda = 0$ the opening and closing profiles are equal to the

original image ($\Pi_{\gamma_0} = \gamma_R^0(f) = \Pi_{\phi_0} = \phi_R^0(f) = f$) and thus they are considered only once (see Fig. 3.1)

$$MP(f) = \left\{ \begin{array}{ll} \Pi_{\phi_\lambda}(f), & \lambda = (n-1+i) \quad i \in [1, n]; \\ \Pi_{\gamma_\lambda}(f), & \lambda = (i-n-1) \quad i \in [n+1, 2n+1]; \end{array} \right\}. \quad (3.3)$$

The derivative of a MP, denoted as *differential morphological profile* (DMP) [72], can be computed as the differences between two adjacent levels of the MP,

$$DMP(f) = \left\{ \begin{array}{ll} \Delta_{\phi_\lambda}(f), & \lambda = (n-1+i), \quad i \in [1, n]; \\ \Delta_{\gamma_\lambda}(f), & \lambda = (i-n-1), \quad i \in [n+1, 2n]; \end{array} \right\} \quad (3.4)$$

with the differential closing profile Δ_{ϕ_λ} and differential opening profile Δ_{γ_λ} simply defined as

$$\Delta_\gamma = \{\Delta_{\gamma_\lambda} : \Delta_{\gamma_\lambda} = \Pi_{\gamma_{\lambda-1}} - \Pi_{\gamma_\lambda}\} \quad \lambda = 1, 2, \dots, n; \quad (3.5)$$

$$\Delta_\phi = \{\Delta_{\phi_\lambda} : \Delta_{\phi_\lambda} = \Pi_{\phi_\lambda} - \Pi_{\phi_{\lambda-1}}\} \quad \lambda = 1, 2, \dots, n. \quad (3.6)$$

The DMP stores the residuals of the sequential transformations applied to the image. This can be particular useful when the multi-scale analysis has to be visualized, since the most important components of the profiles are more evident than when the MP is considered.

Moreover, from the DMP the information on the scale of the objects in the image can be extracted. In [72], this information was used for generating from the image a multiscale segmentation map, called *morphological characteristic*. In greater detail, each pixel in the image is labeled with the index of the level in the MP in which the maximum of its derivative (i.e., DMP) occurs.

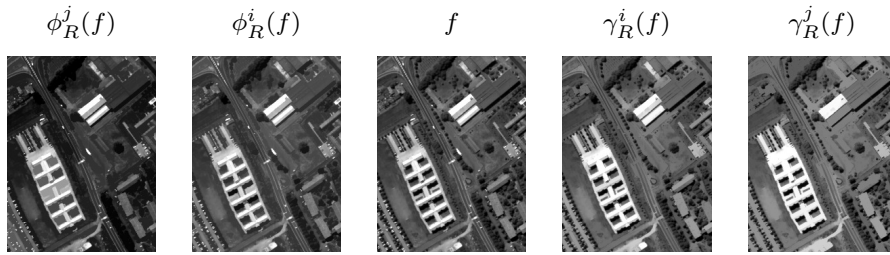


Figure 3.1: Example of MP composed by 5 levels, obtained by 2 openings and 2 closings ($j > i$). For generating this MP a squared SE was considered, with size of 5 (i) and 9 (j) pixels.

3.2.2 Experimental Analysis and Discussion

Morphological profiles were first applied in [72] for segmenting two 800×800 pixels HR panchromatic images acquired by Indian Remote

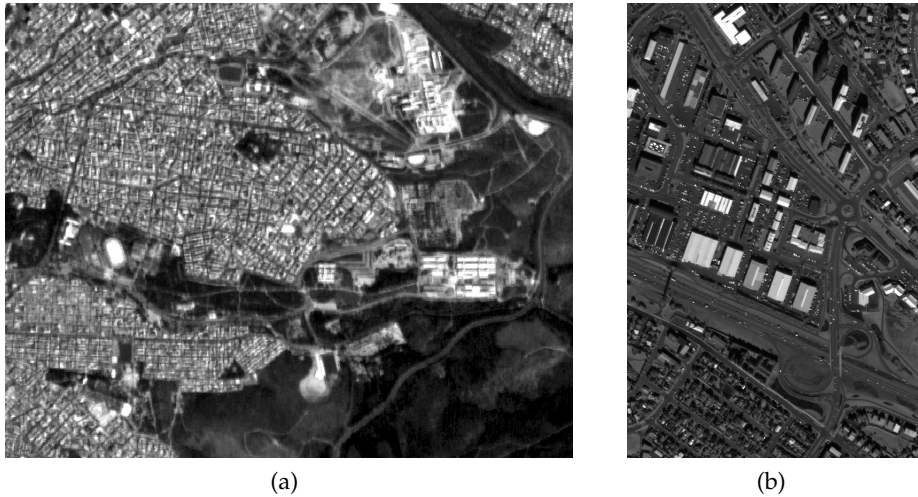


Figure 3.2: Panchromatic images. (a) IRS-1C image of the city of Athens, Greece (800×800 pixels, 5.8 m geometrical resolution, spectral range $0.5\text{-}0.75 \mu\text{m}$); (b) IKONOS image of the city of Reykjavik, Iceland (975×639 pixels, 1m geometrical resolution, spectral range $0.53\text{-}0.93 \mu\text{m}$).

Sensing 1C (IRS-1C) with a 5 m geometric resolution on a dense urban area of Milan, Italy, and on an agricultural area of Athens, Greece. The application of operators by reconstruction to the two images showed a better representation of the geometry of the objects in the scene with respect to the processing with standard morphological operators. Moreover, the segmentation maps obtained by the morphological characteristic of the images were not affected by the oversegmentation effect that was noticeable when a classical watershed segmentation was performed.

In [111], the MPs were applied for the first time in a classification task. An IRS-1C panchromatic image of Athen, Greece, (Figure 3.2a) and an IKONOS panchromatic image from Reykjavik, Iceland, (Figure 3.2b) were classified with a conjugate gradient neural network. In both the experiments, eight closings and eight openings were applied to the original images leading to a 17-dimensional feature vector considered as input to the neural network. In order to reduce the dimensionality of the filtered data, two feature extraction methods and a feature selection technique were investigated. The considered approaches were: i) discriminant analysis feature extraction (DAFE) [2]; ii) decision boundary feature extraction (DBFE) [2]; and iii) a simple feature selection based on sorting the indexes of the DMP using the value of the discrete derivative. The obtained classification results showed as the use of the features extracted by the MP increased the

overall accuracy from 69.4% and 70.9% of the original panchromatic image to 77.7% and 95.1% when considering the entire differential profile for the IRS-C1 and IKONOS image, respectively. Among the techniques of feature reduction, the DBFE outperformed DAFE and the feature selection technique. However, lower accuracies than those obtained by considering the whole DMP were obtained.

A morphological profile was built in [112] by applying alternating sequential filters (ASF) by reconstruction instead of the operators of opening or closing by reconstruction. Alternating sequential filters by reconstruction are iterative sequential applications of an opening and a closing by reconstruction (or vice versa) of increasing size. The MP built on ASF were applied to the IKONOS panchromatic image in Figure 3.2b. The feature extracted were classified by a neural network. Although the standard MP performed better than the one with ASF on the original, the latter showed to be more robust when analyzing the image corrupted by Gaussian noise.

In [113], the DMP was interpreted as a fuzzy measure of the characteristic size and contrast of the objects in the image. The fuzzy measure extracted from the DMP was compared to predefined possibility distributions in order to derive a membership degree for the thematic classes of the samples in the image. The decision is taken by selecting the class with the highest membership degree. The experimental results were obtained from the analysis of the Reykjavik IKONOS image in Figure 3.2b.

In order to perform a better modeling of the spatial features in the image, in [114] the computation of two MPs with SEs of different shape was proposed for classification. The authors considered in their analysis a disk-shaped SE and a linear SE with different orientations (which generate directional profiles [84]). While the MP built with the former SE is suitable to extract the smallest size of the structures, the latter allows one to infer the largest size of the objects. Moreover, an interesting variant of the geodesic reconstruction called “partial reconstruction” was presented. The proposed reconstruction procedure performs a partial geodesic reconstruction (the iterative process is converging to idempotency). This leads to reaching a trade-off between the preservation of the objects geometries and a reduction of the over segmentation effect introduced by standard reconstruction. Two study areas were considered in the analysis, an IKONOS and a Quickbird panchromatic images both acquired on the area of Ghent (Belgium). The proposed technique significantly outperformed the results obtained without considering any spatial feature in the analysis. Furthermore, an increase in the overall accuracies with respect to the case with standard reconstruction of about 2% and 7% was achieved

by considering the two MPs built with partial reconstruction for the two sites, respectively.

3.3 EXTENDED MORPHOLOGICAL PROFILES FOR THE ANALYSIS OF MULTISPECTRAL AND HYPERSPECTRAL IMAGES

3.3.1 Extended Morphological Profile

The extension of the MP to hyperspectral data presented in [115], which led to the definition of the Extended Morphological Profile, is achieved through a two step procedure. At first, the multidimensional data is reduced through a PCA to few informative dimensions (i.e., the first principal components, PCs). The PCs corresponds to the eigenvectors of the estimated covariance matrix of the data and are ordered increasingly according to the values of the correspondent eigenvalues. The first PCs are meaningful for data representation since they account for most of the variance of the data in the original feature space. In general, the first considered PCs accumulate most of the total variance of the data (e.g., usually a threshold on 99% is taken). Subsequently, on each PC a full MP is computed. Thus, the EMP of the first c principal components can be formalized by

$$EMP(f) = \{MP(PC_1), MP(PC_2), \dots, MP(PC_c)\}. \quad (3.7)$$

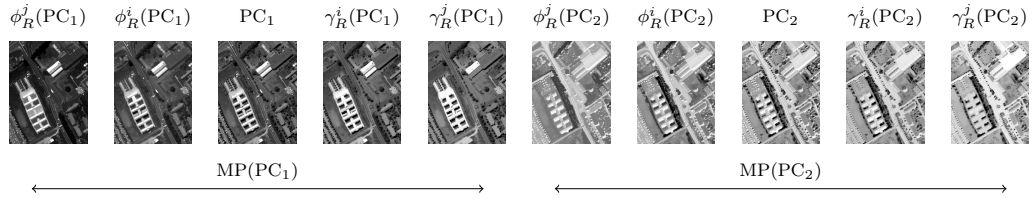


Figure 3.3: Example of EMP computed on the first two PCs and composed by 5 levels for each MP.

As seen from (3.7), the EMP is the concatenation of MPs on a single stack. Since the dimensionality of the EMP can rapidly increase when increasing the number of considered PCs and the levels of the MP, in [115] the application of feature extraction techniques was proposed in order to decrease the curse of dimensionality phenomenon [116]. Feature extraction techniques for classification should be considered in order to achieve a dimensionality reduction and an effective separation of the distributions of the classes in the transformed feature space [117].

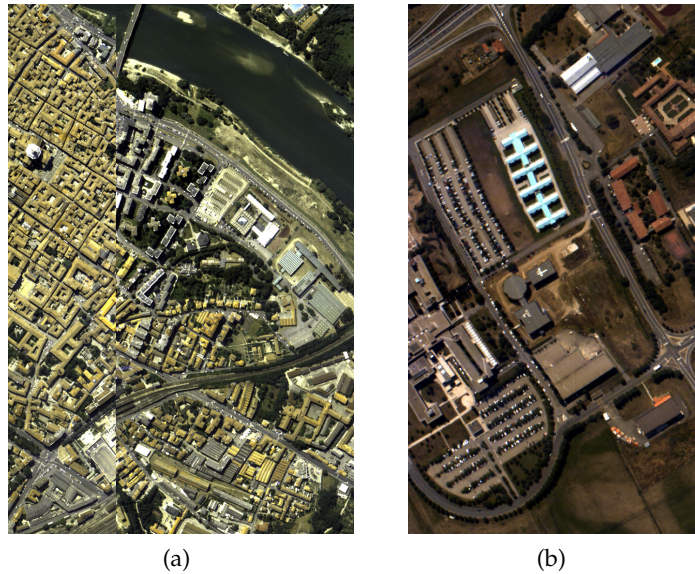
3.3.2 *Experimental Analysis and Discussion*

Figure 3.4: Hyperspectral images acquired by ROSIS-03 sensor over the area of Pavia (Italy) with 2.6m of spatial resolution. (a) Pavia, city center, 1096×715 pixels, 102 spectral bands; (b) Pavia, University area, 610×340 pixels, 103 spectral bands. ¹

The extended morphological transformations based on the ordering of the pixels multidimensional values done by considering spectral-distance metrics were applied in [118] to two hyperspectral images acquired by AVIRIS and DAIS sensors. The AVIRIS image was acquired on Salinas Valley (CA) and is composed by 512×217 pixels with 192 spectral bands with 3.7m of spatial resolution. The DAIS image showed a 400×400 pixels scene of the center of Pavia (Italy) with a 5m geometrical resolution. The classification accuracies obtained by the presented techniques outperformed ones achieved by considering only the original hyperspectral images up to 8% and 7% for the two images, respectively.

The EMP presented in Sect. 3.3.1 was applied in [115] to two hyperspectral images, one acquired by the DAIS sensor on the center of Pavia (400×400 pixels, 80 spectral bands, 2.4 geometrical resolution) and the other collected by the Hyperspectral Digital Imagery Collection Experiment (HYDICE) over the Washington DC Mall area (1280×307 , 189 spectral bands, 2.8m spatial resolution). The experiments were obtained by considering the first two PCs for building the EMP. When considering the features extracted by the EMP, the overall accuracy in classifying the test sites with a neural network sig-

nificantly increased with respect to considering only the hyperspectral data (+45% and +12% for the two images, respectively). Moreover, DAFE, DBFE, and NWFE [2] were considered for reducing the dimensionality of the data before the classification. Although a significant reduction of the dimensionality of the data was achieved (i.e., reducing the load for the classification stage) no increase in terms of overall accuracy were accounted with respect to considering the EMP with full dimensionality. However, among the considered feature extraction techniques, in both cases NWFE performed the best among the others in terms of classification accuracies reaching values of accuracy close to those obtained by the full EMP.

In [119] the features extracted by an EMP computed on the first PC were considered by using five classifiers (Maximum Likelihood for Gaussian data, Fisher linear discriminant, the ECHO classifier, Fuzzy ARTMAP and a feed forward neural network classifier) along with two feature extraction techniques (DAFE and DBFE). The data used in the experiments involved two test sites on the urban area of Pavia, Italy, acquired with the Digital Airborne Imaging Spectrometer (DAIS). Each hyperspectral image was composed of 80 channels with a spatial resolution of 2.6m. When considering the morphological features the overall accuracy increased by more than 27% with respect to considering the first PC alone. Moreover, the reduction of the feature size with the DBFE technique further improved the accuracy of about 2%.

In [120], ICA was considered instead of PCA for computing the EMP. ICA, in contrast to PCA, leads to a better extraction of the information sources (especially when they are non Gaussian). In experiments an hyperspectral image of the center of Pavia (Italy) acquired by the ROSIS-03 sensor (see 3.4a) was considered. The classification was performed with a maximum likelihood classifier. The overall accuracy obtained by the EMP built on the independent components outperformed by 5% the overall accuracy of the classification of the original hyperspectral data.

Kernel Principal Component Analysis instead of the conventional PCA was considered in [121] as feature reduction technique for computing the EMP. Results were obtained for three hyperspectral images, two acquired on the city of Pavia (Italy) (Figure 3.4a, 3.4b) and one on Washington DC Mall (1280×307 , 189 spectral bands, 2.8m spatial resolution). An SVM classifier with linear and Gaussian kernels was considered in the experiments. The results obtained proved that KPCA can extract more informative components with respect to PCA. In fact, the EMP computed on the KPCs increased up to +20% and +5% the

overall accuracy obtained by the classification of the hyperspectral data and with the EMP with PCA, respectively.

Several feature extraction and selection methods were considered for building the EMP. The classification maps obtained with a random forest and an SVM classifier applied to the hyperspectral images reported in Figure 3.4a and 3.4b, showed how the EMP with PCA is not adequate in terms of overall accuracy with respect to other techniques. In particular, NWFE and BDFS performed the best on the experiments with both the classifiers.

The work presented in [122] was devoted to the fusion of spatial features extracted through a standard EMP and the original hyperspectral data. This approach was proposed to increase the amount of spectral information considered in the classification task. The experimental analysis was carried out on two hyperspectral images of the city of Pavia (Italy) both acquired by ROSIS-03 sensor. The two original images are shown in Figure 3.4a and 3.4b. Feature extraction techniques were also employed for reducing the dimensionality of the data and an SVM classifier was used for generating the classification maps. For the university site (see Figure 3.4b), the overall accuracy increased from 79% to 84% (without feature extraction) and to 88% (with feature extraction), with respect to the EMP obtained with the proposed approach.

In [123], an extension of the segmentation procedure based on the analysis of DMPs for panchromatic images [72] was proposed. The novel segmentation technique was developed for automatic object detection in high-resolution images by combining spectral and structural information. In contrast to [72], the DMPs computed on the first PCs extracted from the images were analyzed in order to extract the connected components that best represent each object in the scene. Three hyperspectral images were considered: the image of the center of Pavia (Figure 3.4a), the HYDICE image acquired over Washington DC Mall (1280×307 , 189 spectral bands, 2.8m spatial resolution), and a 500×500 pansharpened IKONOS image of Ankara (Turkey). The obtained results showed a more precise segmentation of the images and a reduced oversegmentation effect with respect to the maps obtained by the morphological characteristic of [72].

3.4 CONCLUSION

In this chapter an overview on the use of the morphological profile (MP) in remote sensing applications has been given. The MP proved to be an effective tool for the analysis of high geometrical resolution remote sensing images because it is defined as a composition of

opening and closing by reconstruction transformations. Operators by reconstruction permit to filter the image by entirely preserving the geometry of those structures that are not erased from the scene.

The definition of the extended morphological profile (EMP) for multispectral and hyperspectral images was presented. The vectorial image is reduced through Principal Component Analysis for constructing the EMP to a reduced number of images, on which MPs are computed. The EMP is finally obtained as the concatenation of the single MPs.

An overview of results obtained by experimental analysis of various techniques developed using the MP and EMP were reported. A significant increase in classification accuracies was observed when features extracted by MP/EMP (or their variants or extensions) were used for classification in comparison to approaches that only use spectral information.

Part II

PROPOSED TECHNIQUES FOR IMAGE
CLASSIFICATION AND OBJECT EXTRACTION

ATTRIBUTE PROFILES

Abstract. This chapter is devoted to present the concept of Attribute Profile. At first, the motivations that led to the definition of the AP are given. Subsequently, the AP is theoretically introduced. Considerations on the computational complexity are also reported. Finally, the effectiveness of AP is assessed on a classification task.

4.1 INTRODUCTION

As can be observed from the literature reviewed in Ch. 3, the computation of a multi-scale processing (e.g., by MPs, DMPs, EMPs) has proven to be effective in extracting informative spatial features from the analyzed images. For example, MPs computed with a compact SE (e.g., square, disk, etc) proved to be suitable for modeling the size of the objects in the image (e.g., in [111] this information was exploited for discriminating small buildings from large ones). Nevertheless, profiles built by filters based on SEs have their main limitation in the capability to model other feature than the size of the objects. The computation of two MPs was proposed for modeling both the length and the width of the structures [114]. In greater detail, one MP is built by disk-shaped SEs for extracting the smallest size of the structures, while the other employs linear SEs (which generate directional profiles) for characterizing the objects maximum size (along the orientation of the SE). This is useful for defining the minimal and maximal length but, as all the possible lengths and orientations cannot be practically investigated, such analysis is computationally intensive. Furthermore, if one attempts to filter the image according to different degrees of spectral homogeneity or according to different shape descriptors, the results would be rather cumbersome. This limitation is particularly important when the discriminative power of the analysis could have been increased by modeling other features rather than the size (e.g., contrast, texture, geometry, etc.).

This chapter was published in:

M. Dalla Mura, J. A. Benediktsson, B. Waske, and L. Bruzzone, "Morphological attribute profiles for the analysis of very high resolution images," *IEEE Transactions on Geoscience and Remote Sensing*, vol. 48, no. 10, pp. 3747 – 3762, Oct. 2010.

Attribute filters can overcome this limitation of the MPs [88]. Due to their flexibility they can perform a processing of an image based on many different types of features. In fact, the attributes can be of any type. For example, they can be purely geometric, textural, based on the contrast, etc.

In this chapter, we present Attribute Profiles for characterizing the spatial information of VHR data by using a multilevel approach based on morphological attribute filters. APs are proposed to be an extension of the morphological profiles and of their derivative concepts, which are conventionally defined for openings and closings by reconstruction. Thus, the proposed theoretical framework permits the definition of a more general set of profiles based on the morphological attribute operators. The profiles built by morphological attribute filters permit a more flexible investigation of the scene, leading to a better modeling of the spatial information. Moreover, thanks to an efficient implementation, their application becomes computationally less demanding than conventional profiles built with operators by reconstruction.

4.2 LIMITATIONS OF MORPHOLOGICAL PROFILES

The main limitation of MPs lies in the partial analysis that is performed with the computation of the profile. In greater detail, MPs attempt to model the spatial information within the scene by analyzing the interaction of a set of SEs of fixed shape and increasing size with the objects in the image. Although this is a powerful tool for performing an investigation on the scale of the structures (thanks to the suitability of the SEs for modeling the size of the objects), it leads only to a partial characterization of the objects in the scene. In fact, one could aim at a description of the image based on other features (e.g., shape, texture, etc.) rather than the size in order to increase the discriminative power of the analysis. From a theoretical viewpoint, filters by reconstruction based on SEs could be used to model other geometrical features, e.g., to represent the information on the shape of the regions by analyzing a set of MPs generated by SEs of different shapes. Nonetheless, the generation of profiles for different shapes would be computationally unfeasible. In fact, in order to perform an analysis aimed at modeling the shape characteristic, the range of the possible sizes assumed by all the components in the image should be investigated by each profile in order to remove the dependence of the results to the scale.

Another important limitation is the strong constraint given by the use of a SE for modeling the concepts of different characteristics of the spatial information (e.g., size, shape, homogeneity, etc.). This limitation is particularly evident when features more complex than the geometrical

primitives of size and shape are required (e.g., shape factor, length of the skeleton of a region, etc.). Moreover, SEs are intrinsically unsuitable to describe features related to the graylevel characteristics of the regions (e.g., spectral homogeneity, contrast, etc.).

A final limitation of MPs is the computational complexity associated with their generation. The original image has to be completely processed for each level of the profile, which requires two complete processing of the image, one performed by a closing and the other by an opening transformation. Thus, the complexity increases linearly with the number of levels included in the profile.

4.3 DEFINITION OF ATTRIBUTE PROFILES

The definition of an attribute opening profile is quite straightforward since a sequence of attribute openings with a family of increasing criteria $T = \{T_\lambda : \lambda = 0, \dots, n\}$, with $T_0 = true \quad \forall X \subseteq E$, leads to a granulometry. Thus, attribute opening profiles can be mathematically defined as

$$\Pi_{\gamma^T}(f) = \{\Pi_{\gamma^{T_\lambda}} : \Pi_{\gamma^{T_\lambda}} = \gamma^{T_\lambda}(f), \forall \lambda \in [0, \dots, n]\}. \quad (4.1)$$

As for a MP, when $\lambda = 0$, $\Pi_{\gamma^{T_0}}(f) = \gamma^{T_0}(f) = f$. We point out that this definition of *attribute opening profile* includes also the morphological opening profile by reconstruction, since openings by reconstruction are a particular set of attribute openings. By comparing attribute profiles to conventional MPs, it can be noticed that both perform multi-scale analysis of the image since the SE/criterion, driven by the increasing scalar λ , progressively erases from the image larger structures. Moreover, attribute opening profiles provide the same capabilities in processing the image as for openings by reconstruction but adding more flexibility in the definition of the filtering criterion. For example, if we consider a compact SE (e.g., square-, disk-shaped), the structures are removed from the scene if the SE does not fit in them. Thus, the image is processed according to the smallest size of the regions. If we consider instead the length of the diagonal of the box bounding each region as an attribute, then the structures are filtered according to a measure of their global extension, which is still related to the concept of scale but in a different way with respect to considering the smallest size of the objects. Moreover, if we take into account the area of the regions a different measure of the size of the objects is provided. Thus, by selecting different type of attributes, even if they are all increasing measures, different characterizations of the scale of the structures are generated.

If we consider other types of attributes not constrained by the increas-

ingness property, a different behavior is achieved by the filters. For instance, it is possible to assess how the image reacts to a filtering done on multiple levels with an attribute invariant to changes in scale. This would permit to characterize the image by extracting information related to the shape of the structures through a measure which is independent of their size. Thus, the application of attribute thinning in a multi-level approach leads to *attribute thinning profiles*. However, their definition is not direct as for attribute opening profiles. In fact, since attribute thinnings are not increasing, the absorption law might not be satisfied in the profile. This can result in sequential elements of the profile that are not ordered. For example, regions erased at a certain level of the profile might appear again in subsequent levels associated to more relaxed criteria. This is an undesirable effect especially if a derivative of the profile needs to be computed. In order to build a consistent profile on attribute thinnings it is necessary that the absorption law is fulfilled by the filtered images, leading the AP to be a set of cumulative functions. This can be obtained by constraining the criteria used in the filtering. The family of non-increasing criteria $U = \{U_\lambda : \lambda = 0, \dots, n\}$ considered for computing the profile *has to be an ordered set*. Moreover, the criteria have to be consistently either in the form of $U_\lambda = a(X) > \tau_\lambda$ or $U_\lambda = a(X) < \tau_\lambda$ for all the connected component $X \subseteq E$, and $\tau_i \leq \tau_j$ for $i \leq j$, with a denoting a generic non-increasing attribute computed on the component X , and τ_λ being the scalar value taken as the threshold at the level λ of the profile. If the criteria are ordered and defined as mentioned above, then the following rule holds: If a connected set $X \subseteq E$ does not satisfy the criterion U_i (i.e., $U_i(X) = false$), then also $U_j(X) = false$, with $i \leq j$ and $U_i, U_j \in U$. Thus, for binary trivial thinning it holds that if $\tilde{F}^{U_i}(X) = \emptyset \Rightarrow \tilde{F}^{U_j}(X) = \emptyset$ and this leads $\tilde{F}^{U_i}(F) \subseteq \tilde{F}^{U_j}(F)$ for binary attribute thinning. In the grayscale case it becomes $\tilde{\gamma}^{U_i}(f) \subseteq \tilde{\gamma}^{U_j}(f)$. The latter property corresponds to the absorption law that can be expressed also as $\tilde{\gamma}^{U_i} \tilde{\gamma}^{U_j}(f) = \tilde{\gamma}^{U_{\max(U_i, U_j)}}(f)$. Thus, by selecting these criteria, the profile is behaving like a granulometry.

Consequently, it is possible to define an attribute thinning profile, based on a set of ordered criteria $U_\lambda = a(X) > \tau_\lambda$, with $U_0 = true \quad \forall X \in E$ as:

$$\Pi_{\tilde{\gamma}^U}(f) = \{\Pi_{\tilde{\gamma}^{U_\lambda}} : \Pi_{\tilde{\gamma}^{U_\lambda}} = \tilde{\gamma}^{U_\lambda}(f), \forall \lambda \in [0, \dots, n]\}. \quad (4.2)$$

Actually $\Pi_{\tilde{\gamma}^U}$ includes also Π_{γ^T} in its definition since the attribute thinning profile produces the same results as for the attribute openings if the criteria U fulfill the more restrictive property of increasingness. By duality, the *attribute closing profile* can be defined as

$$\Pi_{\phi^T}(f) = \{\Pi_{\phi^{\tau_\lambda}} : \Pi_{\phi^{\tau_\lambda}} = \phi^{\tau_\lambda}(f), \forall \phi \in [0, \dots, n]\}, \quad (4.3)$$

and analogously to 3.3, we can define an attribute profile as:

$$AP(f) = \Pi(f) = \left\{ \Pi_i : \left\langle \begin{array}{l} \Pi_i = \Pi_{\phi^{u_\lambda}}, \quad \lambda = (n - 1 + i), \quad \forall \lambda \in [1, n]; \\ \Pi_i = \Pi_{\gamma^{u_\lambda}}, \quad \lambda = (i - n - 1), \quad \forall \lambda \in [n + 1, 2n + 1] \end{array} \right\rangle \right\}. \quad (4.4)$$

The AP can also be expressed in an alternative formulation as:

$$AP(f) = \left\{ \phi^{u_{\lambda_L}}(f), \phi^{u_{\lambda_{L-1}}}(f), \dots, \phi^{u_{\lambda_1}}(f), f, \gamma^{u_{\lambda_1}}(f), \dots, \gamma^{u_{\lambda_{L-1}}}(f), \gamma^{u_{\lambda_L}}(f) \right\}, \quad (4.5)$$

with $2L + 1$ the number of levels in the profile.

Attribute thinning profiles permit us to perform a multi-level analysis of the image based on attributes (represented by ordered criteria) not necessarily related to the scale of the structures of the image. In fact, the choice of attributes like the shape factor, the spatial moments, etc., results in an AP that represents a multi-level (not multi-scale) decomposition of the image according only to the shape of the regions. Furthermore, the attribute can also be a measure which is not related to the geometry of the regions but to the graylevels of their pixels. For example, the scene can be simplified by removing structures according to homogeneity instead of their scale or shape. As for MPs, the residuals of the progressive filtering can be important. Thus we can extend 3.4 by introducing the *differential attribute profile* (DAP) for the set of non-increasing criteria U , is

$$DAP(f) = \Delta(f) = \left\{ \Delta_i : \left\langle \begin{array}{l} \Delta_i = \Delta_{\phi^{u_\lambda}}, \quad \lambda = (n - 1 + i), \quad \forall \lambda \in [1, n]; \\ \Delta_i = \Delta_{\gamma^{u_\lambda}}, \quad \lambda = (i - n), \quad \forall \lambda \in [n + 1, 2n] \end{array} \right\rangle \right\}. \quad (4.6)$$

where $\Delta_{\phi^{u_\lambda}}$ and $\Delta_{\gamma^{u_\lambda}}$ represent the differential thickening and thinning profiles, respectively, whose definition is straightforward and thus not reported.

Examples of a DMP and three DAPs computed on a panchromatic Quickbird image of the city of Trento (Italy) for four different thematic classes are presented in Figure 4.1. The attributes selected for the three DAPs are: i) area; ii) moment of inertia; and iii) standard deviation. By analyzing the differential profiles, as expected, it can be noticed that the DMP shows a similar behavior to the DAP with the area attribute, since both process the image according to the scale of the objects. The DAPs built on the moment of inertia and the standard deviation have a different behavior from the scale attributes. However, given a region, regardless of the type of attribute considered, the active responses of the pixels belonging to the region in the profile are all located either in the opening or closing part of the profile. In fact, dark objects are detected in the closing profile and bright ones on the opening side.

The diversity shown by considering the DAPs built on different types of attributes results in features that potentially can increase in the separability of the information classes.

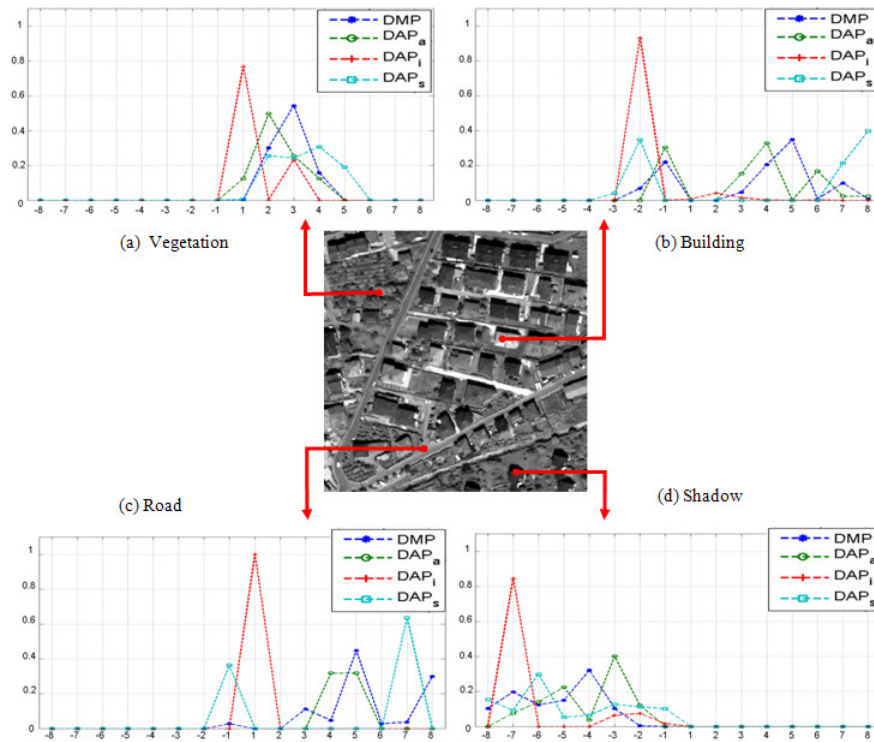


Figure 4.1: Examples of four differential profiles computed on four samples belonging to different thematic classes (Vegetation, Road, Building, and Shadow) from a panchromatic Quickbird image of Trento (Italy). The values of the shown profiles are normalized in the range $[0,1]$. The horizontal axis reports the levels of the profiles. In the legend, DMP refers to the conventional DMP built by a squared-SE, DAP_a , DAP_i , DAP_s denote the differential attribute profiles built on the area, moment of inertia and standard deviation attribute, respectively. The subtractive rule was considered for the non-increasing criteria.

4.4 ANALYSIS OF THE COMPLEXITY

The main advantage, in terms of computational complexity, of the approach based on the max-tree with respect to the use of operators by reconstruction for performing multi-level filtering relies on the fact that the image has not to be completely processed at each level of the profile. In fact, the tree structure is built only once from the original image and after the attribute is computed on the components

of the image, the same data structure is pruned by a set of thresholds λ generating the filtered images at the different levels. Moreover, we point out that, if an attribute can be computed incrementally (e.g., area, volume, standard deviation, etc.), the computation of the attribute can be embedded in the creation of the tree, thus avoiding visiting all the nodes further. If a multi-level multi-attribute analysis is performed, the processing can further take advantage from the architecture based on the max-tree. In fact, the tree is still created only once, and the investigated attributes can be computed on the nodes, if possible, directly during the creation of the tree. However, even if the attributes need to be computed off-line after the creation of the tree, they can be calculated simultaneously at the visiting of each node, requiring a single scan of the tree. Moreover, during the computation of the attributes, their dependences can be exploited. For example, if the standard deviation and the area attributes need to be computed, the former requires in its definition the computation of the area, which can be directly exploited from the second attribute. Obviously, this further optimizes the analysis. Finally, the evaluation stage simply checks the criteria against the attributes values of the nodes in the tree. This is the only operation in the entire analysis that linearly depends on the number of levels and attributes considered. If we quantitatively analyze the computational complexity of the implementation of the different operators, the conventional opening by reconstruction based on the iterative geodesic reconstruction [82] has a worst-case time complexity with an upper bound of $O(N^2)$, where N is the number of pixels in the image. When computing a granulometry by reconstruction composed by L levels, the computational complexity has an order of $2LN^2$ in the worst-case. Vincent [124] proposed an efficient algorithm based on first-input-first-output queue and two raster scans of the image which is an order of magnitude faster than the conventional technique and, thus, can reduce the load of computing a profile. Nevertheless, the image has to be entirely processed $2L$ times, regardless the algorithm considered. Instead, when considering an approach based on the max-tree, the computational complexity of the analysis can be reduced. The most demanding stage of an attribute filtering based on the max-tree is the creation of the tree that relies on a flood-filling algorithm. This algorithm is linear with respect to both the number of pixels and the connectivity [125]. The pruning of the tree and the image restitution are both $O(N)$ operations. Thus, the computational cost of a profile is $O(NG + 4LN)$, being G the number of graylevels in the image. On parallel machines, the max-tree computation is further speeded up according to a slightly varying implementation based on the union-find algorithm. More

considerations on the memory use of max-trees according to their implementation can be found in [126].

4.5 EXPERIMENTAL RESULTS

4.5.1 Data set Description

The experimental analysis was carried out by classifying two portions taken from a large VHR panchromatic image acquired by the Quickbird sensor on July 2006 with geometric resolution of 0.6 m. We did not consider the multi-spectral images acquired by the Quickbird scanner in order to focus the analysis only on the capabilities of different APs to model the geometrical/spatial information. This choice is also reasonable for some operational conditions when satellites that acquire only the panchromatic band (e.g., WorldView 1) are used. The two considered images are made up by 400×400 (Figure 4.2a) and 900×900 (Figure 4.3a) pixels, respectively. Both the images represent

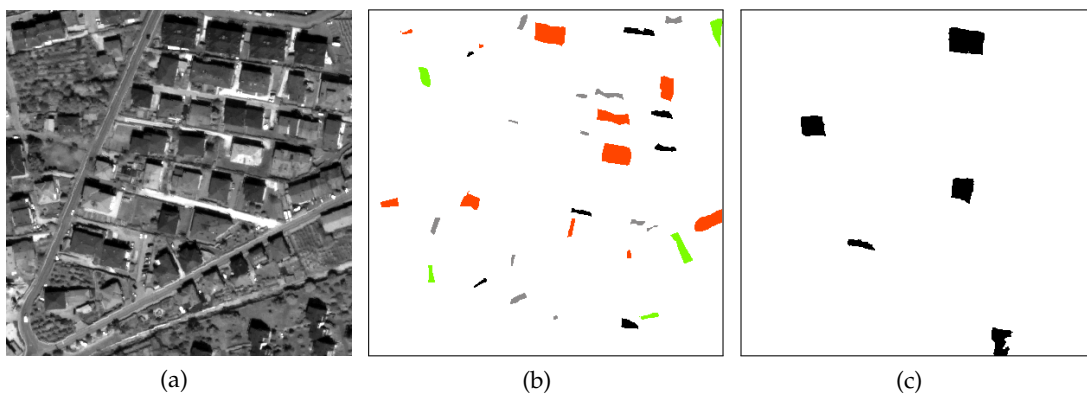


Figure 4.2: Data set 1. (a) Panchromatic image of 400×400 pixels; (b) map of the test areas; and (c) map of the objects selected for the assessment of the geometrical accuracy. Thematic classes: ■ road, ■ building, ■ shadow, ■ vegetation.

two complex urban areas belonging to the city of Trento, Italy. Most of the surveyed buildings are residential with heterogeneous size and shape. Some large industrial buildings are also present in the scene. The presence of shadows can be observed especially in proximities of buildings. All these factors contribute to the complexity of the considered scene. The pixels of the two images were grouped into four informative classes: Road, Building, Shadow and Vegetation. For both images a training set, composed by samples randomly selected from labeled areas not included in the test sets, was considered and two

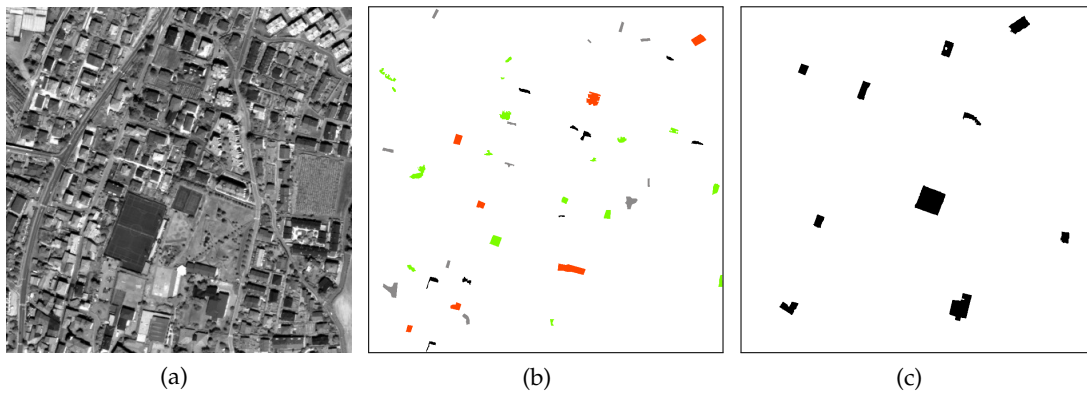


Figure 4.3: Data set 2. (a) Panchromatic image of 900×900 pixels; (b) map of the test areas; and (c) map of the objects selected for the assessment of the geometrical accuracy. Thematic classes: ■ road, ■ building, ■ shadow, ■ vegetation.

independent test sets were defined by photo-interpretation in order to evaluate the performances of the classification. One test set is devoted to the evaluation of the thematic accuracy, while the other checks the geometric precision of the classification map on a set of selected objects in the scene according to the protocol proposed in [127, 128]. The geometrical accuracy is evaluated by a set of five indexes modeling: over-segmentation (OS), under-segmentation (US), fragmentation (FG), shape factor (SH) and errors on the objects borders (ED). The index modeling the OS gives a measure of the overlap between the region which mostly covers a reference objects in the classification map and the area of reference objects. The US error computes how much the regions correspondent to the reference objects are larger than the reference objects. The FR index refers to a descriptor of how the areas of the reference objects are fragmented in different regions in the classification map. Finally, the SH and the ED measures indicate how the shapes and the edges respectively of the reference objects differ to those of the correspondent regions in the reference map. All the error indexes range from 0 to 1 (in the tables the values are given in percentages), with zero representing a perfect match and one the greatest divergence between the reference objects and the correspondent regions in the classification map. For further information on the geometric error indexes the reader can refer to [128]. The two test sets are reported in Figure 4.2b-4.2c and 4.3b-4.3c for data set 1 and 2 respectively. The number of samples selected for training and testing the two data sets are reported in Table 4.1.

Table 4.1: Number of samples per class for the training and test set for the two data sets.

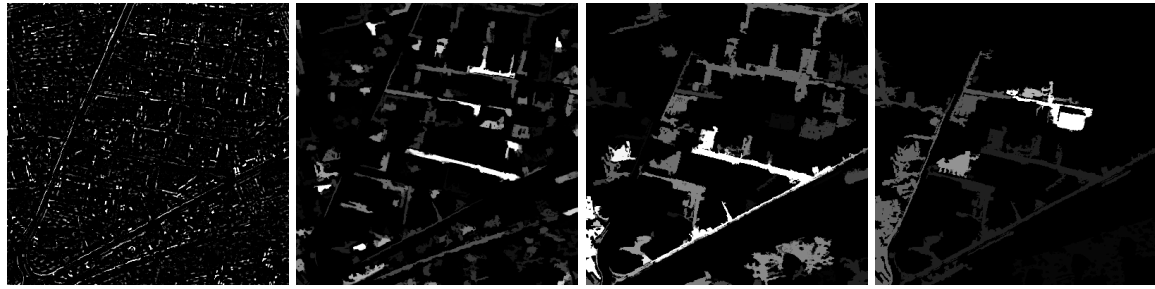
Land Cover	Data set 1		Data set 2	
	Train	Test	Train	Test
Roads	199	907	300	3068
Buildings	209	3330	300	4184
Shadow	255	853	300	1715
Vegetation	222	1030	300	4568
Total	855	6120	1200	13535

4.5.2 Results

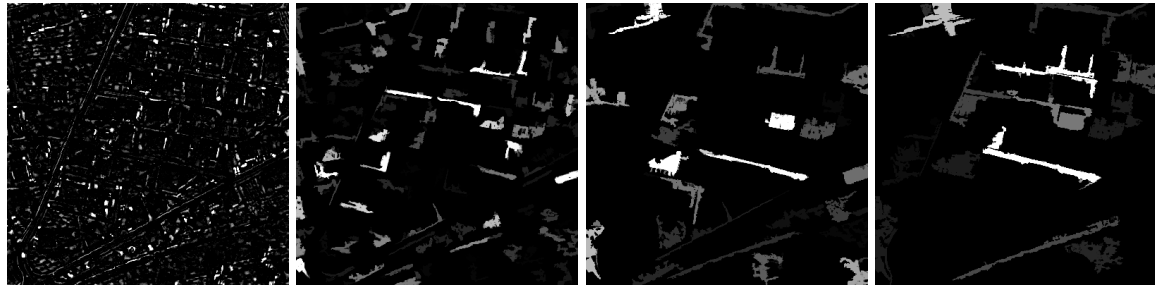
For both the images a 17-dimensional morphological profile was generated using a squared SE with size increasing in 8 steps (7, 13, 19, 25, 31, 37, 43, and 49). These values were arbitrarily chosen and since they range from 4.2 to 29.4 meters they are able to model the size of the heterogeneous objects in the scene. Three attribute profiles with the same dimensionality of the MP were also created following the approach based on the max-tree data structure. All the filtering transformations were performed on the already constructed tree in order to reduce the computational burden. For all the APs, the considered criterion was “the attribute must be greater than λ ”. Three different attributes were considered for the construction of the AP: the area, first moment of Hu, and the standard deviation. The AP with the area attribute describes the scale of the structures in the scene; it is the only increasing attribute among the three selected. In order to create the profile with the area attribute, the following values of λ were selected: 49, 169, 361, 625, 961, 1369, 1849 and 2401. Although, these values correspond to the square of the SE sizes used for creating the MP, the multi-scale analysis obtained models the scale of the objects in the scene with a different criterion with respect to the MP. The second attribute considered is the moment of inertia. The original image was filtered by progressively suppressing from the scene those regions with attribute smaller than the following increasing thresholds: 0.2, 0.3, 0.4, 0.5, 0.6, 0.7, 0.8 and 0.9. The AP based on the standard deviation attribute performs a multi-level decomposition of the objects in the scene that is not related to the geometry of the regions but models the homogeneity of the graylevels of the pixels in the regions. The profile was built according to the following reference values of the standard deviation: 10, 20, 30, 40, 50, 60, 70 and 80. As for the definition of the

SE sizes in the MP, the threshold values of λ were arbitrarily selected in order to cover the significant range of variation of the attribute for all the connected components of the image. Different analyses were carried out on the data. At first, each AP was considered separately and then, all the features extracted by the APs were taken into account simultaneously. In order to compare the behavior of the different profiles, we chose to present the derivatives of the constructed profiles (i.e., DMP and DAPs) because the differences among them are perceptually more visible than by analyzing the correspondent morphological/attribute profiles. The DMP (Figure 4.4a) is visually similar to the DAP built by evaluating the area attribute (Figure 4.4b). Many regions which are suppressed at a certain level in the DMP are present at the same level in the DAP. However, some other objects are not revealed at the same level in the two profiles but in adjacent levels. For example, the thin and elongated region in the middle of the scene that is present in the second and third image from the left (levels 3 and 5 respectively) in the DMP, in the DAP results in the third and fourth (respectively 5 and 7). These differences in the two differential profiles are mainly due to the different modeling of the concept of scale and to the choice done for the step size of the SEs and of the values of the thresholds λ , for the area attribute. In particular, the filters based on the area attribute remove the structures from the image according to their cardinality, whereas the operators by reconstruction with a square SE interact to the smallest size of each region. Thus this different behavior is particularly evident when considering elongated regions. Different conclusions can be drawn by comparing the DMP to the DAPs generated by the moment of inertia and the standard deviation. At first it is evident that at higher levels of the profiles (i.e., related to large values of λ), also regions that are spatially smaller than some others, appeared in previous levels, are present. This is due to the non-increasingness of the selected criterion.

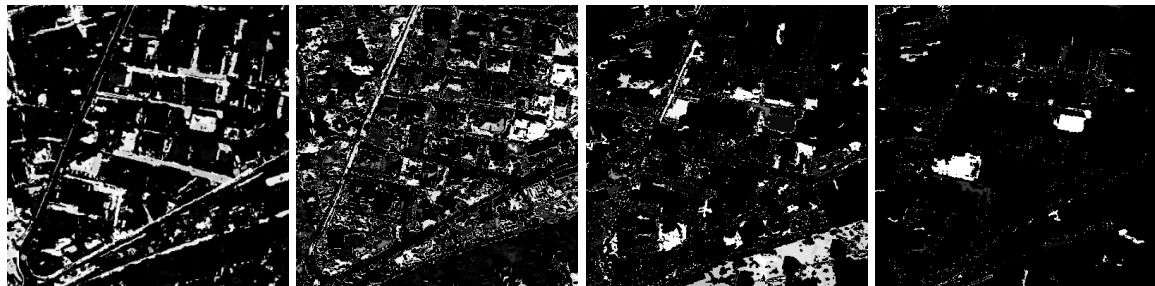
In order to quantitatively compare the capabilities of the proposed profiles in modeling the spatial characteristics of the scene we classified the original image using each profile. A random forest technique with 200 trees was used for the classification [129]. The random forest classifier is formed by an ensemble of decision tree classifiers. We chose to use this non-parametric classifier because of the high redundancy shown by the profiles that can be critical for the estimation of the statistics in classical parametric classifiers. The classification is achieved by selecting the output of the ensembles of the tree classifiers according to a majority voting. The features considered by the classifier were the panchromatic band and the generated profiles. For the definition of the split on each node in the random forest, the number of considered



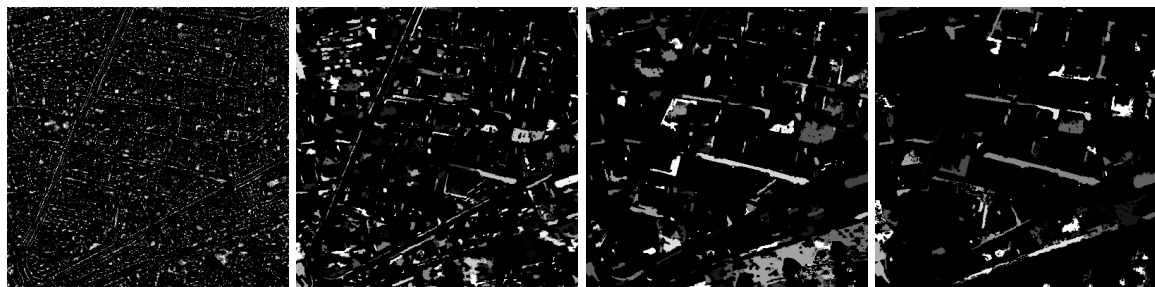
(a)



(b)



(c)



(d)

Figure 4.4: Extracts of differential profiles built on the first data set. (a) DMP created by a SE with a square shape; DAPs with (b) area attribute, (c) moment of inertia attribute, and (d) standard deviation attribute. For all the profiles the levels 1, 3, 5, and 7 are reported from left to right. All the images are stretched for visual purposes.

variables was correspondent to the square root of the number of input features. The aim of this analysis was to investigate how the accuracy (both thematic and geometric) varies when including in the analysis the knowledge gathered on the spatial domain by the profiles. In particular, the results obtained by considering the panchromatic band and a conventional MP were compared to those obtained by different APs. Table 4.2 and 4.3 show the thematic error index, in terms of percentage overall error (OE) and the kappa error (κ E) on the test set, and the five geometric error indexes. The kappa error is computed as $1-\kappa$ in percentage, with κ the kappa coefficient [130]. Furthermore, the accuracies obtained by each class are shown in Table 4.4 and 4.5. In particular, the producer and user accuracy are reported. We recall that the PA is computed, for each class, as the total number of the patterns correctly classified divided by the total number of the patterns belonging to the considered class in the reference map. The PA measures how many reference patterns are correctly classified by each class. The UA is obtained by dividing the total number of correctly classified patterns for each class by the total number of patterns classified to the same class. The UA indicates how many samples associated to a class are actually belonging to that class in the reference. More information on PA and UA can be found in [130]. In the tables, we refer to each AP as AP_{attr} , with *attr* a letter identifying the attribute (*a* area, *i* moment of inertia, *s* standard deviation). AP_{all} denotes all the APs considered together.

By analyzing the thematic accuracies reported in Table 4.2 for the original panchromatic band, one can observe that a clear increase of the accuracy is obtained by using jointly the features that model the spatial information. The accuracy achieved by considering the MP is comparable to the one obtained by the single APs with moment of inertia and standard deviation attributes. Instead, the AP constructed on the area attribute produced the highest overall error and kappa error among the profiles. This is due to the selected thresholds used for computing the filtering, which might not properly model the great variety in the scale of the objects for the considered scene. The best results according to the thematic accuracy are obtained by the joint use of the AP with moment of inertia and the AP with standard deviation attribute, which reduced the overall classification error by about 24% and the kappa error of 32%, with respect to the use of the only original panchromatic image. The improvement was about 9% in overall error and 14% in kappa error, with respect to the conventional MP. Even if the global accuracies are in general quite small, making more complex the visual interpretation of the maps, by evaluating the geometric indexes, one can see that the classification of the panchromatic

image shows a large over-segmentation error (thus, a small under-segmentation error) with respect to the maps obtained by considering the profiles. This behavior is also confirmed by a visual inspection of the classification maps shown in Figure 4.5. In fact, it is possible to observe that the classification map obtained with the panchromatic image (Figure 4.5a) is highly fragmented, whereas the other maps are more homogeneous. As best case, when considering the map obtained by the AP with moment of inertia, a reduction by about 29% and 7% in the over-segmentation and fragmentation error respectively is achieved. This effect can be noticed in the row of buildings at the top of the image. Nevertheless, the AP inertia shows a high US error which can be due to the missed recognition of the buildings on the bottom of the image and the generation of broad areas. The lowest US error among the profiles and the overall lowest ED error are achieved, by considering the AP with moment of inertia and the AP with standard deviation attribute together. Table 4.3 shows the error rates on the test set obtained by analyzing the data set 2. As for the previous data set, the thematic errors decrease when considering the spatial information provided by the profiles. Also in this case, the results obtained by considering a single AP are similar to those generated by the MP (this is also clear from the classification maps in Figure 4.6). In this experiment the AP built on the area attribute results in a thematic error only slightly smaller than the one of the original panchromatic image (about 4% in both overall and kappa errors). However, as confirmed by the map, the geometrical errors are similar with those obtained by considering the other profiles. Again, the highest thematic accuracy is obtained when considering the APs with moment of inertia and standard deviation attributes. The thematic errors are reduced by about 28% in the overall error and 38% in kappa errors with respect to the original panchromatic image and by about 12% and 17% (overall and kappa errors) against the conventional MP. As for the first data set better accuracies are obtained by considering only the AP with moment of inertia and the AP with standard deviation attribute than considering together also the AP with area attribute. This can be due to the increase in the dimensionality of the feature space given by considering also the AP with area attribute, which makes the analysis more complex (i.e., Hughes phenomenon) without providing enough additional independent information than to the other APs. However, one should observe that the selection of the threshold values λ_s affects the capability of the computed profile in modeling the spatial features of the objects. Thus, an AP with different threshold values for the area attribute might provide features which are more discriminant. In addition, also the geometry of the reference objects is globally more

Table 4.2: Errors obtained by classifying the panchromatic image along with morphological/attribute profiles for data set 1.

Features	Thematic Error Index			Geometric Error Indexes			
	OE (%)	κ E (%)	OS (%)	US (%)	ED (%)	FG (%)	SH (%)
PAN	46.5	63.9	40.6	21.9	61.9	18.8	18.7
MP	32.4	45.9	12.8	51.4	66.5	12.7	15.0
AP _a	46.9	54.2	15.3	46.5	62.5	15.3	18.2
AP _i	33.6	41.5	11.7	55.9	69.0	11.6	12.8
AP _s	33.0	47.7	13.8	51.2	66.7	13.7	13.8
AP _i + AP _s	23.0	32.4	13.4	46.8	61.9	13.4	16.1
AP _{all}	30.5	37.9	13.2	43.6	62.9	13.2	16.9

Table 4.3: Errors obtained by classifying the panchromatic image along with morphological/attribute profiles for data set 2.

Features	Thematic Error Index			Geometric Error Indexes			
	OE (%)	κ E (%)	OS (%)	US (%)	ED (%)	FG (%)	SH (%)
PAN	56.2	77.2	60.8	16.6	71.4	23.0	16.6
MP	39.9	56.4	44.8	18.1	50.9	3.4	15.0
AP _a	52.4	73.4	44.3	12.7	61.7	13.9	15.7
AP _i	40.5	56.8	15.8	71.4	82.9	4.9	20.9
AP _s	41.1	57.9	34.6	52.0	70.7	11.0	15.8
AP _i + AP _s	28.1	39.1	27.0	44.2	62.4	10.3	16.4
AP _{all}	28.3	39.4	27.7	46.3	64.9	15.2	15.5

precisely preserved by the AP with moment of inertia and AP with standard deviation attribute considered together in comparison to the other single profiles. In particular, the over-segmentation error in the map obtained by considering all the APs decreases of about 34% and 18% compared to that of the map generated by the only panchromatic image and by the MP, respectively. This can be observed as a more uniform classification of the vegetated areas in the middle of the image and of some roads. As for data set 1, the AP inertia shows small US and FG errors but high US error, which can be due to the presence of large areas associated to the Vegetation class.

By considering Table 4.4 and 4.5, it is possible to make a detailed class-by-class analysis by considering the producer accuracy (PA) and user accuracy (UA) obtained. The two results for both the data sets

Table 4.4: Class specific Producer Accuracy (PA) and User Accuracy (UA) obtained by classifying the panchromatic image along with morphological/attribute profiles for data set 1. The best accuracies obtained are marked in bold.

Features	Road		Building		Shadow		Vegetation	
	PA (%)	UA (%)						
PAN	29.5	62.1	76.1	42.4	94.0	97.1	32.0	45.7
MP	31.6	73.5	90.7	55.1	92.5	97.4	74.0	78.5
AP _a	33.1	77.2	71.0	33.2	92.5	97.4	39.6	59.8
AP _i	41.1	76.6	93.9	49.7	87.6	97.5	51.3	85.6
AP _s	32.4	87.8	90.7	46.5	94.3	97.1	85.8	90.0
AP _i + AP _s	96.6	45.6	62.5	96.8	98.0	94.7	89.1	79.0
AP _{all}	41.8	89.5	93.4	51.0	92.2	97.4	62.7	88.9

Table 4.5: Class specific Producer Accuracy (PA) and User Accuracy (UA) obtained by classifying the panchromatic image along with morphological/attribute profiles for data set 2. The best accuracies obtained are marked in bold.

Features	Road		Building		Shadow		Vegetation	
	PA (%)	UA (%)						
PAN	39.8	47.7	34.0	29.3	85.8	90.3	38.1	37.0
MP	60.2	22.6	67.2	52.7	88.6	94.3	49.8	79.3
AP _a	60.4	40.7	33.4	25.1	89.4	93.4	38.9	55.7
AP _i	87.4	69.5	56.9	11.6	87.1	92.2	45.8	84.4
AP _s	68.0	15.1	51.5	71.1	86.6	94.1	56.1	64.1
AP _i + AP _s	69.2	91.1	66.5	69.8	93.2	86.7	70.6	60.1
AP _{all}	92.2	69.9	70.8	60.1	88.1	93.8	59.0	75.2

are analyzed together in order to observe trends in the obtained results. Focusing the attention on the specific thematic classes, we can underline as, with respect to the other attributes, the AP with moment of inertia performed well in identifying the roads, in particular for data set 2. However, for both data sets, the best results were obtained by considering all the APs. When considering the Building class, the conventional MP, the AP with standard deviation attribute and the AP with all the attributes performed the best and gave comparable results. For this particular class, good results were also obtained by the AP with moment of inertia but only in data set 1. The class Shadow was globally well classified by all the profiles and no particular trend in the results was noticed. Finally, the vegetated areas were extracted well by the AP with the standard deviation attribute especially in data set 1. The MP and the AP with moment of inertia and the one with all the attributes also reached similar results.

4.6 CONCLUSION

In this chapter attribute profiles have been introduced for classification of very high resolution remote sensing images and differential attribute profiles have been proposed and formally defined. The motivation of this work relies on the need to improve the flexibility, the capability of modeling different kind of objects, and the computational load associated with the widely used conventional morphological profiles and their derivative.

Attribute profiles can be used for extracting information from the spatial domain by reducing the limitations of the morphological profiles. This approach allows one to analyze the original image in a multi-level fashion by the application of a sequence of morphological attribute operators. These operators are adaptive morphological connected filters, which include in their general definition also opening and closing by reconstruction. Attribute filters are flexible tools that enable to analyze an image not only on the basis of the scale of the structures (as for operators by reconstruction), but also according to other measures/attributes computed on the regions. Thus, it is possible to perform a multi-level analysis of the scene by exploiting measures related to many different geometric primitives (e.g., shape), the graylevel of the pixels, or any other parameter that can be computed on the regions. We propose to compute the attribute profiles according to an effective implementation based on the max-tree, i.e., an efficient representation of the data, which leads to a reduction of the computational load of about one order of magnitude with respect to morphological profiles. The proposed technique was applied to two very high resolution

panchromatic images acquired by Quickbird satellite on the city of Trento, Italy. Three attribute profiles, based on different attributes, were extracted from the panchromatic band. We considered i) the area (which is related to the MP created with a squared SE); ii) the moment of inertia (which is a descriptor of the geometry of a region invariant to the scale); and iii) the standard deviation of the graylevels of the pixels (which measures the homogeneity of the regions). The data were classified by a random forest classifier. The obtained maps were evaluated by checking their thematic accuracy and the geometric precision in representing some reference objects in the scene. The results pointed out the effectiveness of the proposed APs, which involved a sharply higher thematic and geometric accuracy with respect to considering the only panchromatic band. Moreover, the profiles built on different attributes led to similar results in terms of accuracy but also conveyed different and complementary information into the classification process. In fact, the joint use of the three attribute profiles in the classification tasks resulted in a decrease of the classification kappa errors up to 38% and 17% with respect to the only panchromatic image and to the MP, respectively. The obtained classification maps are also more precise in the representation of the geometry of the regions as proven by the geometrical error indexes.

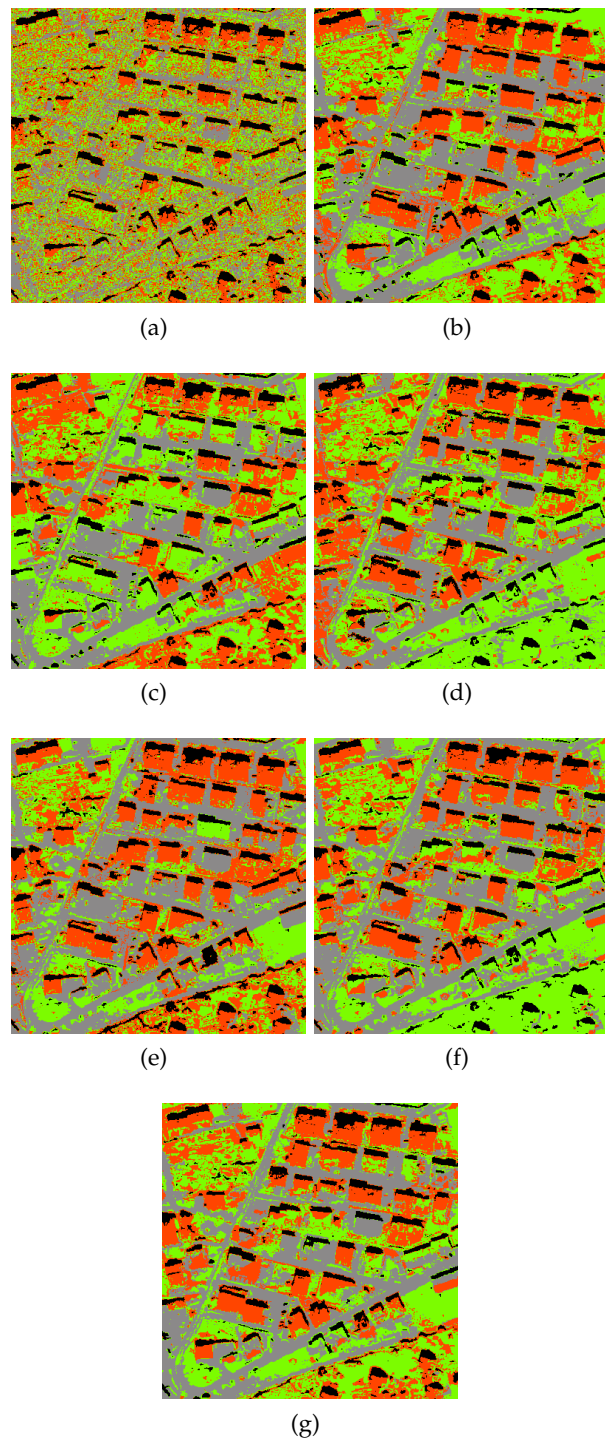


Figure 4.5: Data set 1. Classification maps obtained by: (a) panchromatic image only; (b) MP; (c) AP_{a_i} ; (d) AP_{i_i} ; (e) AP_{s_i} ; (f) $AP_{i_i} + AP_{s_i}$; and (g) AP_{all} . Thematic classes: ■ road, ■ building, ■ shadow, ■ vegetation.

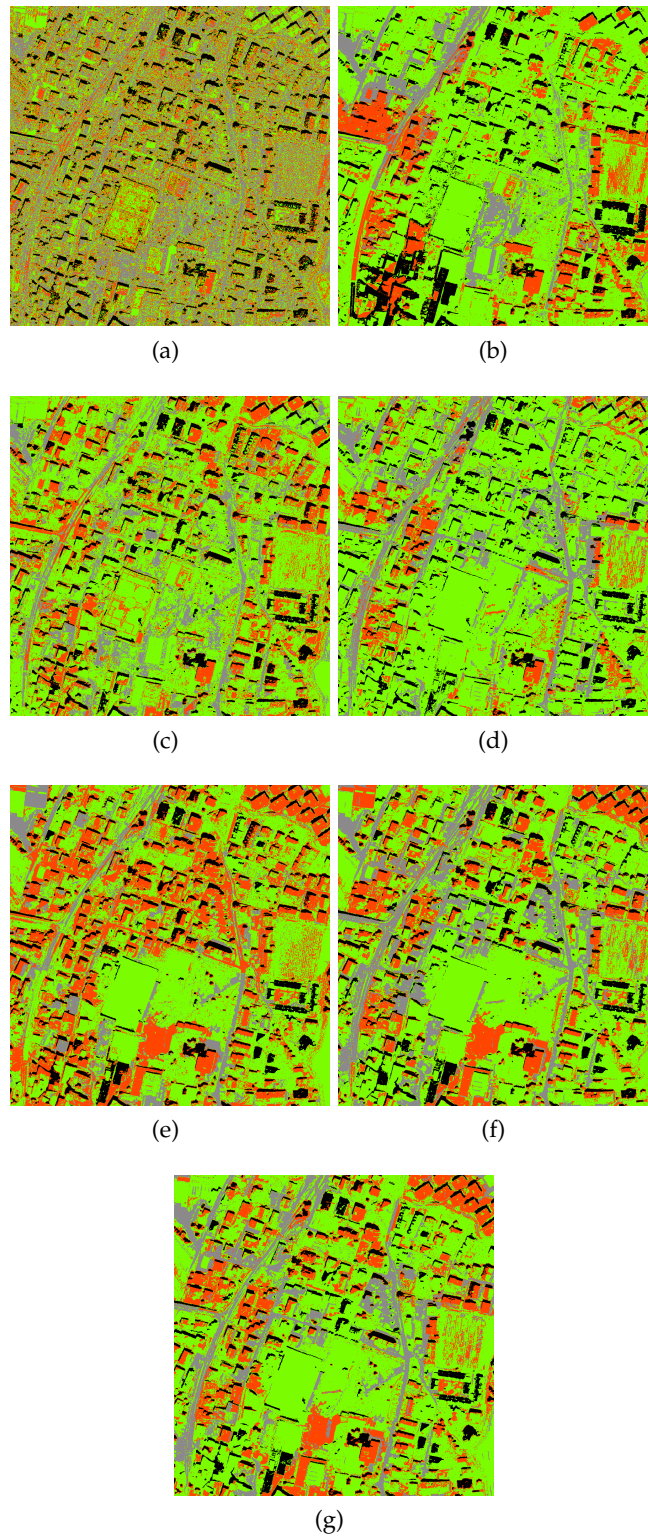


Figure 4.6: Data set 2. Classification maps obtained by: (a) panchromatic image only; (b) MP; (c) AP_{a_i} ; (d) AP_{i_i} ; (e) AP_{s_i} ; (f) $AP_i + AP_{s_i}$; and (g) AP_{all} . Thematic classes: ■ road, ■ building, ■ shadow, ■ vegetation.

Abstract. In this chapter an extension of the attribute profile concept suitable for handling hyperspectral images is presented. The issues related to the extension of morphological operators for the analysis of multitone images is briefly presented along with a review of solutions appeared in the literature. The definition of Extended Attribute Profile and Extended Multi-Attribute Profile is then given. Finally the results obtained by employing the proposed techniques for the classification of two hyperspectral images are reported.

5.1 INTRODUCTION

When dealing with hyperspectral data, the spectral values of the pixels carry important information and it must be taken into account in the data analysis (see [110] for a review of the main techniques for hyperspectral image processing). Along with the spectral response of the pixels, if the geometrical resolution is high, the characteristics of the objects in the spatial domain are also informative. In this scenario, the extension of mathematical morphology tools (e.g., MPs) to multi-valued data is not straightforward since an ordering relation between the elements of this set of data is not natively defined (i.e., there is no ordering relation between vectors). In [115], this issue was addressed by reducing the original dimensionality of the hyperspectral data by computing the MP on each of the first principal components (i.e., scalar images) extracted from the data by the Principal Component Analysis. The definition of the EMP and a review of works based on the EMP can be found in 3.3.1 and 3.3.2, respectively.

In this chapter, Extended Attribute Profiles (EAPs) and Extended Multi-Attribute Profiles (EMAPs) are presented for the analysis of hyperspectral high resolution images. These extended profiles are based on morphological attribute filters and, through a multi-level analysis, are capable to extract spatial features that can better model the spatial information, with respect to conventional extended morphological pro-

This chapter was published in:

M. Dalla Mura, J. A. Benediktsson, B. Waske, and L. Bruzzone, "Extended profiles with morphological attribute filters for the analysis of hyperspectral data," *International Journal of Remote Sensing*, vol. 31, no. 22, pp. 5975–5991, Nov. 2010.

files. The features extracted by the proposed extended profiles were considered for a classification task. Two hyperspectral high resolution data sets acquired on the city of Pavia, Italy, were considered in the analysis. The effectiveness of the introduced operators in modeling the spatial information was proved by the higher classification accuracies obtained with respect to those achieved by a conventional extended morphological profile.

We propose the definition of the Extended Attribute Profile and Extended Multi-Attribute Profile which rely on the application of the APs to hyperspectral data and to a straightforward further extension to a multi-attribute scenario, respectively. The proposed operators can also be considered as an extension of EMPs since an AP includes in its definition the MP. The proposed techniques were applied to the classification of two high resolution hyperspectral data sets acquired on the city of Pavia, Italy. The morphological features extracted were classified by a random forest classifier.

5.2 PROBLEM OF EXTENDING THE MORPHOLOGICAL OPERATORS TO MULTI-TONE IMAGES

The extension of the concept of a morphological profile from the analysis of single-tone images to multi-tone images (e.g., multispectral and hyperspectral imagery) is certainly a non trivial task because the extension of the morphological operators for scalar to multivariate values is an ill-posed problem. In fact, the output of a generic morphological operator processing an image, is usually the result of a function computed on an ordered set of values (e.g., the infimum for erosion, the median for the median filter, the supremum for dilation, etc.). When dealing with scalar images, the ordering of the values mapped by the image $f(p) \rightarrow k$, with $p \in E$ and $k \in \{0, \dots, K\} \subset \mathbb{Z}$, is well defined. The scalar elements in the partially ordered set $\{0, \dots, K\}$ have an unique infimum and supremum. Thus, the morphological operators are well defined. In contrast, when the image destination domain becomes a subset of a multivariate domain, e.g., $f(p) \rightarrow \mathbf{k}$, $\mathbf{k} \in \mathbb{Z}^n$ the ordering relation between the mapped vectorial values is not defined anymore. For this reason, the direct application of concepts seen in previous sections to multi- or hyperspectral images is not possible.

In order to overcome this issue several solutions have been presented in the literature. One possible approach relies on the arbitrary re-definition of the concepts of morphological filters for handling multi-valued images by forcing an ordering relation on the vectorial set of values. In in [118], Plaza *et al.* proposed a reduced vector

ordering scheme based on the spectral purity index of the pixel vectors. The input vectors are ordered according to a spectral-based distance measure (i.e., scalar value). Three distance measures commonly used in hyperspectral analysis were considered: i) spectral angle distance (SAD); ii) spectral information divergence (SID); and iii) hidden Markov model-based information divergence (HMMID). Having defined an ordering relation between vectorial values, the definitions of the morphological operators of opening and closing by reconstruction computed according to this ordering relation can be applied to the hyperspectral data. A reader who is interested in greater details on the extensions of the mathematical morphology concept to multi-valued images can refer to [131, 132, 133, 134].

Another approach for extending morphological transformations to vectorial data deals at first with the reduction of the hyperspectral data to only one (or few) channels and subsequently to the application of the morphological operators to each obtained image separately.

The reduction of the dimensionality can be done by means of several techniques. The first work based on this approach considered Principal Component Analysis (PCA) as feature reduction technique [120, 115] (see Sec. 3.3.2 for details). In [120] Independent Component Analysis was used. Kernel PCA (KPCA) was exploited in [121, 135]. In [136] the reduction of the dimensionality was performed by PCA, KPCA, Non-parametric Weighted Feature Extraction (NWFE), Decision Boundary Feature Extraction (DBFE) and Bhattacharyya Distance Feature Selection (BDFS) techniques [2].

5.3 EXTENDED PROFILES WITH ATTRIBUTE FILTERS

Analogously to the definition of EMPs, we can compute the APs (as defined in 4.4) on the c principal components extracted from the original hyperspectral data. This leads to the definition of the Extended Attribute Profile:

$$\text{EAP} = \{\text{AP}(\text{PC}_1), \text{AP}(\text{PC}_2), \dots, \text{AP}(\text{PC}_c)\}. \quad (5.1)$$

A scheme of the EAP is reported in Figure 5.1. We remind the reader that the EAP includes in its definition the EMP (because the operators by reconstruction can be viewed as a particular set of morphological attribute filters) and, thus, it can be considered as its generalization. The main advantage in using the EAP instead of the EMP relies on the great flexibility given by the definition of the attributes used in the processing for modeling the spatial features that need to be extracted. Moreover, the computation of the filters on the max-tree structure reduces the computational complexity with respect to the

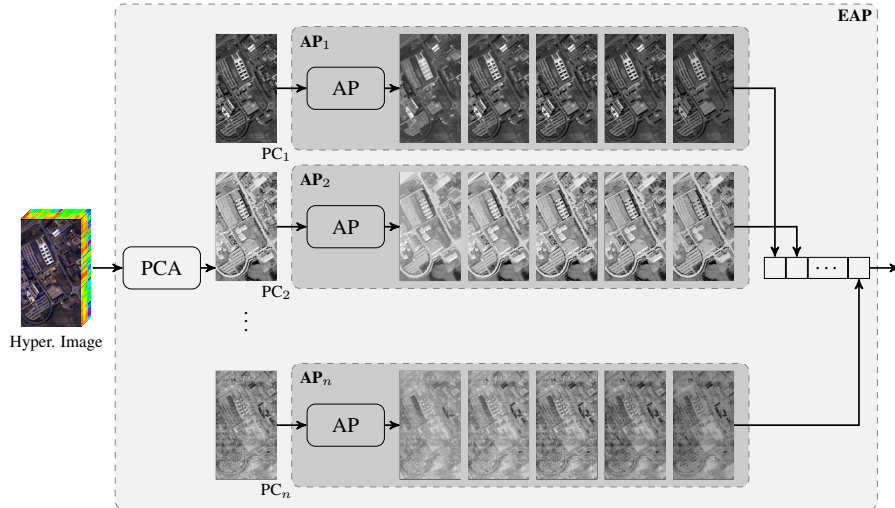


Figure 5.1: Architecture for computing an Extended Attribute Profile.

EMP because the tree (both max- and min-) is built once for each principal component and filtered multiple times according to the required number of levels. Samples of EAPs created on different attributes are presented in Figure 5.2. From the figure it is possible to notice how the thickening and thinning transformations computed with different attributes process the original images in different ways. In particular, one can observe how the profiles built with the area and the length of the diagonal attributes perform differently even if both the attributes are increasing. When considering the EAP with moment of inertia, it is possible to observe how the effect of the filtering is significantly different from those of the other EAPs. In this profile the elongated structures are revealed. The profile with standard deviation attribute also performs differently from the others. For example, one can see that the processing preserves some small regions of high contrast which are instead erased in the other attributes.

Moreover, since APs created by different attributes to extract different information from the scene, the idea of EAP is further evolved to Extended Multi-Attribute Profile EMAP. The EMAP merges different EAPs in a single data structure. A EMAP composed by m different EAPs can be easily formulated as

$$\text{EMAP} = \{ \text{EAP}_{a_1}, \text{EAP}'_{a_2}, \dots, \text{EAP}'_{a_m} \} \quad (5.2)$$

with a_i a generic attribute and $\text{EAP}' = \text{EAP} \setminus \{ \text{PC}_1, \dots, \text{PC}_c \}$. The latter relation is necessary for avoiding the multiple presence of the c principal components (we remind that $\text{AP}_{a_1,i}(f) = \text{AP}_{a_2,i}(f) = \dots = \text{AP}_{a_m,i}(f) = f$ for the level $i = n + 1$). The computation of the EMAP structure is shown in Figure 5.3.

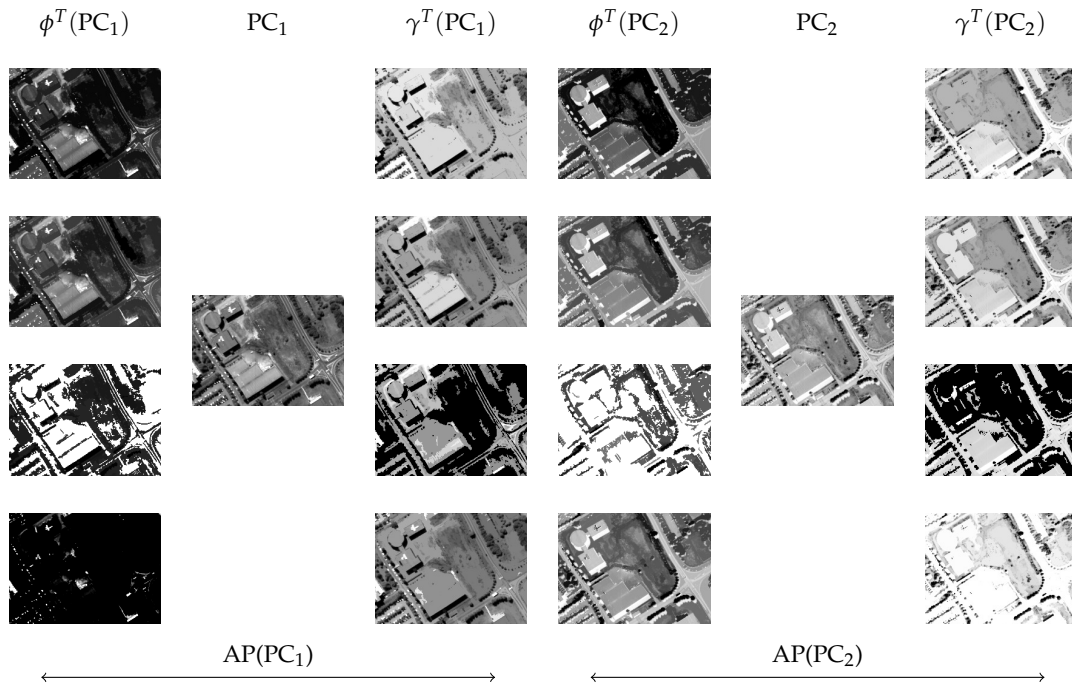


Figure 5.2: Examples of EAPs computed on the first two PCs of a portion of the University data set. Each row shows an EAP built by different attributes. Attributes, starting from the first row, are: area, length of the diagonal of the bounding box, moment of inertia and standard deviation. Each EAP is composed by the concatenation of two APs computed on PC_1 and PC_2 . Each AP is made up of three levels, a thickening image ϕ^T , the original PC and a thinning image γ^T . All the thickening and thinning transformations were computed with the following attributes value, λ s: Area: 5000; Length of the diagonal: 100; Moment of inertia: 0.5; Standard deviation: 50.

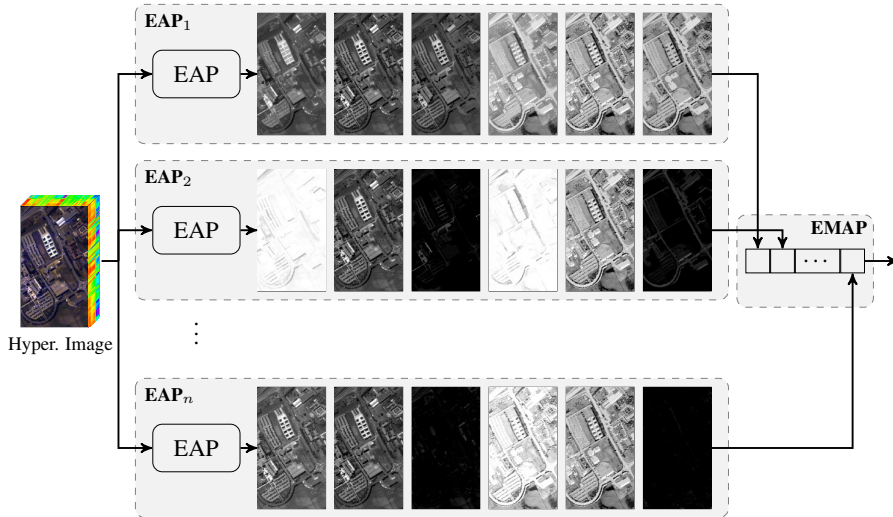


Figure 5.3: Architecture for computing an Extended Multi-Attribute Profile.

It is clear that, although the EMAP leads to an increase in the dimensionality of the features, it gains greater capabilities in extracting spatial information with respect to a single EAP. Moreover, the load in the computation required by an EMAP is slightly greater than the one of a single EAP, since the max- and min-tree are computed only once for each PCs and they are filtered with different attributes at different levels.

5.4 EXPERIMENTAL RESULTS

5.4.1 Data set Description

The experiments were carried out on two widely used data sets acquired on the city of Pavia, Italy (for a review of works carried out on this images refer to [137]). The surveyed scenes are urban areas, one set was acquired on a portion of the city centre while the other shows the University area. The data were acquired by the hyperspectral airborne sensor ROSIS-03 (Reflective Optics Systems Imaging Spectrometer). The sensor acquired 115 spectral bands ranging from $0,43\mu m$ to $0,86\mu m$ and the geometrical resolution of the images is 1.3 m. The considered data were atmospherically corrected but not geometrically (e.g., it is possible to notice the geometrical distortions due to the displacement of the airborne platform during the acquisition). The first data set, which represents the highly dense city centre (in the following referred as Centre), is a 1096×489 pixels portion of the original imaged scene. For this data set, 102 bands out of the 115 were considered due to

noise. Nine thematic classes were considered: Water, Tree, Meadow, Self-blocking Bricks, Soil, Asphalt, Bitumen, Tile, and Shadow. The image acquired over the University area is composed by 103 bands (12 bands were removed due to noise) of 610×340 pixels. Nine thematic classes were identified in this scene: Trees, Asphalt, Bitumen, Gravel, Metal sheets, Shadows, Self-blocking Bricks, Meadows, and Bare soil. The train and test sets for the two data sets are described in Table 5.1. The true color images and the related reference maps are shown in Figure 5.4.

5.4.2 Experimental Set Up

For the three data sets, the first four principal components were initially considered in the analysis in order to explain more than the 99% of the total variance of the multivariate original data. Table 5.2 reports the values of variance and cumulative variance accounted by the PCs for each data set.

An EMP with 4 levels (i.e., leading to a stack of 36 features, 9 for each PC) was computed with a disk-shaped SE of radius increased with a step size of 2. Four attributes were considered in the analysis:

1. a , area of the regions;
2. d , diagonal of the box bounding the region (as the area, it is a measure of the size of the regions);
3. i , first moment invariant of Hu, or moment of inertia (it measures the elongation of the regions), [138];
4. s , standard deviation of the gray-level values of the pixels in the regions (index related to the homogeneity of the regions).

For each attribute an EAP was computed. Below the values of the λ used in the filtering are reported:

1. $EAP_a: \lambda_a = [100 \ 500 \ 1000 \ 5000]$;
2. $EAP_d: \lambda_d = [10 \ 25 \ 50 \ 100]$;
3. $EAP_i: \lambda_i = [0.2 \ 0.3 \ 0.4 \ 0.5]$;
4. $EAP_s: \lambda_s = [20 \ 30 \ 40 \ 50]$.

The features obtained by the computation of the four EAPs were also used for creating an EMAP, thus, based on EAP_a , EAP_d , EAP_n and EAP_s .

The original PCs and the extended profiles were analyzed by a Random Forest (RF) classifier. A RF is an ensemble of decision trees

[129]. In the learning phase of the classifier, each decision tree is trained with a bootstrapped portion of the training set (the samples left out are used for an internal measure of accuracy, called out-of-bag) and selecting a fraction of the available features for defining the split of each node of the tree. The classification of a pattern is achieved by predicting the class label by each tree in the forest and associating the pattern to the class that gathers most of the votes. In the experiments carried out, a RF was composed of an ensemble of 100 trees, which in preliminary experiments showed to be a good trade-off between the accuracy in modeling the problem and the time needed for the learning phase. The number of variables (i.e., features) involved in the training of the classifier was set to the square root of the number of input variables, as suggested by Breiman as default value in [129]. The accuracy of the obtained results was assessed according to the available test sets by measuring the Overall Accuracy (OA), the Average Accuracy (AA) (which is computed as the average of the Producer Accuracies) and the Kappa coefficient (K). In order to avoid redundancy in the next subsections, only the OA will be taken discussed. However, the results for AA and K are reported in the Tables.

5.4.3 Results with Extended Profiles

The results obtained by the analysis carried out on the two data sets proved that the inclusion of features that model the spatial information (e.g., those computed by extended profiles) can significantly improve the classification accuracies (up to 21.9% for the University data set) with respect to considering only the spectral information given by the PCs. For this reason the results obtained by the PCs alone are reported but they will not be further discussed.

For the Centre data set analogous conclusions can be drawn. In general, the results obtained by all the experimental configurations were very good (OA ranging from 96.6% to 98.83%). However, the best accuracies were obtained by the EMAP (see Table 5.3). The gain with respect to the single PCs and the EMP was about 2.2% and 0.6%. It is possible to notice how the accuracies obtained by the EMP are similar to those obtained by the EAPs.

In comparison to the Centre data set, different results were obtained for the University data set (Table 5.4). The EAP built by the area attribute performed the best for the University data set, with a relative increase of OA of about 2.4% and 11.6% as compared to the EMAP and EMP, respectively. The other EAPs performed similarly to the EMP ($\sim \pm 5\%$) and worse than the EMAP in terms of accuracies (at

minimum -3% obtained by the EAP_d). The motivation of the worst performance of the EMAP with respect to the EAP_a can be due to the great difference of the dimensionality of the features generated by the two operators (36 for the EAP versus 132 for the EMAP).

Tables 5.5 and 5.6 report the class specific accuracies (Producer and User Accuracy) for the three data sets.

Details of the classification maps obtained for the two datasets are shown in Figure 5.7 and 5.6. Although it is not possible to clearly indicate which types of objects in the scene benefits of the use of a specific attribute in the classified images, it is clear that the information extracted by the EAPs leads to an overall increase in the precision of the maps.

5.4.4 Results with a Reduced Number of PCs

In order to better investigate the behavior of extended profiles in extracting informative features, we carried out some experiments with a reduced number of PCs. Tables 5.7 and 5.8 report the results in terms of OA, AA and Kappa coefficient, respectively, for the extended profiles computed on the first 3, 2 and 1 PCs. The most notable trend in all the experiments is the steep increase in the accuracy when considering only the first PC and the first two PCs. Concerning the relative overall accuracies obtained by the different extended profiles we can state that for the centre data sets, the EMAP performed always the best in terms of accuracies, except when considering the first two PCs where the best results were obtained by EAP_s (-0.31%) for the Centre data set.

When considering the University data set, by decreasing the number of considered PCs a trend in the difference of OA between the EAP_a and the EMAP is noticed. The improvement in OA of the EAP_a over the EMAP is 2.4% with four PCs (see Section 5.4.3). This difference decreases with the reduction of the number of PCs. In contrast, when considering only one PC the OA obtained by the EMAP exceeds the one of EAP_a by 7.8%.

From this set of experiments, it is possible to conclude that a reduced number of PCs (i.e., with a reduced number of features generated by the profiles) the EMAP outperforms the other extended profiles, in terms of overall accuracies.

5.5 CONCLUSION

In this chapter extended attribute profiles and extended multi-attribute profiles have been proposed for the analysis of high resolution hy-

perspectral images. The introduced extended profiles are based on morphological attribute filters, which have already proven their suitability to the analysis of high resolution images. In particular, this work aims at exploiting the great flexibility in defining the attributes (and thus, in modeling the features related to the chosen attributes) which is provided by this set of morphological operators.

The extended profiles proposed in this work follow the architecture of the previously proposed extended morphological profiles. In greater detail, the attribute filters are applied to a subset of the first principal components extracted from the original data and then concatenated into a single data structure. Extended attribute profiles are based on a multi-level analysis of the principal components based on a single attribute. In contrast, the extended multi-attribute profiles take into account multiple attributes. On the one hand, this leads to an increase in the dimensionality of the extracted features; on the other this results in a greater and more precise modeling of the spatial features.

The proposed techniques were applied to two high resolution hyperspectral images acquired over the city of Pavia, Italy. The data sets represent a portion of the dense urban centre of the city and an university area. Four attributes were considered in the analysis, leading to the generation of four correspondent extended attribute profiles: i) area; ii) diagonal of the bounding box; iii) moment of inertia; and iv) standard deviation. The obtained profiles were also combined together in an extended multi-attribute profile. The features extracted by the extended profiles were considered for classification by a random forest classifier. The single principal components and the features generated by a conventional extended morphological profile were considered for comparison. From the obtained results, it is possible to make the observation that the proposed extended profiles led to better classification accuracies than those generated by both the principal components alone and the extended morphological profile. This result can be explained by the better capability of the extended profiles based on attribute filters in describing spatial features than the conventional approach based on the extended morphological profile. By analyzing the results obtained by the proposed extended profiles it is possible to notice that the classification of multiple attributes achieved the best accuracies for the data set of the centre. Conversely, on the university data set, the extended attribute profile with area attribute outperformed the others. This can be due to the significant increase in the dimensionality of the features generated by the EMAP with respect to the single EAPs, which may affect the generalization capabilities of the classifier.

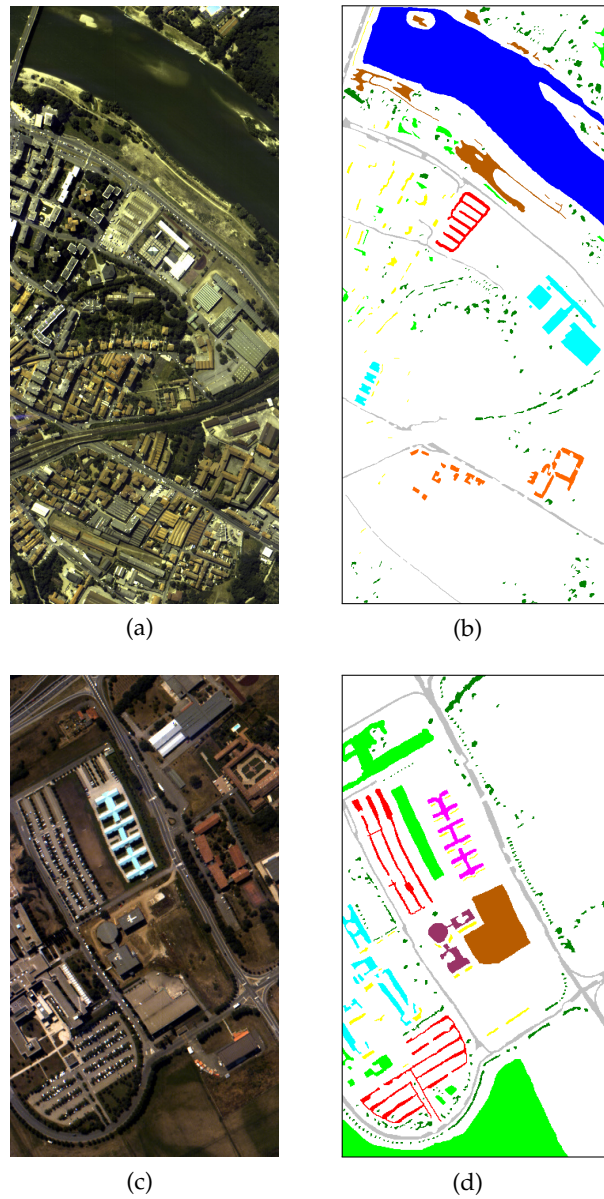


Figure 5.4: True color images and maps of the test sets for the (a)-(b) Centre, (c)-(d) University data sets.

Thematic classes for the Centre: ■ water, ■ trees, ■ asphalt, ■ self-blocking bricks, ■ bitumen, ■ tiles, ■ shadows, ■ meadows, ■ bare soil.

Thematic classes for the University: ■ trees, ■ asphalt, ■ bitumen, ■ gravel, ■ metal sheets, ■ shadows, ■ meadows, ■ self-blocking bricks, ■ bare soil.

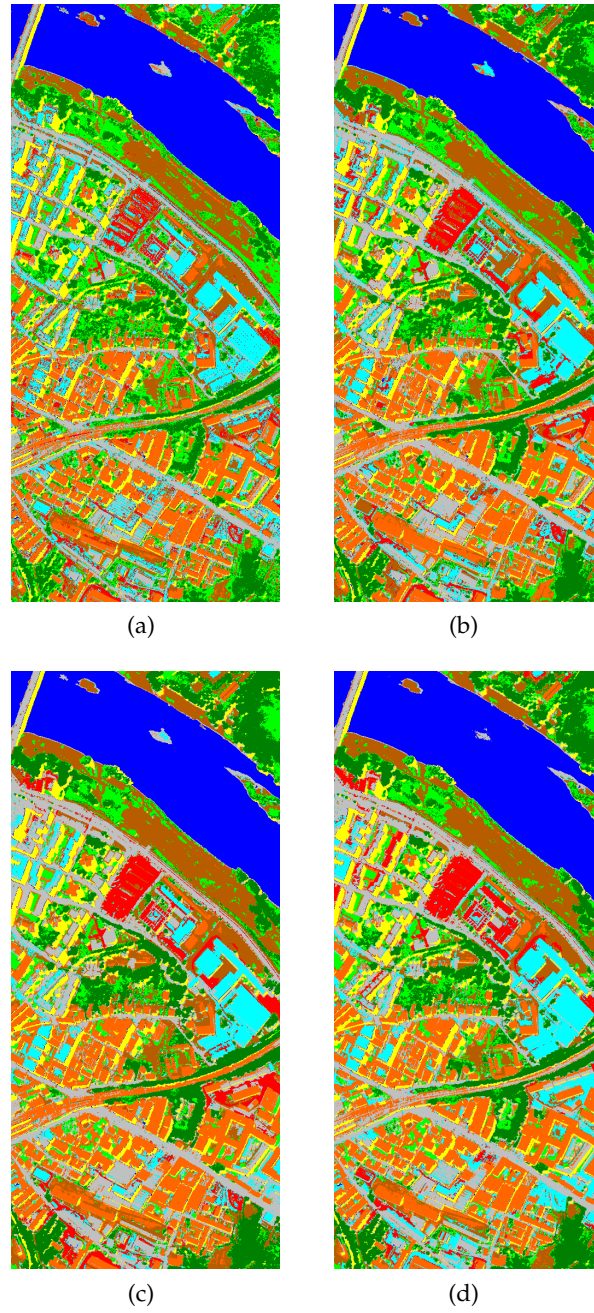


Figure 5.5: Centre data set. Classification maps obtained by: (a) the PCs, (b) the EMP, (c) the EAP_a , and (d) the EMAP.

Thematic classes: ■ water, ■ trees, ■ asphalt, ■ self-blocking briks, ■ bitumen, ■ tiles, ■ shadows, ■ meadows, ■ bare soil.

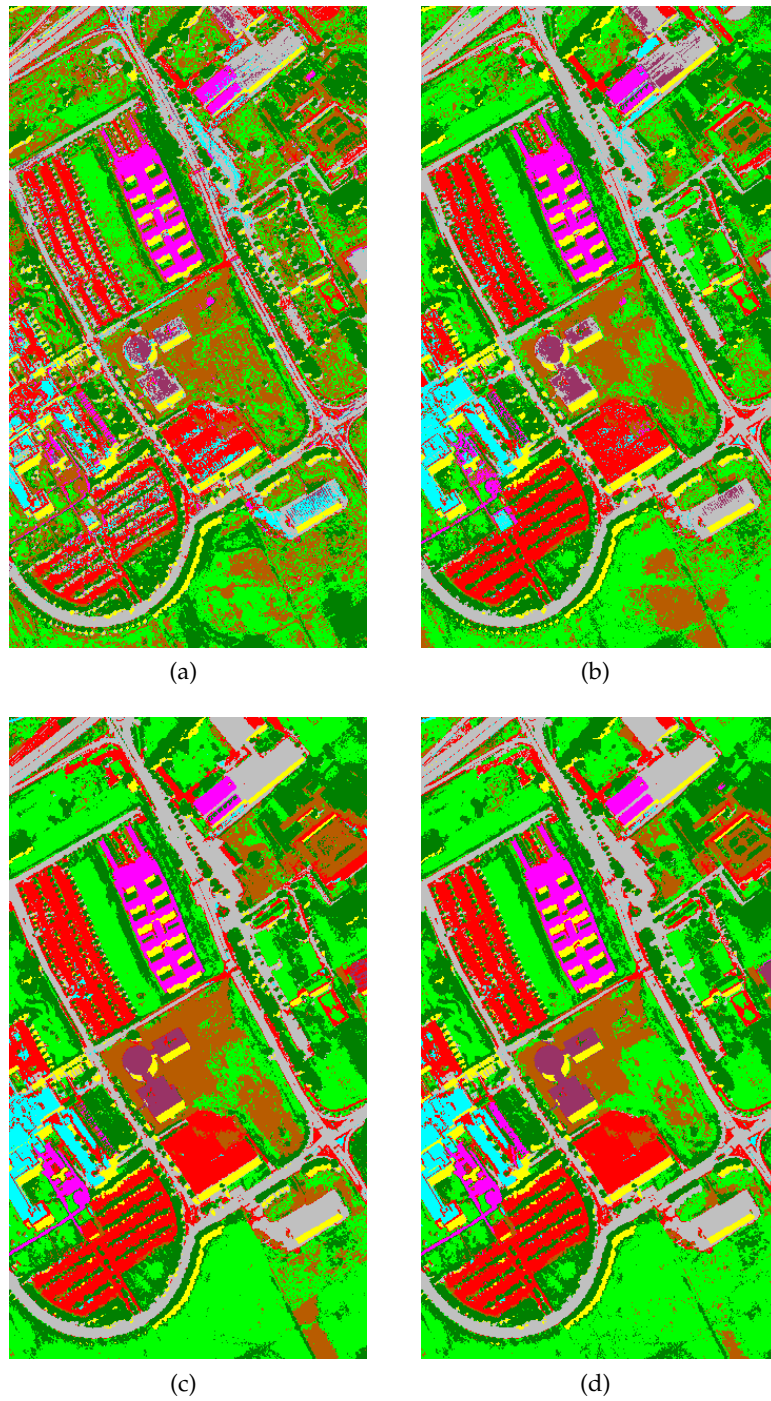


Figure 5.6: University data set. Classification maps obtained by: (a) the PCs, (b) the EMP, (c) the EAP_a , and (d) the EMAP.

Thematic classes: ■ trees, ■ asphalt, ■ bitumen, ■ gravel, ■ metal sheets, ■ shadows, ■ meadows, ■ self-blocking bricks, ■ bare soil.

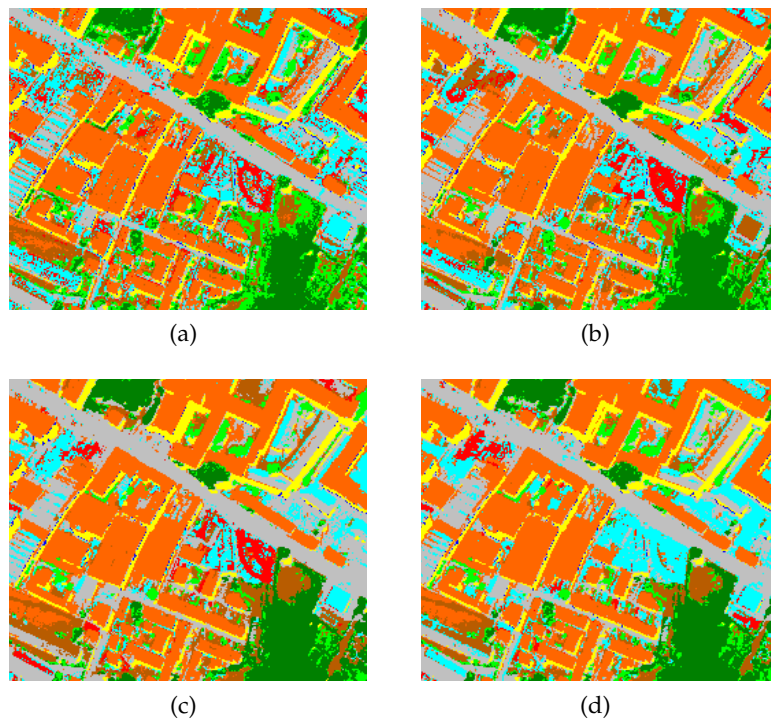


Figure 5.7: Centre data set. Details of the classification maps 5.7 obtained by: (a) the PCs, (b) the EMP, (c) the EAP_a , and (d) the EMAP.

Thematic classes: water, trees, asphalt, self-blocking bricks, bitumen, tiles, shadows, meadows, bare soil.

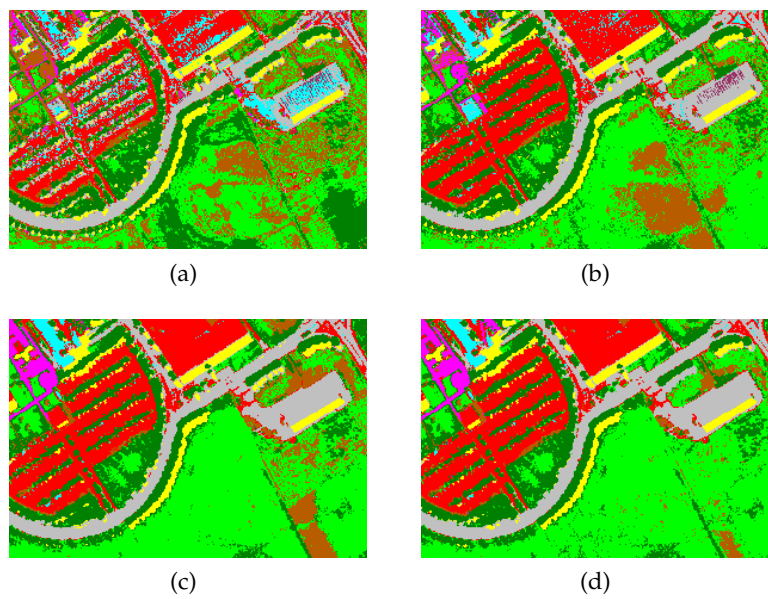


Figure 5.8: University data set. Details of the classification maps in 5.6 obtained by: (a) the PCs, (b) the EMP, (c) the $EAP_{a'}$, and (d) the EMAP.

Thematic classes: ■ trees, ■ asphalt, ■ bitumen, ■ gravel, ■ metal sheets, ■ shadows, ■ meadows, ■ self-blocking bricks, ■ bare soil.

Table 5.1: Number of samples per class for the train and test sets for the Centre and University data sets.

Class	Centre		University	
	Train	Test	Train	Test
Water	745	65278	-	-
Trees	785	6508	524	3064
Meadow	797	2905	540	18649
Metal sheets	-	-	265	1345
Gravel	-	-	392	2099
Bricks	485	2140	514	3682
Bare Soil	820	6549	532	5029
Asphalt	678	7585	548	6631
Bitumen	808	7287	375	1330
Tiles	223	3122	-	-
Shadow	195	2165	231	947
Total	5536	103539	3921	42776

Table 5.2: Variance and Cumulative Variance in percentage explained by each principal component for Centre and University data sets.

	Centre		University	
	Var	Cum. Var.	Var	Cum. Var.
PC ₁	68.15	68.15	58.32	58.32
PC ₂	28.70	96.86	36.10	94.42
PC ₃	2.28	99.14	4.44	98.86
PC ₄	0.32	99.46	0.30	99.16

Table 5.3: Centre data set: Overall Accuracy (OA), Average Accuracy (AA) and Kappa value of the obtained results. The best accuracies obtained are marked in bold.

	PCs	EMP	EAP _a	EAP _d	EAP _n	EAP _s	EMAP
Features	4	36	36	36	36	36	132
OA (%)	96.60	98.27	98.37	98.04	97.97	98.77	98.83
AA (%)	93.24	97.66	97.91	96.74	96.43	97.58	98.02
Kappa	0.94	0.97	0.97	0.97	0.97	0.98	0.98

Table 5.4: University data set: Overall Accuracy (OA), Average Accuracy (AA) and Kappa value of the obtained results. The best accuracies obtained are marked in bold.

	PCs	EMP	EAP _a	EAP _d	EAP _n	EAP _s	EMAP
Features	4	36	36	36	36	36	132
OA (%)	70.42	80.71	92.32	86.84	76.24	78.68	89.89
AA (%)	79.25	86.64	92.00	88.00	84.68	86.27	90.25
Kappa	0.63	0.75	0.90	0.82	0.70	0.73	0.87

Table 5.5: Centre data set: Class specific Producer Accuracy (PA) and User Accuracy (UA) of the obtained results. The best accuracies obtained are marked in bold.

	PCs		EMP		EAP _a		EAP _d		EAP _n		EAP _s		EMAP	
	PA	UA	PA	UA	PA	UA	PA	UA	PA	UA	PA	UA	PA	UA
Water	98.83	100.00	98.87	100.00	98.87	100.00	98.89	100.00	98.86	100.00	100.00	100.00	99.59	100.00
Trees	88.60	97.42	93.53	97.81	91.50	97.54	92.09	97.07	94.15	97.24	90.07	97.94	91.43	97.69
Meadow	94.60	77.19	95.18	86.70	94.60	83.37	93.60	84.49	94.18	86.77	95.59	80.99	94.94	83.55
Bricks	76.17	80.93	97.43	98.63	99.39	99.39	92.06	99.04	88.50	96.68	99.25	99.48	99.30	99.58
Bare Soil	95.02	94.45	99.73	99.50	99.77	99.88	99.68	98.40	98.98	96.52	99.73	99.91	99.79	99.91
Asphalt	93.43	90.70	97.17	96.26	99.71	90.29	97.94	89.00	97.21	92.45	99.26	94.61	99.39	94.26
Bitumen	92.95	89.57	97.19	92.25	97.46	98.11	96.57	97.64	96.24	97.91	94.41	99.26	97.80	99.65
Tiles	99.65	91.50	99.90	91.44	99.94	99.49	99.90	95.88	99.81	87.19	99.90	99.97	99.97	99.21
Shadow	99.91	100.00	99.91	100.00	99.95	100.00	99.95	100.00	99.91	100.00	100.00	100.00	99.95	100.00

Table 5.6: University data set: Class specific Producer Accuracy (PA) and User Accuracy (UA) of the obtained results. The best accuracies obtained are marked in bold.

	PCs		EMP		EAP _t		EAP _d		EAP _n		EAP _s		EMAP	
	PA	UA	PA	UA	PA	UA	PA	UA	PA	UA	PA	UA	PA	UA
Asphalt	77.54	91.49	91.84	96.18	94.60	99.90	93.27	99.74	91.28	98.94	93.49	99.41	94.60	99.75
Meadow	57.50	90.19	72.66	89.34	95.60	92.94	90.99	86.59	66.16	86.44	70.27	86.94	93.82	89.56
Gravel	49.74	60.45	70.84	88.46	67.65	95.75	65.51	92.41	53.36	87.43	61.79	90.19	67.84	96.35
Trees	99.05	51.39	99.28	71.83	98.96	79.14	99.41	68.63	99.31	51.58	98.17	45.51	99.15	73.86
Metal sheets	99.33	93.75	99.55	97.67	99.41	100.00	99.26	100.00	99.63	98.24	98.74	85.24	98.96	99.48
Bare soil	74.49	41.57	67.29	45.67	73.39	97.03	47.35	85.19	58.66	45.00	56.53	58.31	59.30	94.58
Bitumen	69.40	63.18	82.03	96.98	99.77	100.00	98.42	98.72	99.85	99.92	99.92	100.00	100.00	100.00
Bricks	88.08	67.65	98.07	79.91	98.72	79.37	97.80	77.61	95.19	69.83	97.94	76.72	98.56	79.24
Shadow	98.10	98.62	98.20	99.36	99.89	99.27	100.00	98.85	98.63	99.89	99.58	98.74	100.00	98.85

Table 5.7: Centre data set: Overall Accuracy (OA), Average Accuracy (AA) and Kappa value obtained by considering a reduced number of PCs. The best accuracies obtained are marked in bold.

		PCs	EMP	EAP _a	EAP _d	EAP _n	EAP _s	EMAP
OA (%)	PC ₁₋₃	95.99	97.92	98.47	98.16	97.95	98.81	98.96
	PC ₁₋₂	93.57	96.81	97.95	97.44	97.78	98.57	98.26
	PC ₁	51.48	66.41	88.57	86.79	91.36	93.37	94.24
AA (%)	PC ₁₋₃	91.89	96.42	98.26	97.34	96.64	97.61	98.45
	PC ₁₋₂	85.87	94.17	97.31	96.00	96.19	97.03	97.72
	PC ₁	41.97	61.25	80.46	70.49	79.88	85.71	88.46
Kappa	PC ₁₋₃	0.93	0.96	0.97	0.97	0.97	0.98	0.98
	PC ₁₋₂	0.89	0.95	0.97	0.96	0.96	0.98	0.97
	PC ₁	0.35	0.52	0.81	0.77	0.85	0.89	0.90

Table 5.8: University data set: Overall Accuracy (OA), Average Accuracy (AA) and Kappa value obtained by considering a reduced number of PCs. The best accuracies obtained are marked in bold.

		PCs	EMP	EAP _a	EAP _d	EAP _n	EAP _s	EMAP
OA (%)	PC ₁₋₃	64.94	76.62	90.54	79.66	73.22	75.99	88.77
	PC ₁₋₂	61.17	72.69	88.18	80.31	71.04	81.25	86.96
	PC ₁	38.73	46.21	55.34	48.62	44.80	48.23	63.16
AA (%)	PC ₁₋₃	75.44	86.73	91.03	86.04	83.43	85.31	90.43
	PC ₁₋₂	72.21	83.86	88.16	85.94	81.43	85.34	88.23
	PC ₁	50.57	64.08	69.08	64.52	60.52	65.82	73.20
Kappa	PC ₁₋₃	0.57	0.71	0.87	0.74	0.67	0.70	0.85
	PC ₁₋₂	0.53	0.66	0.84	0.75	0.64	0.76	0.83
	PC ₁	0.26	0.37	0.47	0.38	0.34	0.39	0.55

TECHNIQUES BASED ON EXTENDED ATTRIBUTE PROFILES AND DIMENSIONALITY REDUCTION TRANSFORMATIONS

Abstract. In this chapter the role of dimensionality reduction transformations in the computation of the extended attribute profile is investigated. Two techniques are presented for the classification of hyperspectral images. The first technique is based on the computation of the EAPs on the features extracted by Independent Component Analysis. The second technique combines feature extraction transformations on the EAPs. Each technique is presented in a separate section of this chapter.

6.1 CLASSIFICATION OF HYPERSPECTRAL IMAGES BY USING EAPS AND ICA

6.1.1 Introduction

In this section, a technique based on Independent Component Analysis (ICA) and extended morphological attribute profiles is presented for the classification of hyperspectral images. The ICA maps the data into a subspace in which the components are as independent as possible. Attribute profiles, which are extracted by using several attributes, are applied to each image associated with an extracted independent component, leading to a set of extended attribute profiles. Two approaches are presented for including the computed profiles in the analysis. The features extracted by the morphological processing are then classi-

Parts of this chapter were published in:

M. Dalla Mura, A. Villa, J. A. Benediktsson, J. Chanussot, and L. Bruzzone, "Classification of hyperspectral images by using morphological attribute filters and independent component analysis," in *Proc. 2nd Workshop on Hyperspectral Image and Signal Processing: Evolution in Remote Sensing*, Reykjavik, Iceland, 14–16 June 2010.

—, "Classification of hyperspectral images by using extended morphological attribute profiles and independent component analysis," *IEEE Geoscience and Remote Sensing Letters*, vol. 8, no. 3, pp. 541–545, 2010.

M. Dalla Mura, J. Benediktsson, and L. Bruzzone, "Classification of hyperspectral images with extended attribute profiles and feature extraction techniques," in *2010 IEEE International Geoscience and Remote Sensing Symposium (IGARSS)*, 2010, pp. 76–79.

fied with an SVM. The experiments carried out on two hyperspectral images proved the effectiveness of the proposed technique.

6.1.2 Independent Component Analysis

Hyperspectral sensors record images with hundreds of bands and a very high spectral resolution. The very detailed spectral description provided by these kind of images increases the capability to distinguish between land cover classes, thus achieving accurate classification maps. However, the analysis of this huge amount of data presents some methodological issues which need to be addressed. In particular, the high dimensionality of the data is a critical problem, due to the appearance of the Hughes phenomenon: after a certain threshold, if the number of features increases, the generalization capability of the classifier decreases when a fixed number of training samples is used. The threshold mainly depends on the number of samples used to train the classifier. Because of these reasons, feature reduction is often applied as a pre-processing step before the classification of hyperspectral data, in order to avoid the curse of dimensionality, and to reduce the computation time. Although it is not optimal for classification, the PCA is often used for such a task, due to its simplicity and ease of use. The principle of PCA is to project the data into an orthogonal space, so that the eigenvectors correspondent to the greatest eigenvalues retain the maximum variance of the data. Because the PCA is based on the analysis of covariance matrix and second order statistics, it can neglect some important information, especially when few components are retained. In this section, we propose to use ICA for feature reduction, as an effective alternative to PCA. ICA consists of finding a linear decomposition of the observed data into statistically independent components. Given an observation model: $\mathbf{x} = \mathbf{A}\mathbf{s}$ where \mathbf{x} is the vector of the observed signals, \mathbf{A} is a matrix of scalars corresponding to the mixing coefficient and \mathbf{s} is the vector of the source signals, the ICA finds a separating matrix \mathbf{W} such that $\mathbf{y} = \mathbf{W}\mathbf{x} = \mathbf{W}\mathbf{A}\mathbf{s}$, where \mathbf{y} is a vector of independent components (ICs).

Independence is a much stronger assumption than the decorrelation, which can be obtained with PCA or Factor Analysis (FA). In ICA, the concept of independence can be summarized as follows: Each component should not provide any information about higher (than second) order statistics of the other components. However, there are several methods for estimating ICA. In this section we have used the algorithm Joint Approximate Diagonalization of Eigen-matrices (JADE), due to good results shown when used for feature reduction in hyperspectral remote sensing data [139]. Due to space constraints we

refer the reader interested in more details about the general framework of ICA to [140].

6.1.3 Approaches to Deal with Multiple EAPs

The choice of the most suitable attribute and range of thresholding values (λ_s) for extracting the information on the geospatial objects is certainly a complex task, especially when *a priori* information on the scene is not available. A possible approach attempting to overcome this issue relies on the computation of EAPs with different kinds of attributes. However, this leads to the problem of properly exploiting, in the analysis, the different information extracted by the computed EAPs.

A simple strategy is the *Stacked Vector Approach* (SVA), which combines the EAPs by concatenating them in a single vector of features (also called *Extended Multi-Attribute Profile*, EMAP [92]), see Fig. 6.1a. However, even if complementary information can be extracted by considering different attributes, a great redundancy is present in the features extracted. Thus, it is advisable that a classification algorithm with excellent penalization capability is used for classifying the features in order to handle the increased dimensionality which can lead to the Hughes phenomenon.

Another approach is the *Fusion Approach* (FA) that is based on the separate classification of each EAP and on the fusion of the results obtained by the independent classifiers in order to generate the final decision map, see Fig. 6.1b. In comparison to the SVA, the FA keeps low the dimensionality of the data and increases the robustness of the results, especially if the different EAPs generate complementary errors.

An SVM classifier is considered with the *One Against One* (OAO) multiclass strategy. The fusion rule considered when combining the results of the single classifiers relies on the sum the votes of the classifiers applied to the four MPs, assigning each pixel to a class, according to the majority voting scheme. Obviously, other decision criteria can be applied.

6.1.4 Experimental Results

The experimental analysis was carried out on two hyperspectral images acquired over the city of Pavia (Italy) by the ROSIS-03 hyperspectral sensor. Details on the two images can be found in Sec. 5.4.1. In the following we will refer to the two data sets as “University” and “Centre” respectively.

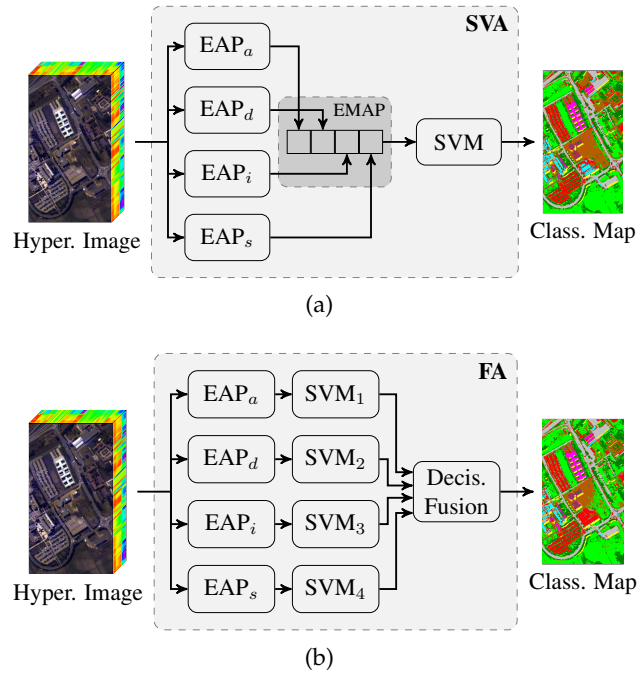


Figure 6.1: Proposed approaches for dealing with multiple EAPs. (a) Stacked Vector Approach (SVA) and (b) Fusion Approach (FA).

In the analysis carried out, all the samples of the training set were used for the University data set while for the Centre data sets, for each class, only 50 samples (randomly chosen from the global 5536 samples available as training) were considered. All the experiments conducted on the latter data set were run ten times with a set of different training samples each time.

From both the two hyperspectral images four components extracted by PCA and ICA were considered. The first four PCs contain more than 99% of the total variance of the data for both the data sets. The components were rescaled to the range $[0,1000]$ and converted to integer in order to be processed by the attribute filters. Four EAPs were computed by considering four different attributes on the components extracted by PCA and ICA: i) a , area of the regions ($\lambda_a = [100 \ 500 \ 1000 \ 5000]$); ii) d , length of the diagonal of the box bounding the region ($\lambda_d = [10 \ 25 \ 50 \ 100]$); iii) i , first moment invariant of Hu, moment of inertia [138] ($\lambda_i = [0.2 \ 0.3 \ 0.4 \ 0.5]$); and iv) s , standard deviation of the gray-level values of the pixels in the regions ($\lambda_s = [20 \ 30 \ 40 \ 50]$). The area and the length of the diagonal of the bounding box extract information on the scale of the objects. The moment of inertia and the standard deviation are not dependent on the size dimension but they are related to the geometry of the objects and the homogeneity of the intensity values of the pixels, respectively. Each

EAP is 36-dimensional, i.e., it is composed of four APs with 9 levels computed on each component extracted. In the sequel, the notation EAP_{attr} denotes the EAP built with the *attr* attribute. The classification maps are obtained by analyzing the features extracted by the extended profiles with an SVM classifier with RBF kernel. The model selection in the training phase of the classifier was based on a gradient descent method, which proved to be computationally less demanding than the exhaustive investigation of the parameters on a grid approach, giving comparable results [141].

The thematic accuracies of the obtained maps (which are presented in Tables 6.1 and 6.2) were assessed by computing the Overall Accuracy (OA), the Average Accuracy (AA) and the Kappa coefficient (K) on the available reference data. The statistical significance of the classification maps obtained by PCA and ICA and the same morphological processing was evaluated with the McNemar's test. All the results were statistically significant.

The obtained results are reported in Table 6.1. It is clear as, in most of the cases, by including the features extracted by the EAPs in the analysis resulted in higher accuracies (up almost 17% of OA) than those obtained by considering only the spectral features. The ICA proved to extract more informative components from the data, leading to better results than those generated by the PCA in all the experiments. When considering the contribution of the single EAPs, the EAPs built with area and the moment of inertia attributes performed the best with the PCA and ICA, respectively. This proves how it can be difficult to select *a priori* the most suitable attribute on the data. In these experiments, considering all the EAPs together, in the SVA architecture, with the ICA gives excellent results in terms of classification accuracies. As far as we know, these accuracies are higher than all those reported in the literature for this data set without post-processing [122, 65]. In contrast, the SVA approach led to low accuracies for the PCA. This can be due to the high variation in terms of accuracy showed by the single EAPs (more than 20% of OA), which affects the overall performances of this approach. The FA is performing well in average and has a robust behavior since in all the experiments the accuracies obtained, when compared to those of the single EAPs, are slightly lower than the best case (less than 2% of OA) and better than all the others. The improved accuracies obtained by the proposed technique are also confirmed by the higher precision shown in the map obtained when considering the ICA and all the EAPs together (see Fig. 6.2c).

Table 6.2 reports the thematic accuracies obtained on the Centre data set (the correspondent classification maps are not reported for space constraints). Similar considerations as for the University data set can

be drawn. For this data set also, it is evident the importance of including the spatial information, which led to an increase in terms of accuracy with respect to considering the original hyperspectral data or the components obtained from the dimensionality reduction technique. The best overall accuracy obtained by using the EAPs, is higher of about 2% than those obtained by the original spectral features and the first components. Considering the PCA and ICA transformations, the latter leads to the best results in most of the cases (except for the single components extracted and for the EAP_s). When looking at the performances obtained by considering the spatial features extracted by the EAPs, one can see that the EAP with area attribute outperformed the other single EAPs with PCA, while when considering the ICA the choice of the standard deviation performed the best among the single EAPs. Moreover, when considering the SVA strategy resulted in the best accuracies with the ICA preprocessing (which is slightly worse than the best EAP). Again, the FA led to results over the average of the accuracies obtained by the single EAPs.

Table 6.1: University data set. Classification accuracies obtained by classifying the hyperspectral image (Spect.), the four components extracted (4 Comp.), each single EAP, and the data with the proposed approaches: Stacked Vector Approach (SVA) and Fusion Approach (FA).

	Spect.	4 Comp.	EAP_a	EAP_d	EAP_i	EAP_s	SVA	FA
Feat.	103	4	36	36	36	36	144	(144)
Principal Component Analysis								
OA (%)	77.89	72.92	90.00	85.42	69.80	86.56	77.81	89.21
κ (%)	72.34	66.25	87.06	81.24	63.22	82.82	71.08	86.06
AA (%)	85.78	81.55	92.04	89.55	82.48	91.15	86.84	92.04
Independent Component Analysis								
OA (%)	77.89	74.64	91.26	87.94	93.57	87.69	94.47	91.69
κ (%)	72.34	68.22	88.55	84.31	91.63	84.14	92.80	89.13
AA (%)	85.78	77.18	92.36	91.72	95.73	90.92	96.58	94.11

Table 6.2: Centre data set. Classification accuracies obtained by classifying the hyperspectral image (Spect.), the four components extracted (4 Comp.), each single EAP, and the data with the proposed approaches: Stacked Vector Approach (SVA) and Fusion Approach (FA). The results reported are the average of the accuracies obtained in 10 trials with 50 training samples per class randomly chosen for each trial.

	Spect.	4 Comp.	EAP _a	EAP _d	EAP _i	EAP _s	SVA	FA
Feat.	102	4	36	36	36	36	144	(144)
Principal Component Analysis								
OA (%)	96.25	96.24	98.40	97.83	97.81	98.48	98.43	98.39
κ (%)	93.59	93.56	97.26	96.27	96.24	97.39	97.31	97.24
AA (%)	92.80	92.65	97.18	96.18	96.23	96.93	97.26	97.21
Independent Component Analysis								
OA (%)	96.25	96.47	98.59	98.18	97.91	97.97	98.69	98.47
κ (%)	93.59	93.94	97.58	96.87	96.42	96.51	97.75	97.38
AA (%)	92.80	92.39	97.50	96.76	96.15	96.18	97.58	97.26

6.1.5 Conclusion

In this section we have presented a technique based on independent component analysis and attribute profiles for the classification of hyperspectral images. In greater details, from the hyperspectral image some independent components are extracted, and different attribute profiles are computed for each one, leading to extended attribute profiles. The features obtained by the morphological processing are then classified with an SVM classifier. We proposed two approaches for considering the features extracted by the different EAPs, one based on the concatenation of the EAPs and one based on the fusion of the classification results obtained on the single EAPs.

The experimental analysis was carried out on two well-known hyperspectral images acquired on the city of Pavia (Italy). The results obtained on these data sets proved that the preprocessing of the hyperspectral data carried out with ICA is more suitable than the PCA for modeling the different sources of information present in the scene. Moreover, from the experiments and results, it was evident how important the spatial features extracted by the EAPs are for classification. The concatenation of the different EAPs gave excellent results in terms of classification accuracies (with respect to other works present in

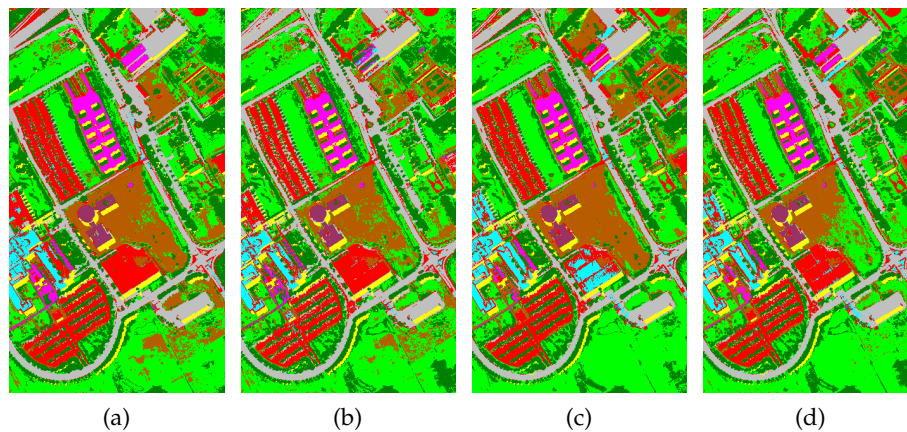


Figure 6.2: ROSIS Pavia University data set. Classification maps obtained by: (a) PCA with area attribute (EAP_a), (b) PCA with FA, (c) ICA with SVA, and (d) ICA with FA.

Thematic classes: ■ trees, ■ asphalt, ■ bitumen, ■ gravel, ■ metal sheets, ■ shadows, ■ meadows, ■ self-blocking bricks, ■ bare soil.

the literature on these data sets). This approach did not perform well only in one case with the PCA, i.e., when the single EAPs led to results significantly different one to the other (range of difference in the overall accuracies greater than 20%). However, this effect did not occur with the ICA, where the obtained results were more uniform and all statistical significant (according to the McNemar's test). The approach based on the fusion of the classification results with the majority voting strategy proved to have a robust behavior leading to accuracies slightly lower than those of the best case obtained with a single EAPs but better than all the others.

6.2 CLASSIFICATION OF HYPERSPECTRAL IMAGES WITH EAPS AND FEATURE EXTRACTION TECHNIQUES

6.2.1 Introduction

In this section we investigate the combined use of morphological attribute filters and feature extraction techniques for the classification of a high resolution hyperspectral image. Although the exploitation of the features extracted by the profiles already proved to improve the accuracies in a classification task [91, 92, 72, 115], the profiles in general increase significantly the dimensionality of the data being analyzed. This effect is further increased when considering multiple APs/EAPs built on different attributes in order to provide richer descriptions of

the spatial information contained in the scene. Furthermore, the information contained in a profile is, in general, intrinsically redundant (e.g., adjacent levels in a profiles can differ one to the other only by few regions in the whole image). The increase in the dimensionality and the high redundancy can be an issue, especially if a classifier non robust to the Hughes phenomenon is considered. The reduction of the dimensionality of the data performed with FE techniques suitable for classification proved to increase the classification accuracies when considering MPs and EMPs. Thus, this approach becomes very interesting when applied to EAPs especially when multiple attributes are considered.

In this section we investigate the classification of HR hyperspectral images based on extended attribute profiles and feature extraction techniques. In particular, extended attribute profiles are computed on the hyperspectral image with different attributes. Subsequently, the dimensionality of the generated profiles is reduced by FE. Three technique have been considered for FE: Discriminant Analysis Feature Extraction (DAFE), Decision Boundary Feature Extraction (DBFE) and Non-Weighted Feature Extraction (NWFE). The feature extracted were considered by two classifiers: Maximum Likelihood (ML) and Random Forest (RF) classifiers.

6.2.2 Feature Extraction Techniques

Three well known feature extraction techniques are considered: DAFE, DBFE and NWFE.

The technique of DAFE performs the Fisher discriminant analysis [2], which is a linear projection of the multivariate data on the $C - 1$ orthogonal directions that are the most discriminant for the C Gaussian distributions estimated on the thematic classes in the image. If the number of features is less than the number of classes, then the number of features becomes the maximum number of discriminant components that can be extracted. The most discriminant features are found as those which maximize a separability criterion $J = tr(\Sigma_W^{-1}\Sigma_B)$ where Σ_W denotes the within-scatter matrix which gives a measure of the overlapping of the different distributions and Σ_B the between-scatter matrix which indicates the separability of the means of the distributions.

The DBFE technique [2], in contrast to DAFE, does not take into account the statistics of the class distributions, since it is based only on the analysis of the boundary that separates the different classes. In greater detail, discriminant features in the DBFE are extracted as directions orthogonal to the decision boundary. However, DBFE is

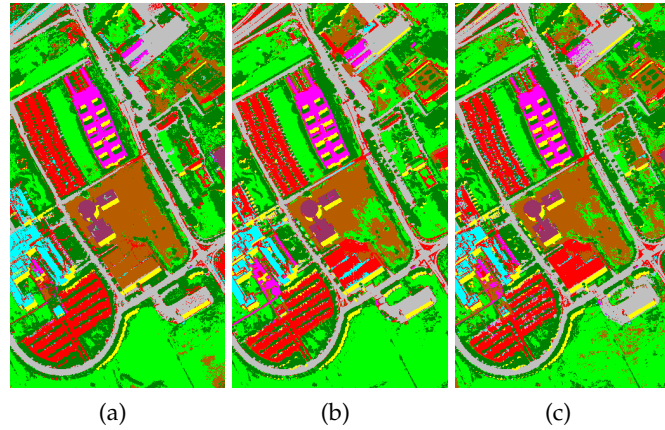


Figure 6.3: ROSIS data set, University of Pavia: Classification maps obtained with RF classifier and EAP_{all} with (a) DAFE; (b) DBFE; (c) NWFE. Thematic classes: ■ asphalt, ■ meadows, ■ gravel, ■ trees, ■ metal sheets, ■ bare soil, ■ bitumen, ■ bricks, ■ shadows.

affected when few training samples are available in the analysis.

The NWFE technique [2] was proposed in order to overcome the limitations of DBFE. NWFE is similar to the DAFE technique but it is based on the estimation of local means (obtained by weighting each sample according to its distance to the decision boundary) and on non-parametric between- and within-scatter matrices.

6.2.3 Experimental Results

The data set considered in the experiments is a 610×340 pixels high resolution hyperspectral image acquired by the airborne sensor ROSIS-03 on the University campus of the city of Pavia (see Sec 5.4.1).

From the hyperspectral data four PCs were considered for the analysis in order to explain more than the 99% of the total variance of the data. Subsequently, four EAPs were computed with different attributes: i) a , area of the regions; ii) d , length of the diagonal of the box bounding the region; iii) i , moment of inertia, [91]; and iv) s , standard deviation of the gray-level values of the pixels in the regions. The area and the length of the diagonal of the bounding box are increasing attributes that are useful to perform a multi-scale analysis of the data. The moment of inertia attribute is also a purely geometric descriptor that measures the elongation of the regions. However, since it is scale invariant, it is not increasing and can be employed for extracting information on the geometry of the regions regardless their scale. Finally, the standard deviation attribute measures the homogeneity of the

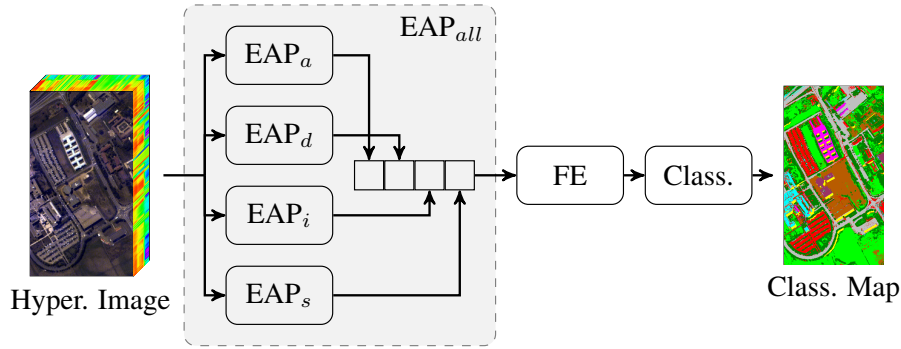


Figure 6.4: Representation of the proposed processing scheme when analyzing all the EAPs together (EAP_{all}).

intensity values of the pixels belonging to each region in the image and thus gives information that is not related to the geometry of the regions but, is dependent on the spectral contrast of the pixels. Four reference values, λ in Eq. (5.1), were considered for building each of the four EAPs, leading to 36-dimensional profiles (composed by four APs of 9 levels computed on the PCs). The λ s values considered are the following: i) EAP_a , $\lambda_a = [100 \ 500 \ 1000 \ 5000]$; ii) EAP_d , $\lambda_d = [10 \ 25 \ 50 \ 100]$; iii) EAP_i , $\lambda_i = [0.2 \ 0.3 \ 0.4 \ 0.5]$; iv) EAP_s , $\lambda_s = [20 \ 30 \ 40 \ 50]$. The concatenation of the four EAPs in a single vector was denoted as EAP_{all} . The feature extraction techniques DAFE, DBFE and NWEF were applied to each of the profiles considered. The estimation of the covariance matrices of the probability density functions for the different class distributions was done by the leave-one-out covariance estimator since the high redundancy present in the profiles led to singular matrices by using the conventional maximum likelihood estimator. A scheme of the processing flow when considering all the profiles (EAP_{all}) is reported in Fig. 6.4.

The features extracted by the FE techniques considered were analyzed by two classifiers: a Maximum Likelihood (ML) classifier with the assumption of Gaussian distributed classes and a Random Forest (RF) classifier. The RF was created with 100 trees. During the training phase of the RF, the number of variables considered in each split of the trees, was set to the square root of the total number of features. The classification results were quantitatively evaluated by measuring the Overall Accuracy (OA) on the reference data. In Table 6.3, the accuracies obtained without the feature extraction techniques are presented. It is possible to notice how similar results are obtained by considering only the hyperspectral channels (*Spectr.*) and the first PCs for all the classifiers. The classification of the EAPs with the ML led to poor results, due to the low reliability of the estimation of the class

distributions as Gaussian in the feature space with full dimensionality. Conversely, the RF proved to be robust to the high dimensionality and capable to handle the information extracted by the EAPs leading to significantly higher accuracies than those obtained without considering any spatial feature. In particular, the EAP_a performed well with respect to the EAPs with other attributes for the RF classifier whereas the EAP_i performed the best for the ML classifier.

In the experiments with FE techniques, the classifiers were applied progressively on an increasing number of the features extracted. The best results are shown in Table 6.4 (the number of features considered is reported in brackets). The importance of the application of a FE is evident from the results. For example, when considering each single EAP and the ML classifier, the gain in terms of accuracies is up to 19% and 34% when compared to the classification of only the hyperspectral data and each EAP without FE, respectively. Also when looking at the RF classifier applied to each single EAP, the use of a FE technique led to better OAs in most of the cases with respect to consider the data without FE, obtaining a gain up to 10%. However, in almost all the experiments, the best accuracies were obtained by performing FE on all the EAPs (EAP_{all}). The best classification in terms of OA was obtained with the RF and the DAFE technique leading to 96.01% of OA (the classification map is reported in Fig. 6.3.c). When comparing the accuracies resulting from each FE technique it is possible to state that in average the application of the NWFEE technique outperformed the results obtained by DAFE and DBFE up to 1.5% and 0.8% of OA, respectively.

Table 6.3: Overall Accuracies obtained without any FE technique. The best accuracy obtained for each classifier is marked in bold.

	Spectr.	PC_s	EAP_a	EAP_d	EAP_i	EAP_s	EAP_{all}
Feats	103	4	36	36	36	36	144
ML	70.47	75.20	72.21	65.05	73.08	54.34	64.19
RF	71.66	69.89	90.99	86.66	82.94	81.64	89.71

6.2.4 Conclusion

In this section we presented a technique that exploits feature extraction techniques applied to the images generated by Extended Attribute Profiles derived from a hyperspectral image for data classification. EAPs can extract useful information but increasing the dimensionality of the data especially when multiple attributes are considered. Three

Table 6.4: Overall Accuracies obtained with the FE techniques. The number of features considered for each experiments is reported in brackets. The best accuracy obtained for each FE and each classifier is marked in bold.

FE Technique	Classifier	EAP _a	EAP _d	EAP _i	EAP _s	EAP _{all}
DAFE	ML	89.97 (7)	84.68 (8)	84.56 (10)	85.41 (8)	91.48 (11)
	RF	92.68 (20)	90.13 (25)	90.84 (35)	86.52 (14)	96.01 (121)
DBFE	ML	88.69 (6)	82.33 (8)	81.47 (7)	85.18 (5)	83.80 (11)
	RF	88.69 (30)	85.07 (36)	82.20 (36)	87.55 (20)	94.50 (81)
NWFE	ML	89.93 (14)	83.03 (4)	87.54 (10)	88.55 (12)	91.18 (11)
	RF	92.99 (24)	87.25 (30)	93.47 (27)	79.83 (5)	91.89 (41)

techniques for reducing the data dimensionality suitable for classification were considered: i) DAFE; ii) DBFE; and iii) NWFE. The features extracted were classified with the ML and RF classifiers.

The experimental analysis carried out on a HR hyperspectral image of Pavia, Italy, proved the importance of the FE stage in the processing chain. When considering the ML classifier, the use of FE brought the greatest gain in terms of accuracy. This can be explained by the sensitiveness of the ML to the Hughes phenomenon. The RF classifier proved to be more robust in presence of high dimensionality and redundant features with respect to the ML. However, in most of the cases the application of a FE technique led to better accuracies with respect to perform the classification on the data with full dimensionality. The RF classifier outperformed in almost all the experiments the other classifiers. The best accuracies were obtained by considering all the EAPs together along with a FE technique. Regarding the FE techniques, the NWFE in average slightly outperformed the other FE techniques in terms of overall classification accuracies.

DUAL TECHNIQUES

Abstract. APs and EAPs handle differently bright and dark structures in the image. However, for some applications it is important to simultaneously operate on bright and dark regions. Dual transformations are then suggested in this scenario. In this chapter we present two techniques based on this approach. Firstly, we show the different effects obtained by applying many attribute filters in an alternating sequence for image simplification. Subsequently, a technique based on self-dual attribute profiles for the classification of VHR panchromatic images is proposed.

7.1 ALTERNATING SEQUENTIAL ATTRIBUTE FILTERS

7.1.1 Introduction

Very high resolution (VHR) remote sensing images can currently reach a geometrical resolution under 50 cm. The increase in geometrical resolution with respect to images of medium resolution (which have a pixel footprint greater than 1 sqm) leads to a significant improvement in the representation of the objects details. For example, chimneys on roofs, cars on roads, tree crowns are now represented in images. If on the one hand such improved resolution increases the capabilities of such imagery, on the other hand, it can make the analysis more complex and demanding [71]. If the VHR image is analyzed by techniques developed for images of lower resolution it is likely that these techniques are not able to deal with the great amount of details present in the image [71]. In fact, the surveyed objects (even those having a homogeneous reflectance) can appear in the image as a fragmented

Parts of this chapter were published in:

M. Dalla Mura, J. A. Benediktsson, and L. Bruzzone, "Alternating sequential filters with morphological attribute operators for the analysis of remote sensing images," in *Image and Signal Processing for Remote Sensing XVI - SPIE Proceeding*, vol. 7830. Toulouse, France: SPIE Publications, Bellingham, WA, 2010, pp. 783 006–1–783 006–8.

Parts are going to appear in:

—, "Self-dual attribute profiles for the analysis of remote sensing images," in *Proc. of 10th Int. Symp. on Mathematical Morphology (ISMM 2011)*, P. Soille, G. K. Ouzounis, and M. Pesaresi, Eds., Intra, Lake Maggiore, Italy, 6th-8th July 2011.

composition of many bright and dark areas, due to phenomena such as the great amount of details, the uneven illumination, the presence of shadows, the natural texture of the surfaces.

Image simplification can be a useful pre-processing operation for analyzing a VHR image. The reduction of the complexity of the scene aims at reducing the presence of uninteresting details and thus enhancing only the components that are informative for the subsequent analysis. However, the simplification process should not affect the characteristics of the interesting objects in order to fully preserve their information for the subsequent analysis.

The image simplification can be obtained by applying Alternating Sequential Filters (ASFs). ASFs are filters defined in the mathematical morphology framework as a sequential application of the alternate composition of either opening and closing or closing and opening. The alternate application of opening and closing (and vice-versa) filters both regions that are brighter (with the opening) and darker (with the closing) than their surrounding greylevels. *Morphological ASFs* are obtained by *morphological opening* and *morphological closing* [82]. An example of the application of a morphological ASF is reported in Figure 7.1(b). It can be noticed how a simplification of the original scene is obtained. However, the geometrical characteristics (e.g., region shapes, edges) of the structures non completely removed by the filtering are not preserved. *ASFs by reconstruction* are better candidates than morphological ASFs for the analysis of VHR images since they are based on *opening by reconstruction* and *closing by reconstruction* [99]. Operators by reconstruction are connected filters and thus they process an image only by merging connected components (regions of connected pixels of iso-intensity graylevel). As shown by the Figure 7.1(c), ASFs by reconstruction are more suitable than morphological ASFs in processing VHR images. The filtering effects that can be obtained by ASFs by reconstruction are limited since operators by reconstruction process the image according to a window with given size and shape (called structuring element, SE). In general, the use of isotropic SEs (e.g., disk or square) in the ASF leads to a simplification of the scene obtained by removing progressively larger regions. When considering lines as SEs, a directional effect is obtained since the image is filtered by removing structures with the same orientation of the SE. However, more complex effects are difficult to achieve (e.g., filter the image according to measures of texture).

Morphological attribute filters can overcome the limitations of the use of SEs. Attribute filters are connected operators and they include in their definition filtering by reconstruction [91]. The filtering effect obtained with attribute filters is mainly due to the type of attribute

selected (e.g., area, length of the perimeter, standard deviation, shape index) leading to a great flexibility in the definition of this family of filters.

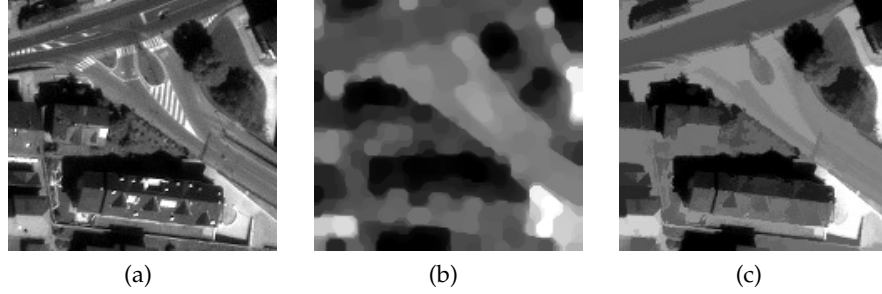


Figure 7.1: Example of Alternating Sequential Filters. (a) Original image; (b) Morphological ASF with sequence morphological opening followed by a morphological closing with disk-shaped structuring element of radius 5 pixels; (c) ASF by reconstruction with sequence opening by reconstruction followed by a closing by reconstruction with disk-shaped structuring element of radius 5 pixels.

In this section we aim at: i) defining Alternating Sequential Attribute Filters (ASAFs), which are ASFs computed with attribute filters; ii) presenting a possible implementation of ASAFs and iii) showing the effects obtained by ASAFs with different attributes for a qualitative analysis.

7.1.2 Definition of ASAF

Alternating Sequential Attribute Filters can be defined as the alternate application of the product of attribute thinning and attribute thickening with progressively stricter criteria. As guideline for the definition of ASAF we follow the presentation of the ASF given in [80]. The product of attribute thinning and attribute thickening composes the alternate core operator that is iteratively applied for performing the filtering. Different compositions of the alternate operator are possible. The main ones are reported below.

- $m_\lambda = \gamma^{T_\lambda} \phi^{T_\lambda}$;
- $n_\lambda = \phi^{T_\lambda} \gamma^{T_\lambda}$;
- $r_\lambda = \phi^{T_\lambda} \gamma^{T_\lambda} \phi^{T_\lambda}$;
- $s_\lambda = \gamma^{T_\lambda} \phi^{T_\lambda} \gamma^{T_\lambda}$.

The ASAF is computed on a family of ordered criteria $\{T_\lambda\}$ with the scalar value λ taken as reference in the predicate, ranging in the interval $[\lambda_1, \lambda_2]$ with step size k . The range of values of λ is increasing monotonically from λ_1 (lowest value) to λ_2 (greatest value). For OP criteria, the criterion T_{λ_1} is the most relaxed predicate (i.e., almost all the regions satisfy the criterion and the image will be slightly affected by the filtering), whereas T_{λ_2} is the strictest predicate (i.e., produces the most severe changes in the image). When considering OR criteria, the severity of the filter is minimal for the criterion T_{λ_2} and maximal for T_{λ_1} .

Let us now consider the alternate product $m_\lambda = \gamma^{T_\lambda} \phi^{T_\lambda}$ as core operator. We show in the following the ASAF definition, which can be straightforwardly extended to the other alternate compositions of thinning and thickening.

- Order-preserving (OP) criterion (e.g., $T = A > \lambda$) with $\lambda_2 \geq \lambda_1$

$$\text{ASAF}_m = M_{T_{\lambda_1}}^{T_{\lambda_2}}(k) = m_{\lambda_2} m_{\lambda_1 + (k-1)(\lambda_2 - \lambda_1)/k} \cdots m_{\lambda_1 + (\lambda_2 - \lambda_1)/k} m_{\lambda_1}. \quad (7.1)$$

- Order-reversing (OR) criterion (e.g., $T = A < \lambda$) with $\lambda_2 \geq \lambda_1$

$$\text{ASAF}_m = M_{T_{\lambda_2}}^{T_{\lambda_1}}(k) = m_{\lambda_1} m_{\lambda_2 - (k-1)(\lambda_2 - \lambda_1)/k} \cdots m_{\lambda_2 - (\lambda_2 - \lambda_1)/k} m_{\lambda_2}. \quad (7.2)$$

For OP criteria, the ASAF is obtained by, at first, computing the alternate filter with criterion T_{λ_1} and increasing step by step the reference value till the criterion T_{λ_2} of the last iteration of the filter. Conversely, for OR criteria, the reference λ is progressively reduced from λ_2 to λ_1 .

As a general guideline, the step size k , regulating the increasing of λ , should be taken as the smallest possible variation that can occur in $\{A\}$, the domain of the (significant) values of the attribute. The progressive increase of the reference value should be the smallest possible in order to obtain the proper simplification effect. Since, only one of the extrema of the range interval of λ defines the severity of the filter (i.e., it can be thought as the “filter size”), the other extremum, which sets the starting point of the filtering, can be fixed without affecting much the filtering effect. Therefore, for OP criteria, λ_1 can be set to the lowest value of the attribute $\wedge\{A\}$ and the ASAF notation can be simplified to $M^{T_{\lambda_2}}$. Analogously, when dealing with OR criteria, it is possible to define λ_2 as $\vee\{A\}$, leading to the filter $M^{T_{\lambda_1}}$. For both (7.1) and (7.2) the absorption law is fulfilled ($M^{T_\lambda} M^{T_\mu} = M^{T_\lambda}$ for $T_\lambda \supseteq T_\mu$).

7.1.3 Implementation of ASAF based on Min- and Max-tree

The implementation of the ASAF based on min- and max-trees is detailed in the following for the alternate operator $m_\lambda = \gamma^{T_\lambda} \phi^{T_\lambda}$ at an arbitrary iteration i of the filtering procedure:

1. Compute the min-tree on the image g (which was already filtered by the previous alternate operators);
2. Compute the attributes and filter the tree according to T_{λ_i} ;
3. Retrieve the filtered image $\phi^{T_{\lambda_i}}(g)$;
4. Compute the max-tree on the filtered image $\phi^{T_{\lambda_i}}(g)$;
5. Compute the attributes and filter the tree according to T_{λ_i} ;
6. Transform the filtered tree back to an image ($\gamma^{T_{\lambda_i}} \phi^{T_{\lambda_i}}(g)$).

By analyzing the implementation of the ASAF as presented above, it is possible to notice how this approach can be computationally demanding (a min- and a max-tree structures are computed for each λ) and for a large range of λ this can be a significant limitation. The main advantage in using the max-tree representation is given by the knowledge of all the possible values of the attribute before filtering the tree. This knowledge helps in speeding up the process since the filtering can be performed only for the significant λ s in the range avoiding to perform a filtering for those λ s that would not produce any change.

In order to speed up the filtering process, it is possible to use faster implementation of the alternating sequence as presented in [80]. However, those are approximations of the ASAF as defined in the previous subsection and they can produce slightly different filtered images. The simplest move to reduce the computational burden of the filter is the increase of the step size k used for defining the increase rate of the range of λ s. Such approximated version of the ASAF is reported below (for a OP criterion and the m_λ operator):

$$\hat{M}^{T_\lambda}(k) = m_\lambda m_{\lambda-k} \dots m_{k+1} m_1. \quad (7.3)$$

Another possible lighter approximated version of the ASAF is given by the following operator:

$$\tilde{M}^{T_\lambda} = \gamma^{T_\lambda} \phi^{T_{\lambda-1}} \gamma^{T_{\lambda-2}} \dots \gamma^{T_2} \phi^{T_1}. \quad (7.4)$$

In this approach, either a thinning or a thickening is computed for each λ . Analogous definitions can be derived for the other alternate operators.

7.1.4 Experimental Results

The effects produced by filtering an image with an ASAF are mainly due to the attribute and the ordering relation of the criterion. The ASAF with increasing attributes leads to a simplification of the image by merging regions of increasing size. Conversely, ASAFs with non-increasing attributes produce a reduction of the complexity of the scene by merging regions according to features related to the shape characteristics of the regions, relative contrast between pixels, etc. The ordering relation used in the definition of the criterion indicates how the feature associated to the attribute is considered in the analysis. For example, if the spectral homogeneity is the feature considered (e.g., estimated by the standard deviation of the values of the pixels), by setting the ordering relation one can define if the simplification of the image will be done by affecting the most or the least homogeneous regions.

7.1.4.1 Experimental Set-up

A GeoEye-1 panchromatic image of 400×400 pixels having a geometrical resolution of 0.5 m was used for the qualitative analysis of the ASAF. The image was acquired on Borgo Valsugana a village close to the city of Trento, Italy. The acquired scene presents heterogeneous residential buildings, roads and some vegetated areas (see Figure 7.2). Four attributes were considered in the analysis: area, length of the

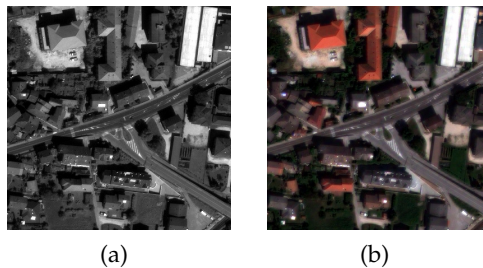


Figure 7.2: GeoEye-1 image of Borgo Valsugana, Trento, Italy. (a) Panchromatic band; (b) True color composition of the pansharpener multispectral channels.

diagonal of the bounding box (denoted for simplicity “diagonal” in the following), moment of inertia and standard deviation. The area and the diagonal are increasing attributes and they give a measure that can be associated to the size of the regions. Conversely, the moment of inertia and the standard deviation are non-increasing attributes. The moment of inertia can be considered as a measure of the spatial elon-

gation of a region. It assumes the lowest value for a disk-shaped region and rapidly increases as soon as the region become more elongated. The standard deviation computed on the graylevel values of the pixels in a region can be related to a measure of the spectral homogeneity. The *min* filtering rule was adopted for increasing criteria, whereas the *subtractive* was chosen for the non increasing ones. For further information on the filtering rules we refer the reader to [91].

The alternate operator used in the composition of the ASAF was m_λ : the sequence of an attribute thinning followed by an attribute thickening. The implementation of the ASAF was carried out with the approximation presented in (7.3), since the direct application of (7.1), (7.2) was computationally too demanding.

7.1.4.2 Results

Figure 7.3 shows the results obtained by applying the ASAF with area and diagonal to the considered image. One can see how a similar effect is obtained with the two attributes. By making the criterion stricter, larger regions are merged together. The Figures 7.3(b) and (d) are associated with the lowest degree of simplification, i.e., they show the scene with small details removed (e.g., the particulars of the roof of the buildings, the white signs on the roads). By increasing the severity of the filters, larger structures are removed (e.g., some buildings, trees, parts of the roads).

Compared to Figure 7.3, a different effect is seen in the filtered images of Figure 7.4. The filtering done with moment of inertia attribute (Figure 7.4(a)–(c)) enhances the elongated regions by progressively removing compact objects. When considering the standard deviation attribute (Figure 7.4(d)–(f)), the image is simplified by merging regions more homogeneous as soon as the criterion is made stricter.

The inverse effect of the ASAFs in Figure 7.4 was obtained by defining the criterion with reversed ordering relation (see Figure 7.5). The less severe filter with moment of inertia attribute removes the most elongated regions (Figure 7.5(a)), whereas the most severe filter (Figure 7.5(c)) only keeps the most compact objects. When considering the standard deviation attribute, the image is filtered by progressively merging homogeneous regions.

7.1.5 Conclusion

In this section we proposed Alternating Sequential Attribute Filters (ASAFs). We defined ASAFs as the sequential application of the product of an attribute thinning and an attribute thickening. Two definition

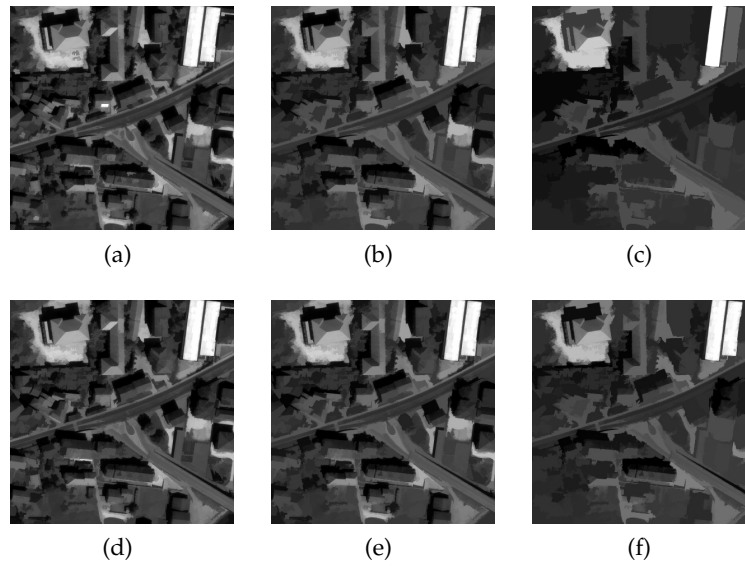


Figure 7.3: ASAF with increasing attributes and order preserving relation. Area attribute: (a) $\lambda = 50, k = 3$; (b) $\lambda = 500, k = 20$; (c) $\lambda = 2500, k = 100$. Length of the diagonal of the bounding box: (d) $\lambda = 20, k = 2$; (e) $\lambda = 40, k = 2$; (f) $\lambda = 80, k = 3$.

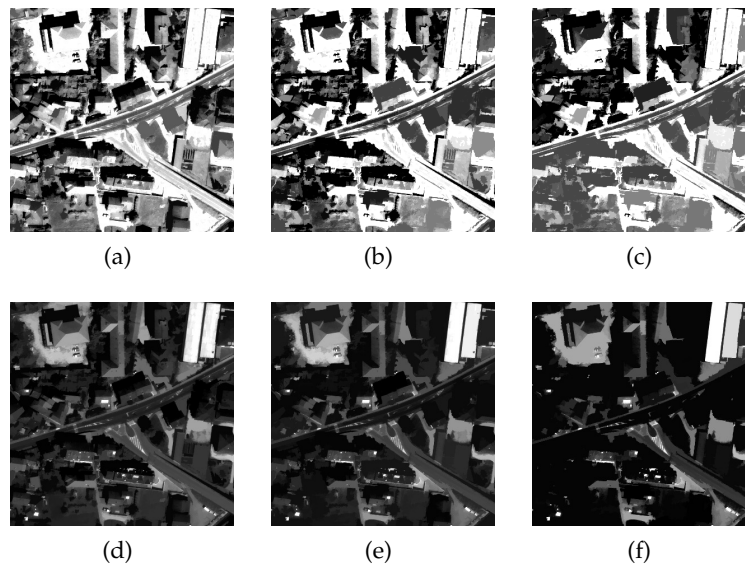


Figure 7.4: ASAF with non-increasing attributes and order preserving relation. Moment of inertia: (a) $\lambda = 0.2, k = 0.01$; (b) $\lambda = 0.225, k = 0.05$; (c) $\lambda = 0.25, k = 0.05$. Standard deviation: (d) $\lambda = 20, k = 1$; (e) $\lambda = 35, k = 3$; (f) $\lambda = 50, k = 4$.

were presented, according to the ordering relation of the criterion considered in the filtering. A possible implementation of the ASAFs based

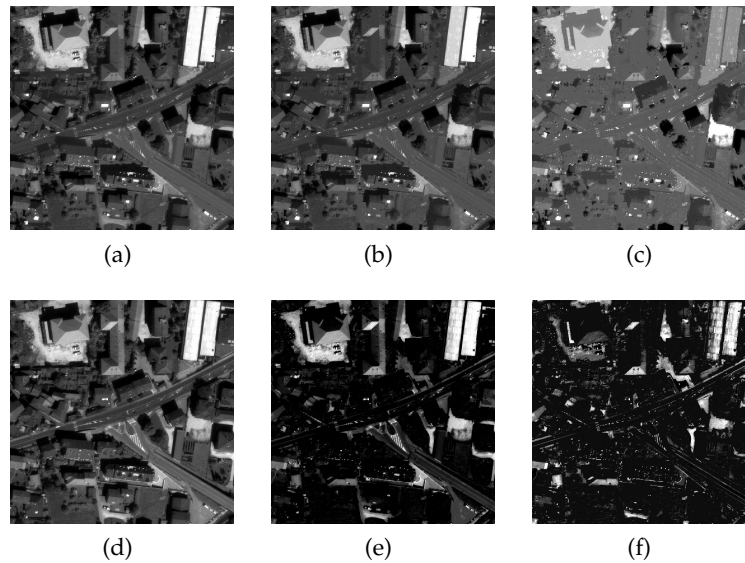


Figure 7.5: ASAF with non-increasing attributes and order reversing relation. Moment of inertia: (a) $\lambda = 0.5, k = 0.1$; (b) $\lambda = 0.4, k = 0.1$; (c) $\lambda = 0.3, k = 0.1$. Standard deviation: (d) $\lambda = 150, k = 10$; (e) $\lambda = 100, k = 10$; (f) $\lambda = 50, k = 10$.

on min- and max-trees was presented. Moreover, two approximated versions of the original definition were reported in order to decrease the computational burden of the processing.

ASAFs were applied to a panchromatic very high resolution image acquired by GeoEye-1. By analyzing the obtained results it was possible to notice how different effects are obtained by considering different criteria (i.e., attributes and ordering relations), thus leading to different ways of simplifying the image.

7.2 SELF-DUAL ATTRIBUTE PROFILES

7.2.1 Introduction

Since the APs are based on the application of either extensive or anti-extensive operators, the multilevel simplification is either obtained on the bright or dark components of the image. If a simultaneous simplification of bright and dark regions is aimed, self-dual operators should be used. The application of self-dual connected operators leads to an image simplification characterized by more homogeneous regions with respect to the results obtained by extensive or anti-extensive connected operators. In a remote sensing scene this effect can be useful for flattening textured areas (e.g., agricultural fields, vegetated areas, etc.)

or removing both dark and bright details. In [93] we investigated the effects of Alternating Sequential Attribute Filters (ASAFs) obtained by the application of attribute thinning and attribute thickening in an alternating sequential approach on a VHR remote sensing image. The selection of different attributes with progressively stricter criteria (i.e., producing greater simplifications of the image) showed how significantly different effects can be obtained on the image. However, the alternating sequence of thinning and thickening operators is not a self-dual operator since the filtering effect is biased by the operator that is applied first. Furthermore, the non approximated computation of ASAFs is computationally very demanding.

In this section we propose to use an inclusion tree for computing the AP instead of the min-tree and max-tree as done in [91]. The inclusion tree is a tree representation of an image which fuses both the min-tree and max-tree of the image in a single data structure [106]. The main advantages for the use of an inclusion tree for the computation of a profile relies on: i) the construction and subsequent manipulation of a single representation of the image embedding the min- and max-tree representation (requiring less resources in term of computational complexity and memory occupation); and ii) the capability of computing extensive, anti-extensive or self-dual connected operators. In this section we focus on the latter aspect investigating Self-Dual Attribute Profiles (SDAPs) which are APs based on self-dual connected operators for the classification of a VHR remote sensing image.

7.2.2 Definition of Self-dual Attribute Profiles

If we take into account the inclusion tree, the AP can be obtained by considering in the filtering the components belonging to the upper level set or lower level set for performing a thinning or thickening, respectively. The phase devoted to the construction of the inclusion tree with the FLST implementation results faster and requires less memory for storing the data than the construction of both a min- and max-tree [106].

The use of an inclusion tree permits also to filter the image with self-dual operators when the inclusion relations defined by the saturation of the components are considered instead of those belonging to the upper or lower level set. Self-dual operators are advisable for the processing of remote sensing images if a simplification leading to more homogeneous regions with respect to the effect obtained by a non dual operator is required.

As an example of this effect, Fig. 7.6 shows the results obtained by

filtering a particular of a VHR remote sensing panchromatic image considering as a predicate $T = \text{card}(C) \geq \lambda$ with $\text{card}(C)$ the cardinality of the connected component C with increasing values of λ . The filtering was computed on a min-, max- and inclusion tree. The operator obtained with the considered predicate on a max-tree (min-tree) was basically an area opening (area closing). When considering the inclusion tree, a self-dual operator (that is called grain filter in [106]) was applied. By analyzing the figure is possible to see how bright and dark details were preserved unaffected in the images filtered with area closing and opening, respectively. For example the bright areas on the roof (probably due to glares of roof windows, metal plates or solar cells) of the building on the top of the image and bright small regions composing the texture of the garden on the bottom right were completely preserved by the area closing. Analogously, the shadows casted on the roof by the dormers and other shaded regions on the vegetated area on the top of the image were unaffected by all the openings. In comparison, the effect of the self-dual filter can be noticed in the production of more homogeneous regions since both bright and dark components were simultaneously filtered. For instance, the particulars on the roofs were removed and the textured areas were completely flattened.

Analogously to the definition of the AP (4.4), it is possible to derive a formulation of Self-Dual Attribute Profiles (i.e., APs built with self-dual operators):

$$SDAP(u) = \left\{ u, \rho^{T_{\lambda_1}}(u), \dots, \rho^{T_{\lambda_{L-1}}}(u), \rho^{T_{\lambda_L}}(u) \right\}, \quad (7.5)$$

with ρ the self-dual operator based on the predicate T , and being $\{T_{\lambda}\}$ a set of L ordered predicates. In contrast to APs, the SDAP is composed by $L + 1$ images while the AP built with the same sequence of λ s is made up of $2L + 1$ images.

7.2.3 Experimental Results

In the experimental analysis a VHR image acquired by GeoEye-1 over Borgo Valsugana a village close to the city of Trento, Italy was considered for classification. The data set is composed by a panchromatic band and four multispectral (MS) pansharpened images (acquired on the visible and near infrared electromagnetic spectrum) of 400×400 pixels with a geometrical resolution of 0.5 m. The Normalized Vegetation Index (NDVI) image was also generated for enhancing the vegetated areas. The NDVI is given by $\frac{NIR-R}{NIR+R}$ with NIR and R the bands acquired on the near infrared and red regions, respectively. The scene presents heterogeneous residential buildings, roads and

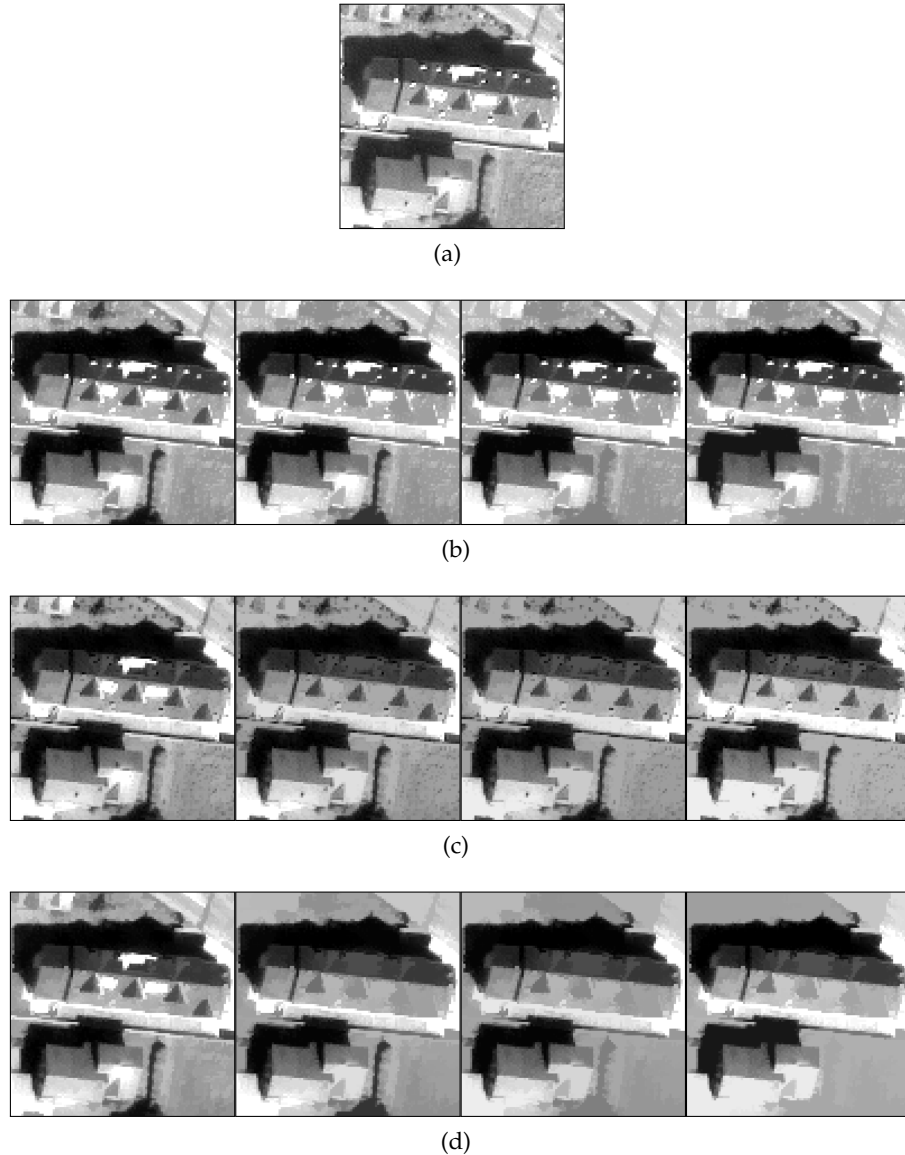


Figure 7.6: Particular of the panchromatic band of 0.5 [m] resolution acquired by GeoEye-1 image of Borgo Valsugana, Trento, Italy reported in Figure 7.7a. (a) Original image; (b) Area opening ($\gamma^{T\lambda}$); (c) Area closing ($\phi^{T\lambda}$); (d) Grain filter ($\rho^{T\lambda}$). The values of area taken as reference and used by all the three operators are $\lambda = \{50, 500, 1000, 2000\}$ (correspondent to images from left to right).

some vegetated areas. Six thematic classes were identified in the image: Buildings, Roads, Trees, Meadows, Shadows and Soil. A reference map of the coverage classes was generated by visual inspection leading to a total of 67977 labeled pixels.

For including the spatial information in the analysis, an AP and a

SDAP with area attribute and 12 reference values ($\lambda = \{5, 25, 50, 100, 150, 200, 300, 500, 750, 1000, 2000, 3000\}$) were computed on the panchromatic image. The AP was computed using the implementation of the min and max-tree included in the C++ Milena library [142] and the SDAP from an adaptation of the code for the inclusion tree provided in the MegaWave2 toolbox ¹.

The data set was classified by 6 different classifiers: Linear Bayes Normal classifier, Quadratic Bayes Normal classifier, Random Forest (RF), 3-Nearest Neighbor, SVM with linear kernel and SVM with RBF kernel. Part of the labeled samples of the reference image was considered for the training of the classifiers, the rest was used for computing the classification accuracy, which was assessed by the Overall Accuracy (OA) and the Kappa coefficient (κ). Two training sets were considered taking for all the classes a total of the 1% (685) and 10% (6801) of the reference samples.

The classification accuracies obtained by considering different features are reported in Table 7.1. With 10% of the samples used for training, it can be seen that considering the images of the SDAP as features and the RF as classifier outperformed in terms of overall accuracies the best results obtained by the spectral features (MS + NDVI) and AP taken singularly of 0.25% and 2.34%, respectively. By a visual inspection of the map correspondent to the best accuracy obtained by the spectral features among all the classifiers (Fig. 7.7d) is possible to notice that the vegetation was well classified (also separating meadows from trees). However, roads and buildings were often mixed and the shapes of some objects were distorted (see the shadow of the building on the top left). In contrast to Fig. 7.7d, the maps obtained by the AP (Fig. 7.7e) and SDAP (Fig. 7.7f) show less confusion between roads and buildings but the natural classes (i.e., soil, meadows and trees) were not correctly detected. Furthermore, Fig. 7.7f in comparison to Fig. 7.7e shows more homogeneous regions (due to the use of self-dual operators in the computation of the profile). When the spectral features are considered along with the AP or SDAP, the best accuracies among all the experiments were obtained. In particular, considering the training set as 10% and the best obtained OAs, there was an increase of accuracy up to about 7% compared to considering both the spectral features and the SDAP singularly and about 9% with respect to considering only the AP. A greater precision in detecting buildings, roads and vegetation is also clear from the maps (Fig. 7.7g, 7.7h). When comparing the best overall accuracies obtained by considering the AP against the SDAP, both with the spectral features, similar results were obtained (with a SVM with RBF kernel and a RF, respectively). However, the

¹ Available at <http://megawave.cmla.ens-cachan.fr>.

results obtained with the SDAP slightly outperformed those achieved with the AP. Again, when comparing Fig. 7.7g and 7.7h, the use of SDAP produced a less noisy map than considering the AP. However, in Fig. 7.7h some shadows in the vegetated areas were not correctly detected as instead occurs in Fig. 7.7g. Satisfactory results are also obtained with a reduced training set (1% of the reference samples) confirming the improvements given by using the SDAP.

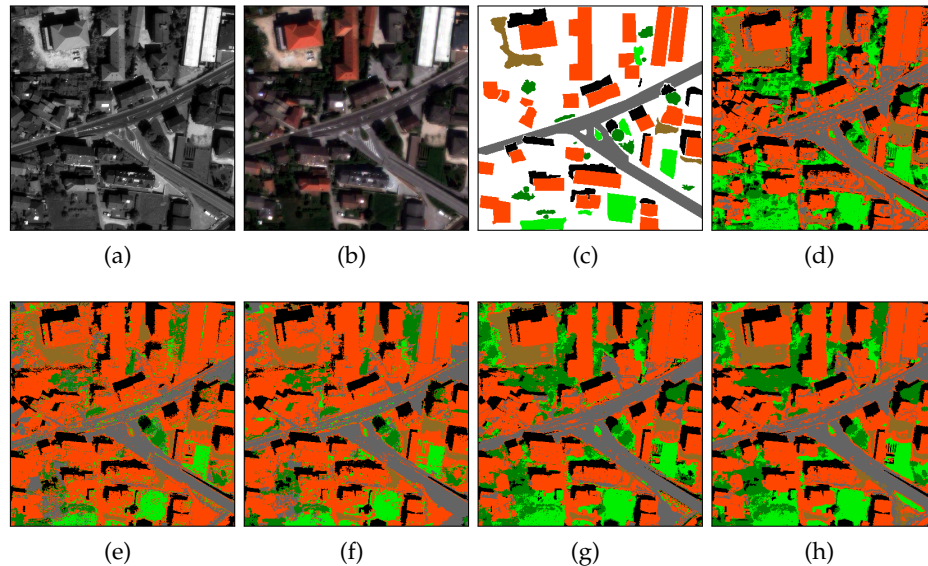


Figure 7.7: GeoEye-1 Borgo Valsugana data set. (a) Panchromatic band; (b) True color composition of the pansharpened multispectral channels; (c) Map of the reference samples. Classification maps (all taking the 10% of the reference samples as training) obtained by: (d) MS + NDVI and SVM with RBF kernel classifier (OA 86.23%); (e) AP and RF classifier (OA 84.14%); (h) SDAP and RF classifier (OA 86.48%); (g) MS + NDVI + AP and SVM with RBF kernel classifier (OA 93.45%); (h) MS + NDVI + SDAP and RF classifier (OA 93.50%). Thematic classes: ■ buildings, ■ roads, ■ trees, ■ meadows, ■ shadows, ■ soil.

7.2.4 Conclusion

In this section we have proposed to compute Attribute Profiles on the inclusion tree of the image instead of considering a min- and max-tree. The use of the inclusion tree as structure representing the image contains the information of both the min- and max-tree. Moreover, on the inclusion tree can also be computed self-dual connected operators, which produce a greater simplification of the image with respect to non dual filters since they operate simultaneously on the bright and

dark components of the image. Thus, we have derived the definition of Self-Dual Attribute Profiles as a version of the APs based on self-dual operators.

In the experimental analysis carried out, we considered for classification a remote sensing image acquired by GeoEye-1 with geometric resolution of 0.5 m on an area close to Trento, Italy. An AP and a SDAP were computed on the panchromatic band with area attribute and same values taken as reference in the computation of the profile. The results obtained showed how including the AP or SDAP as features in the classification of the spectral features greatly improves the accuracies with respect to considering only the spectral information. The use of the SDAP against the AP leads to better results in terms of accuracies in most of the cases (also with a reduced training set). The greater accuracies were also supported by the obtained maps showing regions classified more homogeneously. The best overall accuracies among all the experiments were obtained by the spectral features and the SDAP with a random forest classifier. The obtained results proved that the use of the SDAP is effective for modeling the spatial information of the scene even with a reduced number of features with respect to considering the AP.

Table 7.1: GeoEye-1 Borgo Valsugana data set. Classification accuracies obtained by classifying combinations of the spectral features (MS + NDVI), the AP and SDAP with a linear (Lin.), quadratic (Quadr.), random forest (RF), 3-nearest neighbor (3-NN), SVM with linear kernel (SVM Lin.) and SVM with RBF kernel (SVM RBF) classifiers. The best accuracies for each classifier and among all the experiments are marked in bold and underlined, respectively.

	Lin.		Quadr.		RF		3-NN		SVM Lin.		SVM RBF	
	1%	10%	1%	10%	1%	10%	1%	10%	1%	10%	1%	10%
Train												
	MS + NDVI (5 feats)											
OA (%)	63.12	63.90	73.12	73.03	81.50	85.58	80.57	83.69	69.03	69.25	82.16	86.23
κ (%)	45.72	46.47	63.22	63.27	73.20	79.37	72.27	76.77	51.19	51.21	74.50	80.41
	AP (25 feats)											
OA (%)	62.23	63.34	37.45	22.83	77.35	84.14	71.23	80.29	66.22	67.94	76.15	83.71
κ (%)	41.44	43.12	24.28	12.64	66.85	77.05	58.24	71.55	51.98	51.96	65.91	76.43
	SDAP (13 feats)											
OA (%)	62.97	64.07	54.60	52.36	80.36	86.48	75.27	83.75	61.35	63.25	78.77	83.96
κ (%)	42.37	43.29	42.54	41.64	71.72	80.50	64.08	76.35	33.95	38.18	69.41	77.44
	MS + NDVI + AP (30 feats)											
OA (%)	77.85	78.86	44.30	29.40	87.57	92.58	84.66	90.51	85.95	88.68	88.53	93.45
κ (%)	68.54	70.26	30.30	17.62	82.06	89.37	78.19	86.50	80.30	84.13	83.71	90.68
	MS + NDVI + SDAP (18 feats)											
OA (%)	74.99	76.00	75.34	73.75	<u>89.31</u>	<u>93.50</u>	85.47	90.62	80.04	80.28	88.20	93.33
κ (%)	64.33	65.82	66.17	65.03	<u>84.65</u>	<u>90.70</u>	79.35	86.65	71.06	71.04	83.27	90.48

ATTRIBUTE PROFILES FOR BUILDING EXTRACTION

Abstract. In this chapter we present a technique based on AP for the generation of features suitable for building extraction. In details, we address the issue of selecting the most suitable parameters of the filters by proposing an architecture which embeds in the filtering procedure an optimization step based on genetic algorithms.

8.1 INTRODUCTION

Building extraction from satellites optical images is attracting increasing attention from the remote sensing community thanks to the recent availability of commercial very high resolution (VHR) images. VHR images are characterized by a geometrical resolution of about one meter (e.g., IKONOS sensor) or even sub-meter (e.g., 0.6 m for Quickbird, 0.5 m for World View sensors). This outstanding geometrical resolution permits to address the building extraction task not only by analyzing aerial images, which are costly and not always easily available, but also by considering commercial satellite products. The most important exploitations of the automatic extraction of the buildings are the monitoring of the urban growth, the updating of cartographic and geometric maps, the revision of cadastral databases, etc. However, due to the increased geometrical resolution, the images show a large amount of details in the representation of the surveyed objects leading to a great variety and complexity of the scene. In particular, the buildings, especially in complex urban areas, are heterogeneous in shape, size, orientation, textural characteristics, spectral values, etc. This results in an increased complexity in the definition of a proper procedure able to comprehensively handle those aspects. The limitation of pixel-based techniques are evident and further knowledge on the scene has to be extracted and included in the analysis. For example this can be done by modeling and exploiting the structural informa-

This chapter was published in:

M. Dalla Mura, J. A. Benediktsson, and L. Bruzzone, "Modeling structural information for building extraction with morphological attribute filters," in *Image and Signal Processing for Remote Sensing XV - SPIE Proceeding*, vol. 7477. Berlin, Germany: SPIE, Bellingham, WA, 2009, pp. 747 703–1–747 703–9.

tion of the scene. In general the building extraction task is addressed by an analysis based on a two steps procedure: i) Feature Extraction and; ii) Decision. The first stage is devoted to the preliminary analysis of the data aiming at extracting features, primitives and, in general, any information that can be discriminant for the representation of the buildings. The metadata extracted by this analysis can be considered as an intermediate product in the processing chain. According to the approach involved in this first phase, the obtained results aim at enhancing the information related to buildings. The second step addresses the generation of a final decision map based on the analysis of the intermediate results. In this work we focus our attention only on the first step of the building extraction chain. As already reported in the literature, the extraction of useful information for the detection of buildings in VHR images can be performed by morphological operators based on the geodesic reconstruction, which are tools defined in the mathematical morphology framework [82]. With particular regard to the building extraction task, the MPs and DMPs can be considered for the modeling of the structural information of the building structures. For example, in [143] an automatic building extraction technique is presented, which is based on the extraction of spectral, structural and contextual information. The DMP computed from the image is also used in [143] for extracting the shadows from the image in order to provide contextual information for confirming the inferred position of the buildings. We address the issue of the selection of the most suitable filter parameters for the building extraction problems by integrating an optimization procedure based on genetic algorithms (GAs) in the filtering procedure.

8.2 ATTRIBUTES FOR BUILDING EXTRACTION

The proper approach for the application of attribute filters to VHR images in order to handle the great heterogeneity of the buildings is certainly a multilevel architecture where the image is processed by the same filter type but with different values, λ , used as reference when evaluating the criterion. The building rooftops present in the image do not appear as bright or dark regions but they show different degrees of contrast with respect to their adjacent regions. For this reason, both an extensive and anti-extensive transformations have to be performed. Moreover, since a single attribute could not be enough for modeling the structural characteristics of the filter, we propose a multi-attribute multilevel analysis of the image. The choice of the attributes computed by the filters was made according to the most representative characteristics of the buildings.

The first attribute is purely geometric and aims at modeling the scale of the structures by evaluating the similarity between the shape of each region in the image and the one of a reference structure. The description of the shape is done by the seven moments invariant of Hu. For their definition we refer the reader to [138]. These indexes are invariant to translation, rotation and scaling, so this attribute is non-increasing. These characteristics are important for this task since even buildings of the same shape can assume different orientations, scales and positions in the image. The choice of the reference shape is also very important and problem-dependent. Thus, the multilevel analysis carried out by this attribute shows with which degree the regions in the image are similar to the shape of reference. In the following this attribute will be denoted by H.

Another discriminative characteristic of the buildings with respect to the background is the textural patterns present on the rooftop. In general, the buildings show a relative spectral homogeneity especially when compared to vegetation areas. Thus, the second attribute (denoted by S) is the standard deviation of the values of the pixels belonging to each region. This attribute is purely spectral and so it does not depend on the geometry of the regions; thus, it is non-increasing. The filtering performed with this attribute permits to model the spectral homogeneity of connected areas in the scene. However, the scale of the objects in the image is also a discriminant feature, so the area (referred as A) of the regions is taken into account as third attribute in the analysis.

All the filters evaluate a criterion which is “the selected attribute has to be greater than λ ”. The lambda is the parameter of the filter which has to be tuned.

8.3 FILTERING BY OPTIMIZATION BASED ON GAS

As already mentioned in the introduction, the selection of proper values for λ , which are taken as reference by the filters, is of fundamental importance for generating accurate results. We address this issue by proposing the integration of an optimization procedure based on genetic algorithms (GAs) into the filtering process.

8.3.1 Genetic Algorithms

The genetic algorithm is a widely used technique defined in the framework of evolutionary algorithms for finding solutions in optimization problems. Basically, a GA is defined by a representation of the problem to optimize in terms of genetic biology and by a fitness function

which evaluates the goodness of the found solutions. In greater detail, the variables in the problem are the genes and a possible solution is an individual defined by a set of values which bind the variables in the problem. All the individuals in the population receive a score according to the fitness to the requirement of the problem. The GA keeps evolving the population until a stopping criterion is verified. In general, the evolution terminates when the maximum number of iterations is reached or the population converged to a best solution. The basic operations that can be applied to the individuals are cloning, mutation and crossover. The first is the merely propagation of one individual to the subsequent generation. The mutation results in a change of one or more values in defining an individual. This is necessary in the evolution for maintaining diversity. The crossover combines two genes called parents by crossing them and generates two children by crossed parts of the parents. Different possible crossover techniques are possible: for example, one-point crossover splits the parents in two halves and combines the opposite splits of the parents; two-point crossover do the same with two splitting points, etc. The GA is also driven by the evolutionary strategy that determines which individuals should survive, reproduce and die. The strategy also rules the evolution of the offspring on subsequent generations by determining which individuals should be replaced. For example, an effective replacement is the one performed according to the elitism. This leads to the propagation of only the best individuals through the next generations. For extensive details on GAs we refer the interested reader to [144].

8.3.2 *Parameters Tuning with Genetic Algorithms*

In order to integrate the GA in the filtering process, the problem of selecting the best filters parameters (λ) has to be represented in the domain of genetic. The variables of the problem are the thresholds of the filters and in the GA are the chromosomes. An individual in the population of the GA is thus defined by a particular set of lambdas. The selected fitness function has to evaluate the quality of the solutions. Since a labeled set of values is available for this problem, the score of an individual is taken as the overall thematic accuracy of the map obtained by classifying the filtered images, computed on the labeled set. Other measures of accuracy could be considered for scoring the individuals. For example, the thematic accuracy could be evaluated on specific classes, or the geometric indexes of accuracy could be taken into account [128]. The general architecture of the proposed technique based on APs integrating the optimization procedure is reported in Figure 8.1. The GA is separately applied to each attribute filtering

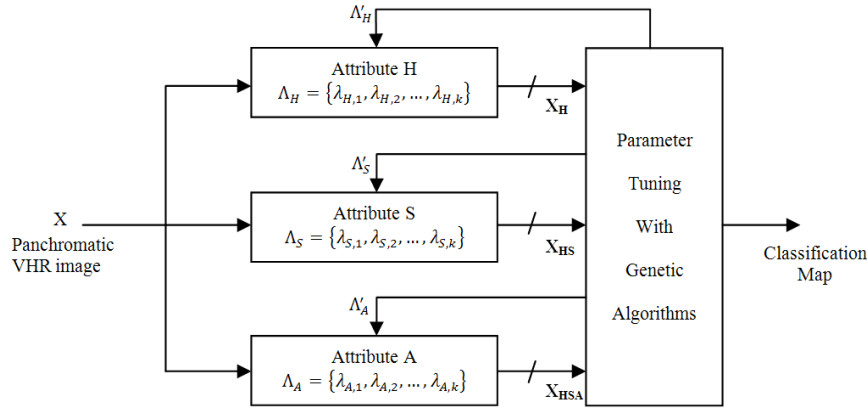


Figure 8.1: General architecture of the proposed technique.

included in the analysis. At first, the optimization generates the best parameters (according to the considered fitness function) for the first filtering. The selected parameter is used both for the thinning and thickening transformations. Subsequently, the parameter of the second level is optimized. In this case, the filtered images obtained by the first filtering are considered as additional features during the evaluation of the solutions identified for the second set of filters. The same is done for the third level. When also the parameters of the last level are found, then the result of the global analysis is simply given by the classification of all the features (the AP with lambdas selected by the GAs).

8.4 EXPERIMENTAL RESULTS

8.4.1 Data set Description

The experiments were carried out on a VHR panchromatic Quickbird image with geometric resolution of 0.6 m, acquired on July 2006 on an area of the city of Trento.

The Figure 8.2 is a 500×500 pixels portion of the entire surveyed scene, showing a complex urban area. Many buildings are present in the image, their heterogeneity is evident by noting the variety in their geometrical characteristics. It is also clear the great heterogeneity in the values of radiance due to different covering materials of the roofs, which in many cases does not show a high contrast with respect to adjacent objects. Moreover, the presence of elements on some roofs (e.g., windows, chimneys), the different illumination of the pitches and the shadows are further increasing the complexity of the recognition task. Four informative classes were considered for describing the

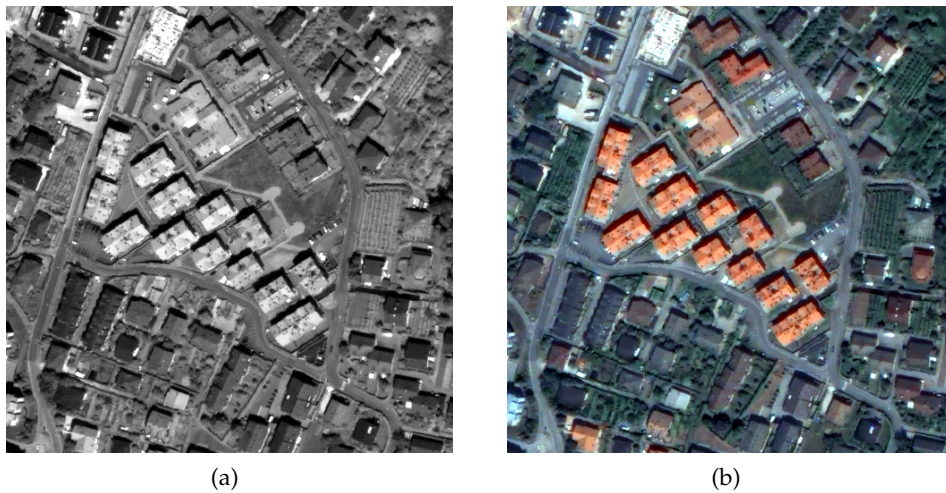


Figure 8.2: Trento data set. (a) Panchromatic band; and (b) true color pan-sharpened image. Both the images are visually enhanced.

objects present in the scene. They are: Road, Building, Shadow and Vegetation.

Table 8.1: Labeled set of pixels reporting the number of pixels for each thematic class for the training and test sets.

Sets	Road	Building	Shadow	Vegetation	Total
Training	58	178	43	88	367
Test	47	178	40	73	348

8.4.2 Experimental Set up

In order to compare the proposed method to a standard technique based on mathematical morphology for the building extraction task, a conventional morphological profile was computed on the original panchromatic image. The profile was built by selecting a SE with squared shape and four sizes (3, 7, 11, and 15 pixels). The obtained filtered images are considered as components of the feature vector given as input to the classification process. The vector is made up of a total of nine components: the original image, four images obtained by the thinning and four by the thickening profile. The multi-attribute analysis was carried out by considering the three attributes presented in Sec. 8.3.2, which are H (the similarity between the geometrical moments invariant of H_u computed on each region and those of a reference shape), S (the standard deviation of the values of the pixels

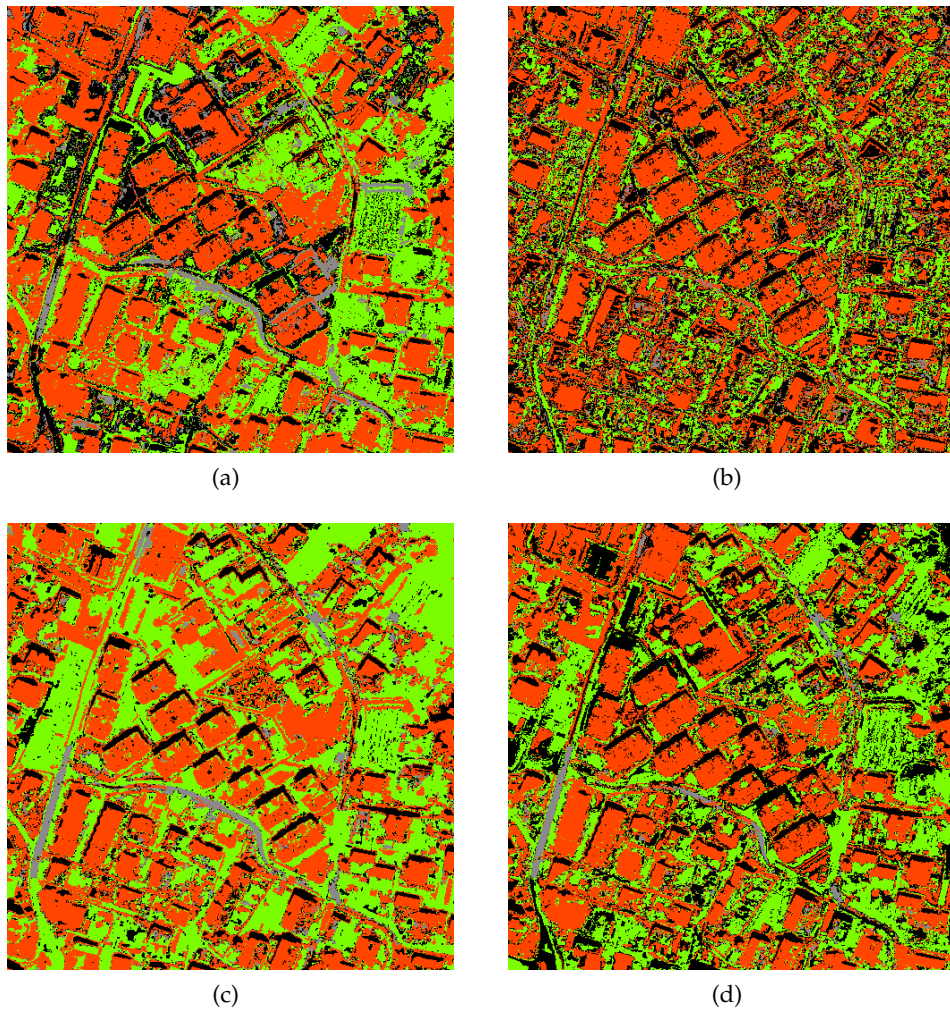


Figure 8.3: Classification maps obtained by: (a) MP; (b) AP with H attribute; (c) AP with HS attributes; (d) AP with HSA attributes.

belonging to each connected component), and A (the cardinality of the regions). The panchromatic image is processed according to the architecture shown in Figure 9.1. For all the attribute filters four different thresholds (λ) were selected leading to eight filtered images for each attribute (four from the anti-extensive and four from the extensive transformations). The total number of features handled by the system when the image is processed with the three attributes is 25 (8 for each attribute plus the original image). The GA used in the tuning of the filters parameters is a standard steady state GA, which is based on overlapping populations and elitism for selecting the best individuals to propagate through the next generations. The operations of mutation and crossover considered in the evolution of the population were the

basic ones since no problem specific implementation was considered. We used the implementation of the GA provided by the open source library GALib¹. The number of iterations was selected as stopping criterion and it was fixed to 500. The evaluation of the individuals of the population was based on a classification process and on the measure of a fitness function based on the overall accuracy of the classification map evaluated on the available labeled set. The experiments were carried out by considering two classifiers both trained on the available training set: a maximum likelihood and a random forest classifier [129]. The random forest classifier selected was composed by the ensemble of 100 decision trees. The number of variables investigated in each split of the tree was the square root of the total number of the input features. We considered for both the classifiers the implementations provided by the open source library OpenCV².

8.4.3 Results

The quantitative results obtained in the experiments are reported in the following tables. Table 8.2 shows the accuracies obtained by considering a maximum likelihood classifier, whereas Table 8.3 is relative to the random forest classifier. For both the tables, the first row refers to the classification of the panchromatic band alone, the second one indicates the results obtained by classifying the original image and its morphological profile. The last three rows report the results obtained by the proposed technique based on AP when the number of attributes considered in the analysis is increased. By analyzing

Table 8.2: Accuracies obtained by the classification with a maximum likelihood classifier of i) the original image, ii) the morphological profile and iii) the proposed method.

Class	Overall Accuracy (%)	Class by Class Accuracy (%)			
		Building	Road	Shadow	Vegetation
Pixel-based	31.89	6.18	0.00	100.00	82.20
MP (Square SE)	61.20	81.75	48.93	100.00	39.72
AP (H)	73.85	82.02	0.00	92.50	89.15
AP (H, S)	75.28	69.66	42.55	100.00	93.97
AP (H, S, A)	76.43	92.69	42.55	70.00	63.85

in details the obtained outcomes it is possible to state that the pixel-

¹ Available at <http://lancet.mit.edu/ga/>.

² Available at <http://opencv.willowgarage.com/wiki/>.

Table 8.3: Accuracies obtained by the classification with a random forest classifier of i) the original image, ii) the morphological profile and iii) the proposed method.

Class	Overall Accuracy (%)	Class by Class Accuracy (%)			
		Building	Road	Shadow	Vegetation
Pixel-based	27.01	6.18	42.55	0.00	100.00
MP (Square SE)	72.98	88.20	42.55	100.00	50.68
AP (H)	68.96	84.83	31.91	100.00	46.57
AP (H, S)	78.45	90.71	40.42	100.00	76.60
AP (H, S, A)	79.88	91.01	42.55	100.00	76.71

based analysis leads to unreliable results, also confirmed by the visual inspection of the classification maps (which are not reported here). This even further confirms the need of the inclusion of information on the spatial domain for better modeling the objects in the scene. When the structural information both modeled by a conventional MP or APs is included in the classification process the overall accuracy is strongly increased. By the joint analysis of the numerical results and the obtained classification maps it was possible to notice how the type of classifier used in the analysis matters. The maximum likelihood classifier proved to be non effective mainly due to the high redundancy shown by the morphological features and possibly their non-gaussian distribution. However, also with this elementary classifier it is possible to notice how the proposed multi-attribute approach improves the accuracies obtained by the use of the MP. The class specific accuracies are not showing a stable trend according to the features used. For this reason we believe that a non parametric classifier such as the RF can better handle the type of features to be analyzed.

We then choose to focus the following analysis only on the results obtained by the RF for which the classification maps are also reported (see Figure 8.3). By comparing the results in Table 3 obtained by including in the analysis the MP and the features generated by the multi-attribute processing, it is possible to state that when considering AP with only the attribute H, the accuracies obtained are definitely better than in the pixel-based case but slightly inferior than those obtained by the MP. This can be related to the attribute used. In fact, the similarity between the geometrical moments computed on each region with the square shape taken as reference might not be so discriminant as a conventional multiscale analysis. We remind that when selecting this attribute, the connected components in the image

are processed by only considering a parameter which is related to their shape and independent on the size of the regions. When the analysis is carried out by considering two attributes, both the overall accuracy and the specific accuracy for the building class overcomes those obtained by the MP. The proposed technique based on three attributes leads to the best accuracies which reach about 80% and 91% with a relative gain with respect to the analysis with MP of about 7% and 3% in overall accuracy and accuracy for the building class, respectively. From a specific evaluation of the maps it is worth noticing how the map obtained by the AP with H attribute appears fragmented. This could be caused by the attribute used which processes the image only according to parameters related to the shape of the regions. The inclusion of the standard deviation attribute in the analysis produces a more homogeneous map (Figure 8.3c) even if the criterion is also non-increasing. This is mainly due to the modeling the textural information on the structures in the image, which result in a better identification of the vegetation, buildings and roads (as confirmed by Table 8.3). The proposed technique based on the three attributes (Figure 8.3d) permits a slightly better characterization of the building objects with respect to the map obtained by the MP.

8.5 CONCLUSION

In this work we presented a morphological multi-attribute technique based on morphological attribute filters for the extraction of features suitable to the building extraction task. Attribute profiles were chosen in order to better modeling the structural information of the scene with respect to techniques based on morphological profiles that usually only perform a multiscale decomposition of the image. Moreover, the computation of morphological filters is also affected by the issue of the selection of proper filter parameters. We addressed this problem by defining an architecture based on genetic algorithms for tuning the parameters of the APs. In greater detail, the proposed technique performs a multi-attribute processing of the image. For illustrating the effectiveness of the proposed architecture on a real image, we proposed to use three attributes related to the characteristics of the buildings which are: i) the similarity between the structures in the image and a square shape taken as reference; ii) the standard deviation of the pixels values; and iii) the area of the regions in the image. The first attribute is related to the shape of the objects, the second to their spectral homogeneity, and the third to their scale. The choice of the parameters defining the multilevel analysis for each attribute is performed by the genetic algorithm, which evaluates the fitness of the proposed

solutions (filter parameters) by classifying the images obtained by the filtering and using the overall accuracy obtained on a reference labeled set. The classification was performed by both a maximum likelihood and a random forest classifier. The obtained results further confirmed the necessity of including information extracted by the spatial domain of the scene in order to generate consistent maps. Moreover, the high redundancy in the features (either generated by a morphological profile or by attribute profiles) is not properly handled by a simple parametric classifier such as the maximum likelihood (which may also be affected by the non gaussian distributions of the features). The results obtained by the proposed technique overcome those obtained by a standard approach based on morphological profiles of about 7% in the overall accuracy of the classification maps, proving the effectiveness of the presented method.

Part III

PROPOSED TECHNIQUES FOR IMAGE
SIMPLIFICATION AND CHANGE DETECTION

A GENERAL APPROACH TO IMAGE SIMPLIFICATION

Abstract. In this chapter a general approach based on morphological connected filters for the spatial simplification of very high resolution remote sensing images is introduced. Different operative scenarios are considered according to the information available on the scene for the analysis. In greater detail, the proposed approach is made up of two steps: i) the selection of the parameters defining the connected filters driven by the information available on the scene and on the specific application; and ii) the application of the tuned filter to the input image.

9.1 INTRODUCTION

The interpretation of remote sensing images is a complex task due to the overwhelming amount of information present in the scene, especially when dealing with images of very high geometrical resolution. In general, the interpretation of the scene can be obtained by considering only part of the whole information contained in the image. All the details that are irrelevant for the image understanding (which are different for different applications) can affect the quality of the analysis and should be removed or attenuated. From a theoretically point of view, the operation that is usually (implicitly or explicitly) done for coping with the huge amount of information is *image simplification in the spatial domain*, which aims at both reducing the complexity of the scene by removing some spatial details from the image and enhancing those characteristics which are more informative in the image for the specific application. In these terms, the image simplification can be thought as an “increase of the signal to noise ratio” of the image, where with signal and noise we intend the information that has to be extracted and removed, respectively. Different simplifications of the image are possible and the type of processing is driven by the application.

Part of this chapter is going to appear in:

M. Dalla Mura, J. Benediktsson, and L. Bruzzone, “A general approach to the spatial simplification of remote sensing images based on morphological connected filters,” in *2011 IEEE International Geoscience and Remote Sensing Symposium (IGARSS)*, 2011, Accepted.

Even a simple low-pass filter can produce a simplification of the image. However, it would also lead to a global degradation of the spatial features of the scene. Image simplification can be done with morphological connected filters [109]. Connected filters only operate on the flat regions of the image without introducing new discontinuities, thus they do not alter the shapes of the regions nor distort their edges. Due to their characteristics, connected filters are then suitable for the analysis of remote sensing images (especially when the spatial resolution is high) since a reduction of the complexity of the image without the detriment of the spatial characteristics of the objects of interest can be obtained [72, 91]. Actually, MPs and APs are composed by a sequence of versions of the original image with a progressively greater degree of spatial simplification. Their effectiveness in applications such as segmentation, classification, object detection, etc. proved how reducing the spatial complexity of the scene is essential for the analysis of remote sensing images.

In this paper we propose a novel general approach based on connected filters for the spatial simplification of remote sensing images. In greater detail, the image simplification is obtained in two stages: i) the parameters of the filters are tuned according to the requirements derived from both the specific application scenario and the available prior information on the scene (settings that define different operative scenarios); and ii) the image is filtered with a proper connected operator and the determined parameters.

9.2 PROPOSED GENERAL APPROACH

The proposed approach is composed of two modules that perform the operations of: i) selection of the parameters and operators; and ii) filtering. The first module interfaces with the external environment, collects information on the type of simplification required (if available) and translates the input requests into the settings of the filter. The second module computes the transformation of the input image through the application of the filter with the selected parameters. The flowchart showing the architecture of the proposed approach is presented in Figure 9.1.

9.2.1 *Selection of the Filter Parameters*

By considering in greater detail the selection of the filter parameters, we identified three possible operative scenarios:

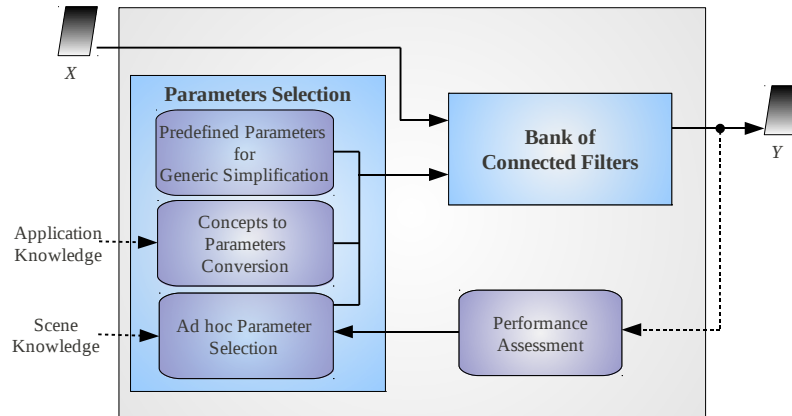


Figure 9.1: Flowchart of the proposed general approach for the simplification of remote sensing images based on connected filters.

1. No prior knowledge on the scene nor on the application is available;
2. No prior knowledge on the scene is available but there is knowledge on the application;
3. Both prior knowledge of the scene and of the application are available.

SCENARIO 1 In the first scenario a generic simplification is performed on the image. Since no hints are given on the kind of information that should be enhanced on the scene, the image can be processed by a predetermined criterion. For example, it can be performed a reduction of the image complexity by attenuating the noisy components (e.g., by removing small regions with greylevel significantly different from their surroundings) and by removing the effects due to the variability of the imaged natural scene which are not very significant for the interpretation of the scene (e.g., flattening small differences of the graylevels in homogeneous regions). Since the simplification obtained in this scenario should be useful for most of the applications, the filtered image should not be significantly different from the original in order to avoid the penalization of some objects or some image features over the others. The automation of the processing is simply done by defining the simplification criterion, since no other external interaction is possible.

SCENARIO 2 As defined for the second scenario, when the simplification aims at enhancing determined objects due to the knowledge of

the application but no specific information on the investigated area is available, the parameters of the filters should be selected in order to model the conceptual case of the analysis. For example, if one aims at highlighting the buildings but no actual knowledge on the buildings present in the image is available, the image can be filtered keeping all those regions with rectangular shape and a proper scale according to a general knowledge of the spatial characteristics of the buildings. The translation of the conceptual features to specific filter parameters (e.g., “keep rectangular regions” \Rightarrow attribute filter with criterion: $\{rectangularity > 0.5\}$) can be done in different ways. For example, the user can manually define the operators and the reference values of the attributes according to its conceptual representation of the objects of interest or, in order to automate the process, the relations between the attribute values and the concepts can be expressed by a fuzzy possibilistic model. In [113], a similar approach based on a fuzzy measurement of the characteristic size and contrast of each object in the scene, obtained from the interpretation of the derivative of the MP, was considered for classification.

SCENARIO 3 The selection of the filter parameters done in the third scenario is based on the information available on the investigated scene. If the available information is a set of labeled samples (i.e., a training set), the reduction of the image complexity generated by the filtering aims at decreasing the intra-class variability of the objects but keeping the inter-class variability. The quality of the simplification obtained is evaluated on the known samples according to a given criterion. The automation of the model selection can be performed iteratively by minimizing a cost function that represents the fitness of the generated result with the input requirements according to the criterion considered in the evaluation until a stopping condition is met.

9.2.2 Filtering

The filtering stage can be performed in different ways according to the connected operators chosen by the previous module. For example, if the objects of interest are “bright” (regions of high reflectance) then an anti-extensive operators (e.g., an attribute thinning) should be considered. When both bright and dark regions should be processed then a dual or self-dual operator is more effective. The different connected operators can be efficiently computed by exploiting the representation of the image as trees, such as min-, max- and inclusion-trees [109].

The architecture of the proposed approach can be also exploited for producing multiple simplifications of the considered image done at different levels (i.e., obtaining MPs and APs).

9.2.3 Discussion

The generality of the proposed approach relies also on the different types of remote sensing images that can be processed. Connected filters natively operates on optical scalar images (e.g., panchromatic band) but they can be extended also to multi- and hyper-spectral images (e.g., as proposed in [92]) or even to images acquired by active systems if proper operators and attributes suitable to modeling the characteristics of the Synthetic Aperture Radar (SAR) signal are selected. The characteristics of SAR images are completely different with respect to optical data. For example, the scene is represented in a geometry referred to the range dimension and furthermore, a multiplicative noise component (speckle) is present.

Several applications can benefit from the proposed approach since the simplification of the image is a fundamental preprocessing step in several tasks. In particular, the simplification aimed at enhancing some objects in the scene can ease the detection and extraction of the targets of interest. Moreover, the classification of the scene can exploit the reduction of the intra-class variability leading to a greater separation of the distributions of the different classes. A simplification producing the suppression of small non significant details can also be useful in the detection and monitoring of changes in the analysis of multitemporal images since it can lead to a reduction of the false alarm rate.

9.3 EXPERIMENTAL RESULTS

In the experimental analysis the first two operative scenarios (see Sec. 9.2.1) were taken into account. A Quickbird panchromatic image of 995×995 pixels and geometrical resolution of 0.6m acquired over a residential urban area of the city of Bam, Iraq, was considered (see Figure 9.3a).

By considering the first scenario, which assumes no knowledge of the application nor of the scene, a generic simplification was computed. The complexity of the original image was reduced by removing small bright and dark areas and by flattening the interior of homogeneous objects performing an adaptive quantization, which is a pruning of

the tree representing the image that keeps only one node in each monotone branch (segment of a branch between two subsequent bifurcations) [106].

When considering the second scenario, two different simplifications of the original image were performed aiming at enhancing a specific class of thematic objects (i.e., buildings) and a more generic set of areas such as the elongated dark structures (e.g., shadows casted by buildings, dark roads). The obtained simplified images are reported in Figure 9.3b, (c). Since no information on the scene was available, the parameters of the filters were estimated from the common knowledge of the characteristics of the objects of interest. It was assumed that buildings were represented in the image as compact and rectangular shaped regions with a size suitable for a residential building. Three attributes were considered: i) *moment of inertia* (measure of the spatial compactness of a region); ii) *rectangularity* (ratio of the area of a region and the area of its bounding box); and iii) *area* (the cardinality of the regions). Since in general the buildings are made of concrete that is characterized by a high reflectance (with respect to vegetated areas) an attribute thinning was considered as the operator performing the filtering. The simplification aimed at enhancing the dark areas was performed by selecting the following attributes: the *moment of inertia* (modeling the elongation) and the *height*, computed as difference between the maximum graylevel of the image and the level of each region (used for selecting the areas based on their low reflectance). The filtering was performed with an attribute thickening operator since the focus was on the dark regions. In these experiments the conversion from the conceptual characteristics of the target objects and the type of operator, attributes and thresholds was done manually. However, this process can be automated, e.g., by defining fuzzy possibilistic functions representing the membership of the attribute values for each operator and the characteristics to be modeled.

Figure 9.2 shows how the simplification performed on a particular of a building rooftop is able to keep most of the information of the scene with less flat regions. The number of connected components was reduced from 2789 for 9.2a to 1059 to 9.2c.

By a visual inspection of Figure 9.3b it is possible to notice that most of the buildings are kept unaffected by the filtering (even with some differences of the graylevel between the original image), while the background is flattened. Analogously, the structures present in Figure 9.3c mainly correspond to the shadows of the buildings and segments of the road network while all the other objects are erased by the filtering.

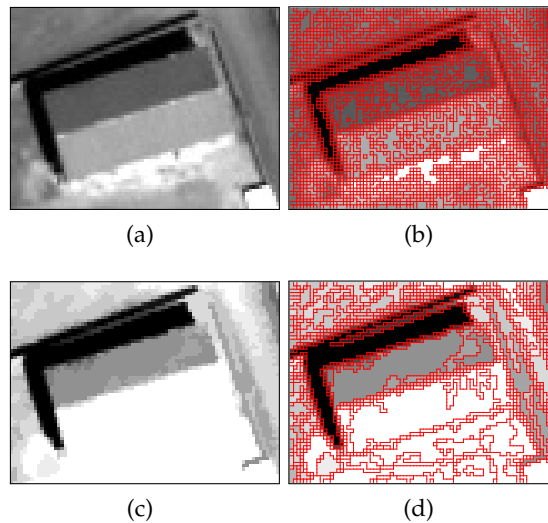


Figure 9.2: Bam data set: (a) Particular (80×60 pixels) of the Quickbird panchromatic image (Figure 9.3a) showing the roof of a building; (b) Contours of the flat regions of (a) (2789 regions); (c) Result of a generic simplification performed on (a) (removal of regions with area < 10 and flattening of object interior performed by adaptive quantization); (d) Contours of the flat regions of (c) (1059 regions). The greylevels of the images are stretched for visual purposes.

9.4 CONCLUSION

In this chapter, a general approach based on morphological connected filters for the spatial simplification of remote sensing images has been defined in three scenarios modeling common different operative conditions. The motivation of this work is the importance of image simplification as preprocessing transformation for several applications aiming at image interpretation and the lack of an explicit definition of an approach including the operations that lead to the process of image simplification. The effectiveness of the proposed approach has been confirmed by the qualitative results obtained on a very high resolution image. Moreover, the generality and the capability to be fully automated make the proposed approach of interest for many remote sensing applications.



(a)



(b)



(c)

Figure 9.3: Bam data set: (a) Quickbird panchromatic image (995×995 pixels); (b) Simplification enhancing the buildings (attribute thinning with criterion $\{(R > 0.3) \wedge (I < 0.5) \wedge (50 < A < 5000)\}$); and (c) Simplification enhancing the elongated dark areas (attribute thickening with criterion $\{(H > 10000) \wedge (I > 1.0)\}$). Attributes: R : rectangularity, I : moment of inertia, A : area, H : height.

CHANGE DETECTION TECHNIQUES BASED ON CONNECTED OPERATORS

Abstract. In this chapter, two multilevel techniques are proposed for change detection. The first presented technique deals with alternating sequential connected filters and self-dual reconstruction filters. The second technique is based on attribute profiles.

10.1 INTRODUCTION ON CHANGE DETECTION ON VHR IMAGES

Human development and natural forces continuously alter landscapes. The analysis of these variations is necessary in many tasks such as monitoring landuse, risk assessment, and the analysis of the worldwide population growth and development. For this reason, *change detection* (CD) has an increasing importance in the field of remote sensing. The images acquired by periodical passes of remote sensing satellites over the same areas permit a regular analysis of changes occurred on the ground. The large amount of available satellite data have led the remote sensing community to focus its attention on unsupervised change-detection techniques, where ground-truth information is not necessary.

In this scenario, with the launch of a new generation of optical satellites, such as IKONOS, Quickbird, Eros A1, very high resolution (VHR) images have been commercially available and their diffusion will further increase with the future World View satellites. The VHR images are characterized by a submetric resolution; thus, the acquired scenes show many details (e.g., small trees, particulars of buildings, cars, etc.) that were not observable by the previous generation sensors. In addition, the high resolution in representing the surveyed scene makes

Parts of this chapter were published in:

M. Dalla Mura, J. A. Benediktsson, F. Bovolo, and L. Bruzzone, "An unsupervised technique based on morphological filters for change detection in very high resolution images," *IEEE Geoscience and Remote Sensing Letters*, vol. 5, no. 3, pp. 433–437, July 2008.

N. Falco, M. Dalla Mura, F. Bovolo, J. A. Benediktsson, and L. Bruzzone, "Study on the capabilities of morphological attribute profiles in change detection on VHR images," in *Image and Signal Processing for Remote Sensing XVI - Proceedings of SPIE*, vol. 7830. Toulouse, France: SPIE, Bellingham, WA, 2010, pp. 783 016–1–783 016–10.

the contextual information a predominant feature in VHR images. In fact, unlike in low and medium spatial resolution images, the relations between adjacent pixels become a fundamental information source for the understanding of the scene. The high geometrical resolution and the contextual information are features particularly important in the urban scenes, opening new perspectives for CD applications.

A widely used unsupervised CD technique for medium resolution images is the change vector analysis (CVA). CVA can be divided into three phases [145]: i) *Pre-processing*, where the multitemporal images are made comparable through co-registration, geometric correction and radiometric calibration; ii) *Image comparison*, where the spectral differences between the two images are represented by computing the spectral change vectors (SCVs); and iii) *Analysis of the results of the comparison*, that aims at extracting the changed regions by generating a map where each pixel is associated to the class of changed ω_c or unchanged ω_u patterns.

In light of the properties of multitemporal VHR images (i.e., presence of a relevant amount of geometrical details, shadows, residual misregistration, multiscale objects), unsupervised CD in these data is a complex task [146]. Most of the CD methodologies presented within the last 30 years [145, 147] for low or medium geometrical resolution imagery cannot handle the geometric and textural information present in VHR images. In particular, standard *pixel-oriented* techniques based on the thresholding of the magnitude of the SCVs, result in change detection maps showing a great number of false alarms and artifacts [146].

According to the specific characteristics of VHR images, *object-oriented* approaches are more suitable to exploit the context relations. These approaches permit to drive the analysis of the multitemporal images by the spatial information extracted from the objects in the scene. In [71], an object-oriented method was presented, which decomposes the images at different resolution levels and exploits the multiscale structure for classification of VHR data. This method was extended to multilevel change detection in [148] by defining a multiscale CVA technique. In greater detail, the decomposition of the image into different levels permits to adaptively take into account the scales of the structures in the scene and to progressively reduce the complexity of the magnitude image. However, only relatively few CD techniques are available for VHR images and further research is necessary on this topic.

In the following two sections, change detection techniques using morphological connected operators are presented.

10.2 AN UNSUPERVISED TECHNIQUE BASED ON MORPHOLOGICAL CONNECTED FILTERS

10.2.1 Introduction

A very promising approach to the analysis of VHR remote sensing images is based on morphological filters. Morphological filters are non-linear operators defined in the *mathematical morphology* (MM) framework and widely applied to image processing problems. MM is based on the operators of erosion ε and dilation δ . The other morphological operators can be constructed by combining these fundamental operators [82]. In image processing, morphological filters are defined by a structuring element (which designs the shape and size of the filter) and a neighborhood transformation (which defines how the values of the pixels included in the SE are processed). The output of the morphological transformation shows how the image interacts with the size and shape of the SE. In this framework, morphological filters are formally defined as image transformations that are *idempotent* and *increasing* [82]. Since opening and closing satisfy these properties, they are morphological filters. The effect of an opening or a closing is basically to simplify the input image by erasing, respectively, bright and dark objects (in the meaning of brighter and darker than surrounding regions) in the scene, while preserving other structures in the image. Morphological filters are intrinsically object-oriented transformations because they focus the processing of the image on areas with a shape and size defined by the SE. These properties and the non-linearity of the morphological operators result very important for the analysis of VHR remote sensing images, especially for reducing the noise components by preserving the geometrical features of the objects into the scene. For these reasons, the application of morphological filters to VHR images was investigated in the context of segmentation [72] and classification [115] problems with convincing results. However, despite its potential effectiveness, MM was not used in change detection problems on VHR images.

In this section, we present a CD technique based on the integrated use of morphological filters and CVA technique. In particular, we define a processing scheme that jointly exploits the SCVs information and the capabilities of MM in properly separating the changes in multi-temporal images from the sources of noise. In addition, we present an analysis aimed at choosing the morphological filter more suitable for the analysis of SCVs derived from multitemporal VHR images.

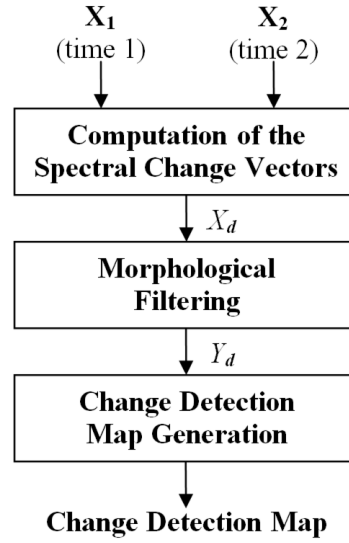


Figure 10.1: General scheme of the proposed technique.

10.2.2 Proposed Change-Detection Technique Based on Morphological Filters and Change Vector Analysis

10.2.2.1 Architecture of the Proposed Change Detection Technique

Let us consider two co-registered multispectral VHR images with B spectral channels, $\mathbf{X}_1 = \{X_1^b, 1 \leq b \leq B\}$ and $\mathbf{X}_2 = \{X_2^b, 1 \leq b \leq B\}$, acquired over the same area at different times t_1 and t_2 , respectively. Here each spectral image X_k^b , with $k = 1, 2$, has size of $I \times J$ pixels: $X_k^b = \{X_k^b(i, j), 1 \leq i \leq I, 1 \leq j \leq J\}$. Let $\Omega = \{\omega_c, \omega_u\}$ be the set of classes associated with changed and unchanged pixels. It is assumed that an adequate pre-processing phase has been applied to the multitemporal images in order to make them as more comparable as possible. In particular geometric corrections, co-registration, and radiometric corrections should be applied to the data.

The proposed CD technique is made up of three steps: i) computation of the SCVs; ii) morphological filtering; iii) generation of the map of changes (Figure 10.1). The comparison between the multitemporal multispectral images \mathbf{X}_1 and \mathbf{X}_2 is obtained through the CVA technique. The magnitude of the SCVs (which is associated to an image called difference image X_d) contains information about the changes occurred between the two acquisitions. As any greyscale image, the difference image can be thought as a topographic map, where the greyscale intensity of each pixel is associated to a measure of elevation. According to this interpretation, a higher intensity value (i.e., a brighter pixel in the image) corresponds to a higher elevation in the related topographic map. Hence, it is possible to characterize the structures present in the

image in terms of convexity and concavity, where these properties are associated to areas of high and low intensity, respectively, w.r.t. the surroundings. The presence of convex regions (areas made up of pixels with high intensity) is due to a difference in the spectral signature of the correspondent regions on the ground (which can be associated to a change occurred between two acquisitions [145]). Different phenomena during the acquisitions (e.g., illumination of the scene, sensor view angle, etc.) and the presence of noise (mainly due to the residual misregistration between the multitemporal images) lead to the presence of convex portions in the magnitude image associated with unchanged areas. In general, the residual misregistration appears in the difference image as thin and elongated convex regions, which corresponds in the scene to the borders of well defined structures (e.g., buildings, streets, rivers etc.) or textured areas (e.g., the patterns on the rural fields) [146]. Differences in the scene illumination and sensor view angle result in shadows with different positions and shapes in the multitemporal images. These differences appear in the magnitude image as convex regions made up of pixels with intensity comparable to those of patterns that belong to changed areas. If no prior information about the shape and the size of the changed objects is available, it is not possible to distinguish a real change from these regions by analyzing only the magnitude of the SCVs. These effects are the main source of errors in the generation of the CD map.

In the proposed technique, after CVA, the complexity of X_d is reduced with the filtering phase, carried out by a morphological filter, which is applied to the magnitude of the SCVs. If the decision phase is based on the analysis of the image statistics computed on the magnitude of the SCVs, the filtering process should not alter the distribution of the data. Thus, the morphological filter should fulfill the property of self-duality, guaranteeing that convex and concave structures are equally processed. The transformation resulting by the application of a morphological filter, depends on the shape and the size of the SE. Filtering with relatively small SEs results in: i) Removing structures that are brighter and darker than the surroundings, ii) reducing noise present into the image, and iii) flattening light textures on the object surfaces. In other words, the size of SE defines the grade of the simplification reached on the resulting image, determining how many details or small changes will be deleted from the image. Obviously, the larger the SE size, the greater the simplification and the coarser the resulting image. The shape of the SE is another important parameter. For CD problems without any *a priori* information about the shape of the changed areas, it is reasonable to chose an isotropic SE that processes the image without preferring any specific direction. In this

scenario the choice of a SE with a disk shape can be considered the most general, because the pixels in the perimeter of the neighborhood have the same distance to the center. On the contrary, if information about the investigated changes is available, the shape and size of the SE can be selected according to the geometrical characteristics of the objects in the scene. For example, in an urban area a rectangular shaped SE would better match the building shapes; in this scenario, the size of the SE could be chosen taking into account the average dimension of the analyzed structures.

Finally, the CD map can be generated according to one of the unsupervised CD techniques proposed in the literature for the analysis of X_d [147]. Each pixel, in the final CD map, belongs to the class of changed ω_c or unchanged ω_u patterns.

10.2.2.2 Morphological Filters for Change Detection in VHR Images

The morphological filters applied to the magnitude of the SCVs permit us to erase convex and concave regions of a defined shape and size. This leads to a simplification of the difference image and a reduction of the noise components. Nevertheless, considering the SCVs computed from two multispectral VHR images, the selection of a proper morphological filter is not a trivial task. The complexity of X_d needs to be reduced preserving its geometrical information. If we consider standard morphological filters, (e.g., morphological opening, γ , which is the dilation of an eroded image, and morphological closing, ϕ , which is the erosion of a dilated image) the simplification of the magnitude image would be reached with a partial loss of the geometrical information.

In order to properly exploit the very high resolution representation of the details in the scene, we propose the use of self-dual reconstruction filters (SDRFs) and alternating sequential filters (ASFs), both based on morphological operators by reconstruction. The morphological filters by reconstruction, defined by new advances in MM, are based on a non-Euclidean metric [149]. This family of filters is effective in applications where the geometrical information has to be preserved. These operators simplify the difference image by erasing the structures that interact with the SE, but preserve the shape of those that are not canceled. Their use permits also to avoid typical drawbacks of the morphological classical operators as the shape noise (i.e., presence in the output image of patterns with the same shape as the SE used) and the shift of the object borders [82], which can compromise the analysis of VHR images.

SDRFs are operators based on the self-dual reconstruction. SDRF could be designed as a median filter, followed by a self-dual recon-

struction using the original image as a mask (this operation retrieves the geometry of structures that are degraded but not erased by the median filter). The application of a median filter and the self-dual reconstruction guarantees the equal processing of concave and convex structures, satisfying the property of self-duality. According to [82], the self-dual reconstruction of the median filter of the difference image X_d can mathematically be expressed as:

$$\Upsilon_d^{SDRF} = R_{X_d}[\zeta^{(i)}(X_d)] \quad (10.1)$$

where R is the self-dual reconstruction operator and $\zeta^{(i)}$ is the median filter operator with SE of size i (defining the SDRF size). By increasing the size of the median filter, a greater simplification of the image (enlarging the flat zones) is achieved.

ASFs, a sequential composition of opening and closing by reconstruction, are defined as follows:

$$\Upsilon_d^{ASF_m} = M_i = m_i \dots m_1(X_d), \quad \text{with } m_i = \gamma_R^{(i)} \phi_R^{(i)}, \quad (10.2)$$

$$\Upsilon_d^{ASF_n} = N_i = n_i \dots n_1(X_d), \quad \text{with } n_i = \phi_R^{(i)} \gamma_R^{(i)}, \quad (10.3)$$

where m_i is the sequence of a closing by reconstruction followed by the dual opening with a SE of size i , while n_i is the combination of an opening followed by a closing. The opening and closing by reconstruction with size i of a general image f are based respectively on the reconstruction by dilation, R^δ , and the reconstruction by erosion, R^ϵ , [82]:

$$\gamma_R^{(i)}(f) = R_f^\delta[\varepsilon^{(i)}(f)] \quad \text{and} \quad \phi_R^{(i)}(f) = R_f^\epsilon[\delta^{(i)}(f)]. \quad (10.4)$$

The reconstruction performed using the original image as a mask leads to the iterative degradation of the image but restores partially its geometrical information. The processing driven by using the original image as a mask consists of progressively "flattening" the object surfaces while preserving their borders. The robustness of ASF against the noise is well known in the literature [84], where it has been used mostly in applications on SAR imagery (e.g., despeckling). Nonetheless, ASF has already been used on VHR imagery for classification. Chanussot *et al.* [112] have shown how this operator is well suited for a progressive simplification of the VHR image. Therefore, the idea of applying this operator to the CD task is very promising. The sequence of an opening and closing (or its dual) can be iterated several times increasing the size of the SE at each iteration. By iterating the filter, larger regions are processed involving a reduction of the image complexity. It is possible to filter the difference image through the sequences of open-close or close-open. These operators are dual with

respect to the set complementation but not self-dual, i.e., leading to different results when one is applied instead of the other. Choosing for instance, n , the open-close sequence, narrow bright structures would be suppressed by the starting opening. By duality, if closing is selected first, as for m , small darker structures would be removed first. Considering VHR images, in the first iteration of the ASF, the SE has the smallest dimension (if we consider a disk, it would have the diameter of 3 pixels equivalent to about 2 meters at nadir on a panchromatic Quickbird image having resolution 0.7 m). The first iteration of the ASF (with the smallest filter size) filters the noise present into the image. After that, the choice of the open and close sequence is not really significant because the geometrical resolution is much higher than the minimum target size [72].

10.2.3 *Experimental Results*

The proposed method was evaluated on a data set of multitemporal and multispectral VHR images acquired by the Quickbird sensor on the Trentino area (Italy) in October 2005 and July 2006. In the pre-processing phase the two images were pan-sharpened generating a new set of multispectral images with the same geometrical resolution of the panchromatic band. The pan-sharpening was carried out by applying the Gram-Schmidt procedure implemented in the ENVI software package [150] to the panchromatic channel and the four bands of the multispectral image. Moreover, the multitemporal images were radiometrically corrected and co-registered. The registration process was carried out by using a polynomial function of order 2 according to 14 ground control points (GCPs), and applying a nearest neighbor interpolation. The final data set was made up of two pan-sharpened multitemporal and multispectral images of 992×992 pixels with a spatial resolution of 0.7 m, which have a residual misregistration of about 1 pixel on GCPs (Figure 10.2). Between the two acquisition dates, two kinds of changes occurred: i) New houses were built in rural area; and ii) some roofs in industrial and urban areas were rebuilt. Different illumination of the scene (due to different acquisition seasons) and a different acquisition angle during the imaging are the reasons for the presence of a great number of not correspondent shadows in the two images. It is worth noting that the different illumination in the two multitemporal images modifies the spectral response of some unchanged areas.

In applying the proposed CD technique, the comparison between the two multitemporal images was carried out by computing the magnitude of the SCVs obtained by CVA after the data normalization.

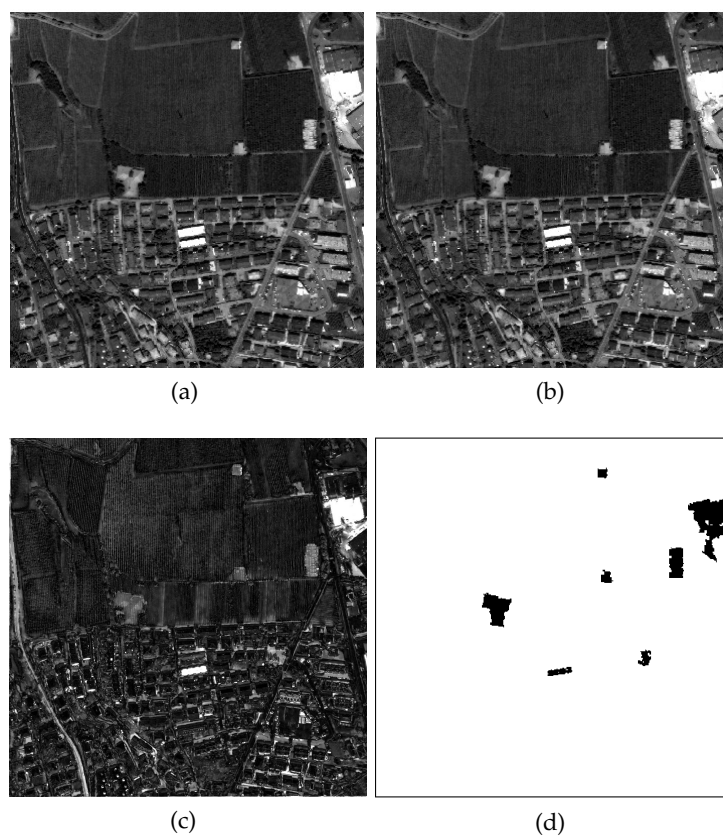


Figure 10.2: Gray scale representation of the pan-sharpened multispectral and multitemporal images acquired in (a) October 2005 and (b) July 2006; (c) magnitude of the spectral change vectors computed from (a) and (b) (the image is visually enhanced) and (d) reference map.

Table 10.1: Change-detection errors (in number of pixels and percentages) obtained by using the proposed technique.

Method	Filter Size	Correct Detections		False Alarms		Missed Alarms		Total Errors	
		pixels	%	pixels	%	pixels	%	pixels	%
Standard CVA		15396	73.60	64502	6.70	5522	26.40	70024	7.12
CVA with SDRF	9	17595	84.11	67682	7.03	3323	15.89	71005	7.22
	13	18692	89.36	69181	7.18	2226	10.64	71407	7.26
	17	18689	89.34	61510	6.39	2229	10.66	63739	6.48
	21	18680	89.30	53963	5.60	2238	10.70	56201	5.71
	25	18680	89.30	47867	4.97	2238	10.70	50105	5.09
CVA with ASF	9	19465	93.05	62605	6.50	1453	6.95	64058	6.51
	13	19682	94.09	47688	4.95	1236	5.91	48924	4.97
	17	19851	94.90	42898	4.45	1067	5.10	43965	4.47
	21	18779	89.77	16382	1.70	2139	10.23	18521	1.88
	25	17880	85.48	15679	1.63	3038	14.52	18717	1.90

The difference image was processed with a SDRF and an ASF by reconstruction using, for both the operators, a SE with disk shape. In ASF, the sequence close-open, m , was chosen. The final map of changes was obtained by thresholding the filtered image with the automatic technique based on the Kittler and Illingworth (KI) method [151] under the Gaussian assumptions. However, other thresholding techniques can be used [152].

In order to allow a quantitative evaluation of the effectiveness of the presented method, the CD map generated by the proposed technique was compared to a reference map (which includes 20918 changed pixels and 963146 unchanged pixels) defined according to the available prior knowledge on the considered area. The results presented in Table 10.1 permit us to assess the effectiveness of the proposed technique with respect to the standard pixel-based CD procedure based on the CVA. In particular, when considering a disk SE of diameter 17 pixels, the number of missed alarms (MAs) sharply decreases of 15.74% and 21.30% for the SDRF and the ASF, respectively; in both cases the false alarms (FAs) decreases to less than 3%.¹ Furthermore, Table 1 shows that by increasing the size of the filters, the number of FAs (mostly due to both the different acquisition conditions at the two dates and the residual registration noise) is progressively reduced. The ASF by

¹ Missed alarms and false alarms are also referred in the literature as false negatives and false positives, respectively.

reconstruction leads to a significant reduction of the number of FAs, but the MA rate is strongly dependent on the filter size. In greater detail, changed regions with the same size of the SE are removed (this implicitly defines a minimum bound on the size of detectable changed objects). If we compare the results obtained by the ASF with those yielded by the SDRF in similar conditions on the SE size, we can observe that with the SDRF the complexity of the difference image is not reduced as much as applying the ASF, but the MA rate is less sensitive to the size of the filter. This was expected from the SDRF definition, which permits the preservation of the structures that are not removed by the median filter even if they are smaller than the SE.²

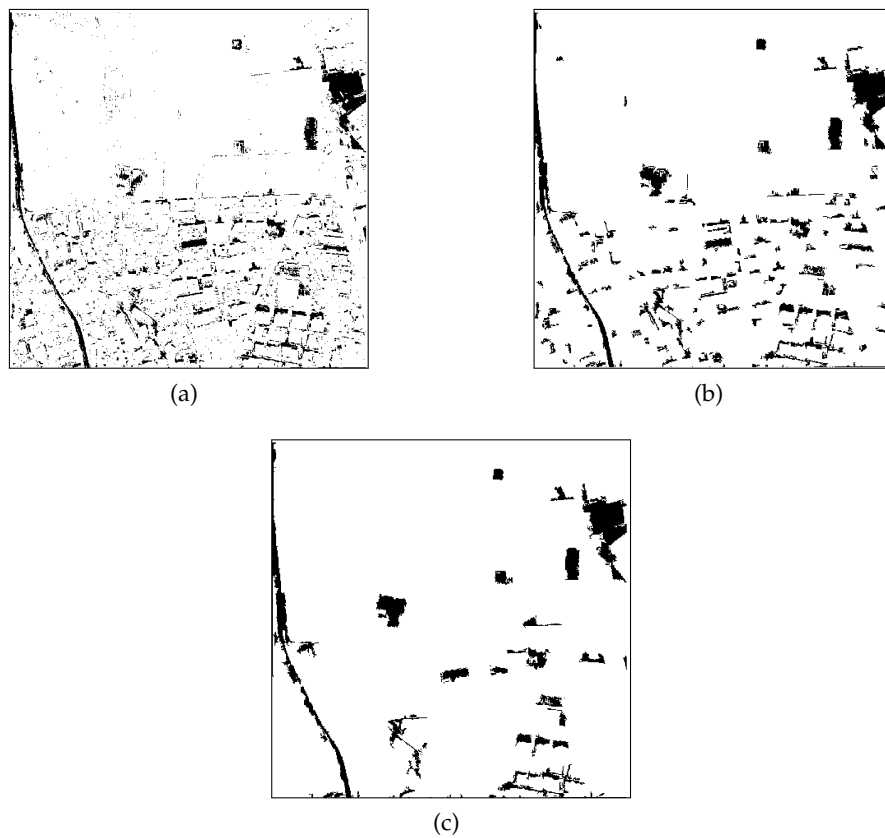


Figure 10.3: Change-detection maps obtained (a) by applying the standard pixel-based method and the proposed technique (b) with a SDRF and (c) with an ASF by reconstruction with open-close sequence. Both the filters were applied with a disk SE diameter of 17 pixels.

² As a general guideline, the maximum value of the filter size should be not higher than the expected minimum size of changed areas.

The qualitative analysis of the CD maps presented in Figure 10.3 confirms the effectiveness of the proposed technique. The comparison of the maps generated by the standard CVA (Figure 10.3a) and the proposed method (Figure 10.3b and 10.3b) with the reference map (Figure 10.2d) leads us to conclude that the use of morphological filters attenuates significantly the noise associated with FAs in the CD process. In particular, the effects of the residual registration noise are strongly reduced by the proposed approach. Moreover, the use of both considered morphological filter types leads to a better exploitation of the spatial correlation of the adjacent pixels in the images, thus increasing the detection of changed structures and reducing the residual noise.

10.2.4 Conclusion

In this section, a technique for change detection in VHR images based on morphological filters has been proposed. The method is based on the integration of morphological filters by reconstruction (alternating sequential filters and self-dual reconstruction filters, specifically selected and tuned for the processing of VHR images) with the CVA technique. This technique exploits the strong non-linearity characteristic of the morphological operators for filtering the VHR images, while preserving their geometrical information and exploiting the contextual relations.

The aforementioned method was evaluated on a data set made up of two real multitemporal and multispectral VHR images. From the analysis of the obtained results, the proposed method confirms to be effective in detecting the changed areas in a more accurate and precise way with respect to the standard pixel-based CVA technique. Moreover, the use of morphological filters by reconstruction, especially the ASFs, permits to decrease the error rate by exploiting the high geometrical resolution of the data with a limited computational effort. In fact, the details of the changed structures are extracted by preserving their geometrical properties.

10.3 STUDY ON THE CAPABILITIES OF MORPHOLOGICAL ATTRIBUTE PROFILES IN CHANGE DETECTION ON VHR IMAGES

10.3.1 Introduction

In this section we propose a change detection technique based on morphological Attribute Profiles (APs) suitable for the analysis of VHR images. In greater detail, this work aims at detecting the changes

occurred on the ground between the two acquisitions by comparing the APs computed on the image of each date. The experimental analysis has been carried out on two VHR multitemporal images acquired by the Quickbird sensor on the city of Bam, Iran, before and after the earthquake occurred on Dec. 26, 2003. The experiments confirm that the APs computed at different dates show different behaviors for changed and unchanged areas. The change detection maps obtained by the proposed technique are able to detect changes in the morphology of the correspondent regions at different dates regardless their spectral variations.

10.3.2 *Proposed Change Detection Technique Based on Morphological Attribute Profiles*

The proposed technique aims at detecting changes by comparing, at each pixel, the behavior of the AP computed on the image of each date. The starting assumption is that on the pixels belonging to unchanged areas, having similar spatial characteristics, the effect of the filtering would be similar, i.e., obtaining similar profiles. Instead, for pixels belonging to changed areas we obtain profiles with significant differences at the considered acquisition dates. For example, if we compare two multitemporal profiles of a single pixel of an unchanged building, in general, they show a similar trend till the level in which the building structure is merged to an adjacent region by the filter. Considering the subsequent levels, profiles can result different since the information of the building structure is lost. However, the comparison of the profiles is not trivial. In fact, if the comparison is performed on all the levels of the profiles inconsistent results might be obtained. By a qualitative analysis of the behaviour of the profiles it came out that the comparison between levels of the profiles is reliable until a certain level (usually when the objects in the image are canceled and thus, their structural characteristics are lost). Because of side effects (e.g., different seasons of acquisition and a different view angle sensor introduce different illumination in the scene and a different shape effect) that involve in radiometric variations, the two classes of change and no-change can be confused, making a direct comparison between the profiles inappropriate. These mismatches between the analyzed images make a spectral comparison of the multitemporal images difficult and thus the characterization of the objects within the scene. In order to give a context meaning to the profile, for each pixel must be taken into account a different range of values of the used attribute. The following technique, focusing on the geometrical changes, aims at performing a comparison of the profiles taking into account the

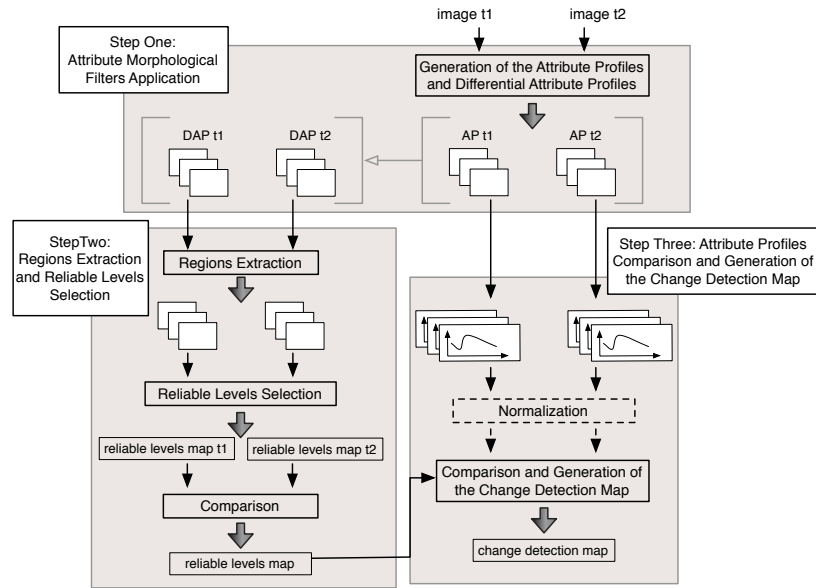


Figure 10.4: General scheme of the proposed technique.

different spatial contextual information on each analyzed pixel. The processing flow of the proposed architecture is based on three main steps:

1. Application of the attribute morphological filters;
2. Regions extraction and reliable levels selection;
3. Comparison of the attribute profiles and generation of the change detection map.

STEP ONE: APPLICATION OF THE APS The first step aims at computing on each multitemporal image an AP and the corresponding DAP, using the attribute of *area*. The obtained images of the APs show a multiscale filtering of the input images. In the closing profile dark regions are shown, whereas in the opening profile we can find the bright ones. The behavior of the APs is characterized by a monotonous decreasing trend of gray levels from the components of closing to opening ones. Since the DAPs are generated by computing the derivative of APs, they show peaks in correspondence of changes in the values of APs. A DAP is calculated as the difference between a given level of the relative AP and the its previous level.

STEP TWO: REGIONS EXTRACTION AND RELIABLE LEVELS SELECTION This phase focuses on the analysis of the DAPs, in order to

extract the objects in the scene. By analyzing the mono-dimensional trend of the DAPs it was noticed that:

- for each peak in the DAP, a region is present in the DAP at the level correspondent to the peak (which is the region canceled by the current level of filtering);
- the intensity value of each peak in the DAP is related to the gray level of the region which was erased by the filter;
- in general, a pixel can have several peaks in the DAP (i.e., the pixel belongs to completely different regions at different levels of resolution);
- some regions are more relevant than others in representing the object which the pixel belongs to.

From the analysis of the DAPs, it is possible to find a level of resolution that can more properly represent each object.

In order to perform the extraction of the regions, it is necessary to apply a binarization to each level of resolution in order to extract all the connected regions that have values greater than zero (see Figure 10.9), since the images of the DAP are in grayscale. Subsequently, we compute some measures on the regions at each level of the profile as proposed in [123], in order to find the levels in which each region is best represented from a perceptual point of view leading to the selection of the reliable levels. Two parameters are taken into account: standard deviation and spatial dimension of a given region. The method is based on the consideration that meaningful regions are homogeneous. Taking into account that a single pixel would be the most homogeneous region, the joint use of the mentioned parameters ensures that a region selected as meaningful will be as spectrally homogeneous and large as possible. Thus, for each region, belonging to each date, the reliable level R is computed according to the following criterion:

$$R = \hat{n} : \max(M(n)) \quad \text{with} \quad M(n) = D(n, \text{parent}(n)) \cdot C(n) \quad (10.5)$$

with n the level in the DAP, $D(\cdot)$ the standard deviation computed between the pixels in region of n and its *parent* region (i.e., the region in the previous level), and $C(\cdot)$ the area of the region.

In general, a given region in the AP becomes large after a number of filtering steps, reaching a level in which it will merge with the surrounding ones (level at which it will appear in the DMP), losing partially or completely its physical structural meaning. Consequently,

the level at which we are interested in, usually corresponds to the value that precedes this effect. This approach was applied on both the closing and opening profiles separately, obtaining for each date a map of the reliable levels for both the closing and opening profiles. Between the obtained maps we computed the maximum in order to generate for both closing and opening operations a unique multi-temporal reliable levels map (Figure 10.5a and 10.5b). Moreover, by considering the greater level (i.e., coarser image) permits to maximize the differences between the profiles associated to the changed areas, since the comparison of the profiles is performed until the selected level. In fact, by performing the comparison of the profiles until the greatest level is reached can show a difference in the behavior of the profiles due to the change.

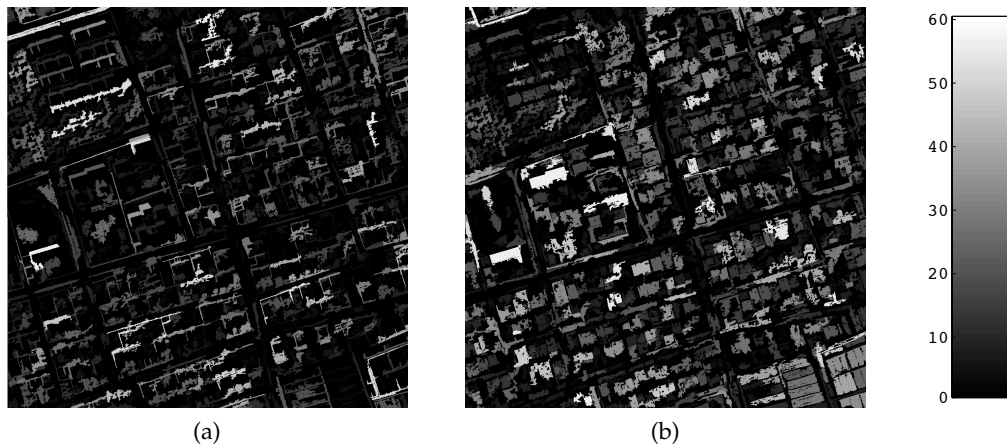


Figure 10.5: Reliable levels maps obtained applying the relation (10.5) to: (a) the closing component; (b) the opening component.

STEP THREE: COMPARISON OF THE ATTRIBUTE PROFILES AND GENERATION OF THE CHANGE DETECTION MAP In the last step, a comparison between the profiles of each pixel belonging to the images of the two dates is performed. Also in this phase, the components of closing and opening are analyzed separately. It is expected that unchanged areas show similar behaviors in the AP, whereas changed zones have a different trend in the profile.

In order to reduce the effects of radiometric variation in acquisition which is not associated to a real change, the values of the APs for each pixel are normalized on all the range of values considered for λ in order to sum to one. Then the APs for each pixel p in the two multitemporal images are compared till the reliable level R , defined at

the previous step. The *change indicator* (CI) is obtained applying the following definition to all pixels:

$$CI(p) = \sum_{l=1}^R |AP_{t1}(p, l) - AP_{t2}(p, l)| \quad (10.6)$$

Finally, the binary change detection map can be obtained by thresholding the above defined change indicator. In our experiment a manual trial and error thresholding procedure was adopted.

10.3.3 Experimental Results

10.3.3.1 Data set description

The proposed method is evaluated on a data set of multitemporal panchromatic images acquired by the Quickbird sensor with geometric resolution of 0.6 m. The images show an area of 1000×1000 pixels of the city of Bam, Iran, acquired in September 2003 and March 2004, Figure 10.6a and 10.6b, respectively. The considered area represents an urban area made up by small buildings. After the earthquake occurred on 26th December 2003, most of the buildings were destroyed, an undamaged area is located in the left side of the images, characterized by some large buildings. It is possible to notice the presence of a different illumination due to the different acquisition seasons which results in shadows differences.



Figure 10.6: Panchromatic images: (a) September 2003; (b) March 2004.

10.3.3.2 Experimental results on two subsets of the considered data set

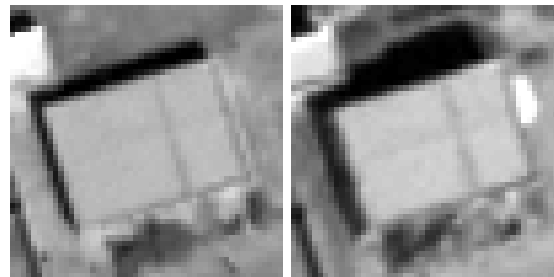
An analysis of the effectiveness of the proposed method is carried out on two small subsets of the considered data set. The two regions are

selected such as one presents a building that did not collapse after the earthquake and one that was completely destroyed.

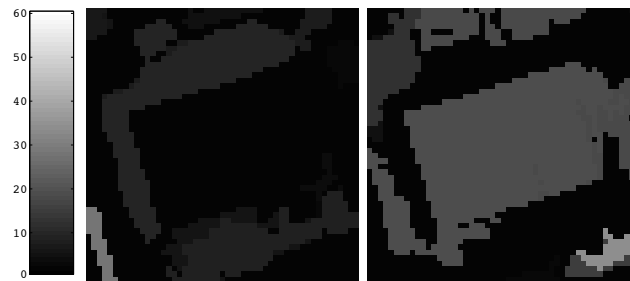
In this example we report the results obtained in steps two and three of the proposed method in order to show the different behaviors of the proposed representation in changed and no-changed areas. In step two we computed the closing and opening components of the reliable levels map applying in (10.5) and computing the maximum between the reliable levels maps belong to both dates. In the third phase the closing and opening components of the change indicator map are obtained applying the comparison (10.6) between the normalized APs. We can see the effectiveness of the meaningful region selection of the method. The changes associated to shadows are shown by the closing component of the change indicator map in Figure 10.7c, while the changes of the buildings are well represented by the opening component in Figure 10.8c.

10.3.3.3 *Experimental results on the entire data set*

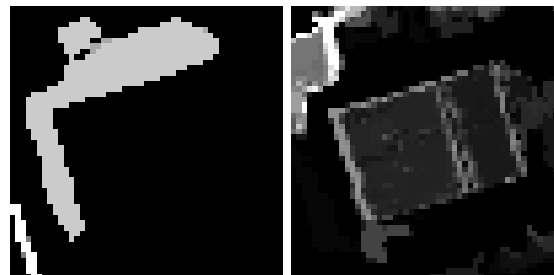
For both images a 121-dimensional AP and a DAP of 120 dimensions were generated using the attribute *area* with a range of values between 0 - 3000, and a constant step increase of 50 pixels. An example of DAPs binarization is shown in Figure 10.9. The chosen range of values is related to the dimension of objects in the scene. The comparison between the two multitemporal images was carried out by computing the difference between the APs taking into account for each pixel its reliable level. The comparison is performed for both the closing and opening profiles (Figure 10.10a and 10.10b). The final change detection maps (Figure 10.11a and 10.11b) are obtained by applying a trial and error thresholding procedure to the change indicator maps. In order to allow a qualitative evaluation of the effectiveness of the proposed approach, the final maps are compared with a change detection map obtained by applying the standard CVA (Figure 10.11c). The proposed technique permits to detect the changes preserving their geometrical information resulting more homogeneous and spatially precise than the map obtained with the standard CVA. For the considered data set: the CD map given by opening shows most of the changes occurred on buildings, while, the CD map corresponding to closing shows the changes mostly due to variations on the shaded areas. The maps obtained with the proposed technique show changes related to the geometrical changes in contrast with the CVA map, which shows spectral changes.



(a)



(b)

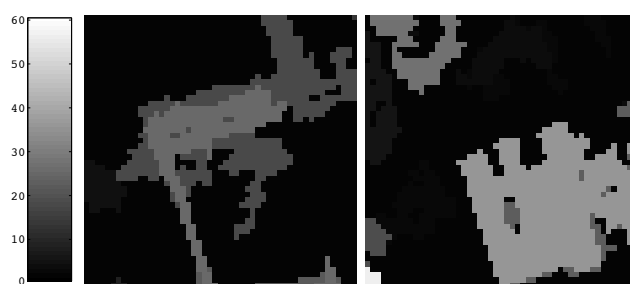


(c)

Figure 10.7: Example of unchanged region: (a) region at dates t_1 and t_2 , left and right respectively; (b) closing and opening components of the reliable levels map, obtained in step two; (c) closing and opening components of the change indicator map, obtained in step three.



(a)



(b)



(c)

Figure 10.8: Example of changed region: (a) region at dates t_1 and t_2 , left and right respectively; (b) closing and opening components of the reliable levels map, obtained in step two; (c) closing and opening components of the change indicator map, obtained in step three.

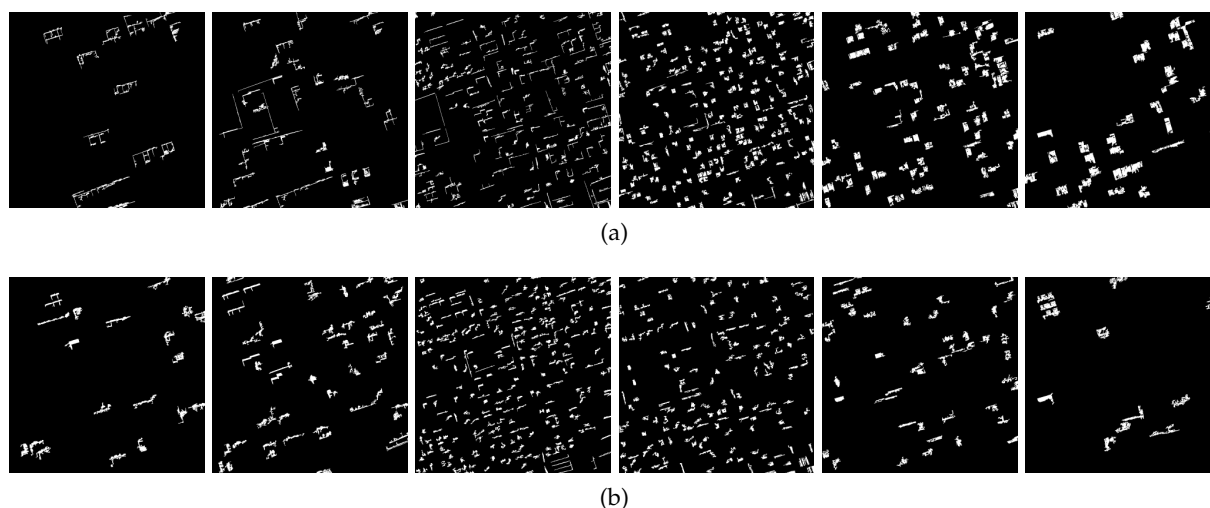


Figure 10.9: DAPs binary maps: (a) September 2003; (b) March 2004. The images show the multilevel behavior of the profiles. From left side we have: closing profile at levels 28, 19, 6 of λ and opening profile at levels 8, 19, 37 of λ .

10.3.4 Conclusion

The APs have proved their effectiveness in integrating the geometric information in the classification and segmentation tasks. In this section we proved their effectiveness also in change detection field. A new change detection technique based on attribute profiles has been proposed for a multitemporal VHR data set.

For each pixel a region-based analysis is performed in order to find the meaningful level of resolution, thus, the APs computed on the image of each date are compared. The attribute filters are able to decrease the complexity of the images and the change detection maps obtained with the proposed method show areas that changed their geometry during the two acquisitions independently from spectral variations.

By applying the proposed approach, geometrical information related to the objects is preserved, and moreover, the application of the APs permits us to automatically separate the changes occurred on dark areas, mostly composed by shadow regions, from those occurred on bright regions, mostly composed by buildings, that appear in closing and opening, respectively.

The qualitative analysis of the results obtained considering two VHR images of Bam, Iran, proved that the change detection maps obtained with the proposed technique are qualitatively more accurate and spatially precise with respect to the one obtained by the standard pixel-based CVA approach. As future developments we plan to: i)

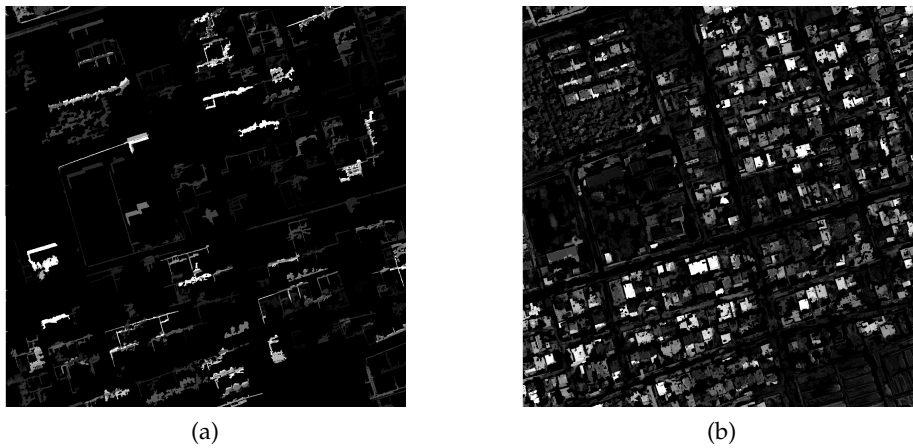


Figure 10.10: Change indicator maps obtained applying the relation (10.6): (a) closing profile; (b) opening profile.

improve the level of automatization of the proposed method; ii) test it on data sets with different characteristics and on different change detection problems; and iii) perform a quantitative evaluation of its performance.

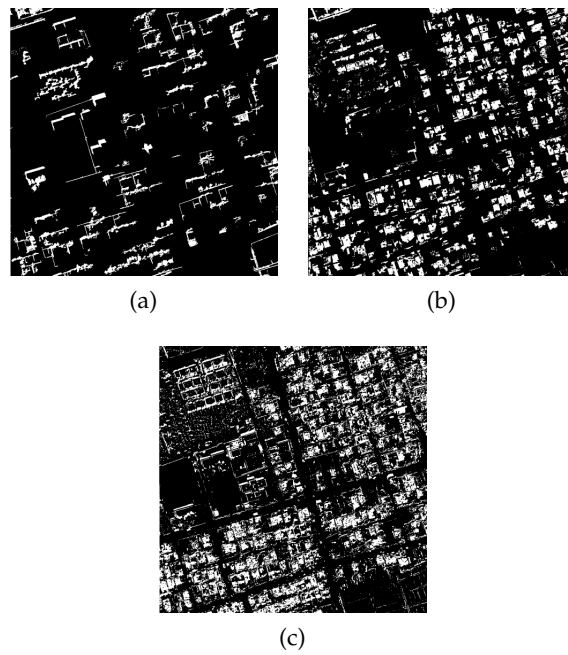


Figure 10.11: Final map obtained after the thresholding: (a) closing component; (b) opening component; (c) CVA.

CONCLUSION

Abstract. This chapter presents a general discussion of the work described in this thesis reviewing the main contributions of this research. Specific concluding remarks on the research topics treated in the dissertation are also given. Finally, perspectives on possible future developments of the work are presented.

The inclusion of the spatial information in any form (e.g., modeled as contextual relations, by descriptors of the structures in the image, as relations between different type of objects, etc.) is essential for all the analysis dealing with optical remote sensing images, especially when the geometrical resolution is high. Thus, the analysis of the scene must take into consideration the characteristics extracted by the spatial domain, along with the spectral signatures of the pixels, for a proper exploitation of all the available informative components. In this applicative scenario, mathematical morphology provides tools for the processing of the data that have already proven their usefulness and effectiveness for conveying spatial information in the analysis.

The work presented in this dissertation addressed the problem to model the spatial information with novel techniques based on mathematical morphology for applications such as: i) thematic classification; ii) image simplification; iii) building extraction; and iv) change detection. The proposed techniques were defined for dealing with panchromatic and multi-/hyperspectral images.

As a general conclusion of the research carried out, the following observations can be made:

- In all the applications addressed by our work, connected operators demonstrated to be suitable for performing analyses that require the preservation of spatial characteristics of structures of interest while suppressing uninteresting components in the scene. Connected operators transform the image by only merging flat regions. Thus, features as edges and shapes cannot be distorted but only either completely canceled or kept unaffected.
- Morphological attribute filters are very flexible operators. Moreover, they are connected operators so they do not alter the edges of the regions. The freedom in selecting the attributes allows one to set up a filtering of the image which can suit the needs

of the application. Attribute filters have a greater capability in performing a transformation that suits the aim of the analysis (e.g., remove small regions, filter out bright objects with squared shape, flatten textured regions) with respect to connected operators based on a structuring element. In fact, operators based on SE can only tune the size and shape of the SE leading to transformations with a limited capability.

- Multilevel architectures are proper approaches to the consistent description of complex scenes. A single scale or single level of filtering usually is not sufficient for handling the heterogeneous characteristics of the objects in real scenes. Multilevel techniques, such as APs and EAPs, are more appropriate for the modeling of the spatial information in complex scenes.
- Representation of the image as a hierarchical structure of regions is very important. Max-tree and inclusion-tree represent an image as a tree structure where each node of the tree maps a region in the image. Such representations have proven to be suitable for the efficient implementation of attribute operators.

With particular regard to the topics treated in this research, some specific observations can be made.

- *Image classification.*

The main novelties introduced by this work consist in the definition and investigation of attribute profiles, extended attribute profiles and self-dual attribute profiles, which are multilevel operators suitable for characterizing the spatial information of the image.

In Ch. 4, we have presented the definition of APs and have reported the experimental analysis carried out for the classification of panchromatic images. APs have proven to be an effective tool for the modeling of the spatial characteristics of the objects. In particular, when the APs are computed on attributes that can model different spatial characteristics, features conveying complementary information in the analysis are obtained. When compared to the conventional morphological profiles, the use of APs based on different attributes led to a gain in terms of accuracies up to 12%. APs are based on the max-tree structure making them appealing also in terms of computational complexity, since their computation requires less resources than for a MP.

Analogously, when hyperspectral images are considered, extended attribute profiles (Ch. 5) led to very accurate results. When compared to the results obtained by the EMP, EAPs based

on different attributes led always to higher accuracies (up to 9%).

In Ch. 6 two techniques based on the EAPs and dimensionality reduction techniques were proposed. The first technique performs the computation of the EAPs on the features extracted by an ICA (instead of the PCA). It was tested on a hyperspectral data set leading to high accuracies. The ICA led to better results than the PCA because it can better model the information sources.

The problem of the high dimensionality of the features when dealing with the EAPs was addressed by proposing a technique based on a dimensionality reduction step performed by feature extraction techniques (DAFE, DBFE and NWE were considered). An improvement in terms of accuracies when considering a feature extraction technique was assessed by the experimental analysis. As confirmed by the results, in this scenario, the reduction of the dimensionality is particularly important for investigating the effect of the Hughes phenomenon on the classifier.

Dual techniques for the analysis of VHR images were also investigated (Ch. 7). Alternating sequential attribute profiles were proposed, they are attribute filters applied in an alternate setting. ASAF has shown to be promising for the capability of performing transformations on both dark and bright components in the image with the flexibility given by the definition of the attributes. However, their high computational complexity is a limit to their application on large scale.

Attribute profiles computed on the inclusion-tree, namely self-dual attribute profiles, were proposed. SDAP were shown to be effective tools for the classification of VHR images. In the experiments carried out, the SDAP outperformed the AP in terms of classification accuracies. The SDAP permits the simultaneous transformations of bright and dark structures in a multilevel setting with a reduced complexity with respect to ASAF.

- *Building extraction.*

A technique based on APs for the extraction of features which can be used for extracting the buildings from the image was proposed in Ch. 8. The technique is based on a genetic algorithm used for optimizing the selection of the parameters when computing the AP. Standard deviation, a shape index and the area were selected as attributes for proper modeling the characteristics of the building structures. The quality of the features obtained by the filters with optimized parameters was assessed

by classifying the features extracted and checking the accuracy in the identification of the buildings.

- *Image simplification.*

For the problem of image simplification, a general approach based on hierarchical representations of the image (e.g., max-tree and inclusion-tree) and a filtering stage adaptively defined according to the information available on the scene were proposed in Ch. 9. An important feature of the proposed approach is the generality. According to the operational scenario, a different processing of the image is performed. The good results obtained in the preliminary experiments make this approach promising for the image simplification task.

- *Change detection.*

In the context of change detection, two techniques were proposed in Ch. 10. The first technique is based on the application of connected operators to the image of the spectral change vector. The simplification of the image obtained by the filtering stage proved that a reduced number of total errors was achieved without distorting the edges of the detected changed areas with respect to the results obtained by a conventional CVA.

The second presented technique deals with APs. From each multitemporal image, an AP is computed. The AP are then analyzed in order to detect significant changes in the trend of the profiles that can be related to the occurrence of a change on the ground. The interesting feature of this technique relies in the capability of providing information on the changes occurred on the morphology of the structure in the scene resulting in a informative component complementary to the one derived by the spectral variation (used in most the conventional approaches). The obtained results again show higher accuracies in terms of detection of the changed areas when compared to those given by the CVA.

On the basis of the study, the analysis and the experiments carried out in the framework of this thesis, we identified some interesting directions of research as future developments of this work.

- In our opinion a further investigations aimed at exploiting more the tree representation of the image should be carried out. In particular, we believe that the tree structure could be better exploited for performing a region-based analysis of the image. Moreover, the combination of the concepts proposed in this thesis and the representation of the image given by binary partition

trees is also of interest. Furthermore, the hierarchical structure of the tree could be also used for gathering information on the composition of the scene according to the relations that exist between the region/objects of the image.

- Another interesting direction would be to extend the presented techniques by considering different notions of connectivity. The proposed techniques are based on the conventional 4- and 8-connectivity rules but general connectivity classes are also available.
- The extension and investigation of the proposed techniques on data acquired by other sensors (e.g., LIDAR and SAR images) should also be of interest. Indeed, very few applications of mathematical morphology techniques on other data than optical images exist.

BIBLIOGRAPHY

- [1] C. Elachi and J. Van Zyl, *Introduction to the Physics and Techniques of Remote Sensing*. Wiley-Interscience, 2006.
- [2] D. A. Landgrebe, *Signal Theory Methods in Multispectral Remote Sensing*. Wiley-Interscience, 2003.
- [3] G. Konecny, *Geoinformation: remote sensing, photogrammetry and geographic information systems*. Taylor & Francis, 2003.
- [4] G. Rees, *Physical principles of remote sensing*, ser. Topics in remote sensing. Cambridge University Press, 2001.
- [5] J. A. Richards and X. Jia, *Remote sensing digital image analysis: an introduction*. Springer Verlag, 2006.
- [6] R. Schowengerdt, *Remote sensing, models, and methods for image processing*, 3, Ed. Academic Press, 2007.
- [7] J. Schott, *Remote sensing: the image chain approach*. Oxford University Press, 2007.
- [8] W. Egan, *Optical Remote Sensing: Science and Technology*. CRC Press, 2003.
- [9] P. Atkinson and P. Curran, "Defining an optimal size of support for remote sensing investigations," *IEEE Transactions on Geoscience and Remote Sensing*, vol. 33, no. 3, pp. 768–776, 1995.
- [10] R. Devillers and R. Jeansoulin, *Fundamentals of spatial data quality*, ser. Geographical information systems series. ISTE, 2006.
- [11] G. Rees, *The remote sensing data book*. Cambridge University Press, 1999.
- [12] M. Borengasser, W. S. Hungate, and R. Watkins, *Hyperspectral Remote Sensing Principles and Applications*, C. Press, Ed., 2008.
- [13] P.-F. Hsieh, L. Lee, and N.-Y. Chen, "Effect of spatial resolution on classification errors of pure and mixed pixels in remote sensing," *IEEE Transactions on Geoscience and Remote Sensing*, vol. 39, no. 12, pp. 2657–2663, Dec. 2001.

- [14] S. Wang, D. B. Elliott, J. B. Campbell, R. W. Erich, and R. M. Haralick, "Spatial reasoning in remotely sensed data," *IEEE Transactions on Geoscience and Remote Sensing*, vol. GE-21, no. 1, pp. 94–101, 1983.
- [15] Q. Weng, *Remote Sensing and GIS Integration: Theories, Methods, and Applications*. McGraw-Hill, 2009.
- [16] V. Mesev, *Integration of GIS and remote sensing*, ser. Mastering GIS. Wiley, 2007.
- [17] S. Jong and F. Meer, *Remote sensing image analysis: including the spatial domain*, ser. Remote sensing and digital image processing. Kluwer Academic, 2004, no. v. 1.
- [18] T. Blaschke, S. Lang, and G. Hay, *Object-based image analysis: spatial concepts for knowledge-driven remote sensing applications*, ser. Lecture notes in geoinformation and cartography. Springer, 2008.
- [19] K. Navulur, *Multispectral Image Analysis Using the Object-Oriented Paradigm*. Boca Raton, FL, USA: CRC Press, Inc., 2006.
- [20] B. S. Daya Sagar and J. Serra, "Spatial information retrieval, analysis, reasoning and modelling," *International Journal of Remote Sensing*, vol. 31, no. 22, pp. 5747–5750, 2010.
- [21] L. Shapiro and G. Stockman, *Computer vision*. Prentice Hall, 2001.
- [22] H. Miller and J. Han, *Geographic data mining and knowledge discovery*, ser. Chapman & Hall/CRC data mining and knowledge discovery series. CRC Press, 2009.
- [23] G. Christakos and C. Panagopoulos, "Space transformation methods in the representation of geophysical random fields," *IEEE Transactions on Geoscience and Remote Sensing*, vol. 30, no. 1, pp. 55–70, Jan. 1992.
- [24] Y. Jhung and P. Swain, "Bayesian contextual classification based on modified m-estimates and markov random fields," *IEEE Transactions on Geoscience and Remote Sensing*, vol. 34, no. 1, pp. 67–75, Jan. 1996.
- [25] B. Tso and R. C. Olsen, "A contextual classification scheme based on MRF model with improved parameter estimation and multi-scale fuzzy line process," *Remote sensing of environment*, vol. 97, no. 1, pp. 127–136, 2005.

- [26] R. Nishii, "A markov random field-based approach to decision-level fusion for remote sensing image classification," *IEEE Transactions on Geoscience and Remote Sensing*, vol. 41, no. 10, pp. 2316–2319, 2003.
- [27] T. Yamazaki and D. Gingras, "Image classification using spectral and spatial information based on MRF models," *IEEE Transactions on Image Processing*, vol. 4, no. 9, pp. 1333–1339, 2002.
- [28] M. Datcu, K. Seidel, and M. Walessa, "Spatial information retrieval from remote-sensing images. i. information theoretical perspective," *IEEE Transactions on Geoscience and Remote Sensing*, vol. 36, no. 5, pp. 1431–1445, Sep. 1998.
- [29] M. Schroder, H. Rehrauer, K. Seidel, and M. Datcu, "Spatial information retrieval from remote-sensing images. II. Gibbs-Markov random fields," *IEEE Transactions on Geoscience and Remote Sensing*, vol. 36, no. 5, pp. 1446–1455, 2002.
- [30] R. Cossu, S. Chaudhuri, and L. Bruzzone, "A context-sensitive bayesian technique for the partially supervised classification of multitemporal images," *IEEE Geoscience and Remote Sensing Letters*, vol. 2, no. 3, pp. 352–356, 2005.
- [31] Y. Zhao, L. Zhang, P. Li, and B. Huang, "Classification of high spatial resolution imagery using improved gaussian markov random-field-based texture features," *IEEE Transactions on Geoscience and Remote Sensing*, vol. 45, no. 5, pp. 1458–1468, May 2007.
- [32] S. Serpico and G. Moser, "Weight parameter optimization by the ho ndash;kashyap algorithm in mrf models for supervised image classification," *IEEE Transactions on Geoscience and Remote Sensing*, vol. 44, no. 12, pp. 3695–3705, 2006.
- [33] F. Melgani and S. Serpico, "A markov random field approach to spatio-temporal contextual image classification," *IEEE Transactions on Geoscience and Remote Sensing*, vol. 41, no. 11, pp. 2478–2487, 2003.
- [34] T. Kasetkasem and P. K. Varshney, "An image change detection algorithm based on markov random field models," *IEEE Transactions on Geoscience and Remote Sensing*, vol. 40, no. 8, pp. 1815–1823, 2002.
- [35] J. Bolton and P. Gader, "Random set framework for context-based classification with hyperspectral imagery," *IEEE Transactions on Geoscience and Remote Sensing*, vol. 47, no. 11, pp. 3810–3821, 2009.

- [36] G. Rellier, X. Descombes, F. Falzon, and J. Zerubia, "Texture feature analysis using a gauss-markov model in hyperspectral image classification," *IEEE Transactions on Geoscience and Remote Sensing*, vol. 42, no. 7, pp. 1543 – 1551, 2004.
- [37] S. Yu, M. Berthod, and G. Giraudon, "Toward robust analysis of satellite images using map information-application to urban area detection," *IEEE Transactions on Geoscience and Remote Sensing*, vol. 37, no. 4, pp. 1925 –1939, Jul. 1999.
- [38] P. Zhong and R. Wang, "Learning sparse crfs for feature selection and classification of hyperspectral imagery," *IEEE Transactions on Geoscience and Remote Sensing*, vol. 46, no. 12, pp. 4186 –4197, 2008.
- [39] —, "A multiple conditional random fields ensemble model for urban area detection in remote sensing optical images," *IEEE Transactions on Geoscience and Remote Sensing*, vol. 45, no. 12, pp. 3978 –3988, 2007.
- [40] —, "Using combination of statistical models and multilevel structural information for detecting urban areas from a single gray-level image," *IEEE Transactions on Geoscience and Remote Sensing*, vol. 45, no. 5, pp. 1469 –1482, May 2007.
- [41] —, "Learning conditional random fields for classification of hyperspectral images," *IEEE Transactions on Image Processing*, vol. 19, no. 7, pp. 1890 –1907, 2010.
- [42] J. R. Welch and K. G. Salter, "A context algorithm for pattern recognition and image interpretation," *IEEE Transactions on Systems, Man and Cybernetics*, vol. SMC-1, no. 1, pp. 24–30, 1971.
- [43] P. H. Swain, H. J. Siegel, and B. W. Smith, "Contextual classification of multispectral remote sensing data using a multiprocessor system," *IEEE Transactions on Geoscience and Remote Sensing*, vol. GE-18, no. 2, pp. 197 –203, 1980.
- [44] J. C. Tilton, S. B. Vardeman, and P. H. Swain, "Estimation of context for statistical classification of multispectral image data," *IEEE Transactions on Geoscience and Remote Sensing*, vol. GE-20, no. 4, pp. 445 –452, 1982.
- [45] N. Khazenie and M. M. Crawford, "Spatial-temporal autocorrelated model for contextual classification," *IEEE Transactions on Geoscience and Remote Sensing*, vol. 28, no. 4, p. 529?539, 1990.

- [46] R. L. Kettig and D. A. Landgrebe, "Classification of multispectral image data by extraction and classification of homogeneous objects," *IEEE Transactions on Geoscience Electronics*, vol. 14, no. 1, pp. 19–26, 1976.
- [47] D. A. Landgrebe, "The development of a spectral-spatial classifier for earth observational data," *Pattern Recognition*, vol. 12, no. 3, pp. 165–175, 1980.
- [48] P. H. Swain, S. B. Vardeman, and J. C. Tilton, "Contextual classification of multispectral image data," *Pattern Recognition*, vol. 13, no. 6, pp. 429–441, 1981.
- [49] A. Speis and G. Healey, "Feature extraction for texture discrimination via random field models with random spatial interaction," *IEEE Transactions on Image Processing*, vol. 5, no. 4, pp. 635–645, 1996.
- [50] A. Laha, N. Pal, and J. Das, "Land cover classification using fuzzy rules and aggregation of contextual information through evidence theory," *IEEE Transactions on Geoscience and Remote Sensing*, vol. 44, no. 6, pp. 1633 – 1641, 2006.
- [51] G. Storvik, R. Fjortoft, and A. Solberg, "A bayesian approach to classification of multiresolution remote sensing data," *IEEE Transactions on Geoscience and Remote Sensing*, vol. 43, no. 3, pp. 539 – 547, 2005.
- [52] R. M. Haralick, K. Shanmugam, and I. H. Dinstein, "Textural features for image classification," *IEEE Transactions on systems, man and cybernetics*, vol. 3, no. 6, pp. 610–621, 1973.
- [53] N. Cressie, *Statistics for spatial data*, ser. Wiley series in probability and mathematical statistics: Applied probability and statistics. J. Wiley, 1993.
- [54] S. Sarkar and G. Healey, "Hyperspectral texture synthesis using histogram and power spectral density matching," *IEEE Transactions on Geoscience and Remote Sensing*, vol. 48, no. 5, pp. 2261–2270, May 2010.
- [55] J. Li and R. Narayanan, "Integrated spectral and spatial information mining in remote sensing imagery," *IEEE Transactions on Geoscience and Remote Sensing*, vol. 42, no. 3, pp. 673–685, 2004.
- [56] S. Meher, B. Shankar, and A. Ghosh, "Wavelet-feature-based classifiers for multispectral remote-sensing images," *IEEE Transactions*

- on *Geoscience and Remote Sensing*, vol. 45, no. 6, pp. 1881–1886, 2007.
- [57] E. Binaghi, I. Gallo, and M. Pepe, “A cognitive pyramid for contextual classification of remote sensing images,” *IEEE Transactions on Geoscience and Remote Sensing*, vol. 41, no. 12, pp. 2906–2922, 2004.
- [58] S. Ahearn, “Combining laplacian images of different spatial frequencies (scales): implications for remote sensing image analysis,” *IEEE Transactions on Geoscience and Remote Sensing*, vol. 26, no. 6, pp. 826–831, Nov. 1988.
- [59] A. Shackelford and C. Davis, “A hierarchical fuzzy classification approach for high-resolution multispectral data over urban areas,” *IEEE Transactions on Geoscience and Remote Sensing*, vol. 41, no. 9, pp. 1920–1932, 2003.
- [60] —, “A combined fuzzy pixel-based and object-based approach for classification of high-resolution multispectral data over urban areas,” *IEEE Transactions on Geoscience and Remote Sensing*, vol. 41, no. 10, pp. 2354–2363, 2003.
- [61] W. Song, J. Keller, T. Haithcoat, and C. Davis, “Automated geospatial conflation of vector road maps to high resolution imagery,” *IEEE Transactions on Image Processing*, vol. 18, no. 2, pp. 388–400, 2009.
- [62] L. Zhang, X. Huang, B. Huang, and P. Li, “A pixel shape index coupled with spectral information for classification of high spatial resolution remotely sensed imagery,” *IEEE Transactions on Geoscience and Remote Sensing*, vol. 44, no. 10, pp. 2950–2961, 2006.
- [63] C. Unsalan and K. Boyer, “Classifying land development in high-resolution panchromatic satellite images using straight-line statistics,” *IEEE Transactions on Geoscience and Remote Sensing*, vol. 42, no. 4, pp. 907–919, 2004.
- [64] Y. Tarabalka, J. Benediktsson, J. Chanussot, and J. Tilton, “Multiple spectral-spatial classification approach for hyperspectral data,” *IEEE Transactions on Geoscience and Remote Sensing*, vol. 48, no. 11, pp. 4122–4132, 2010.
- [65] Y. Tarabalka, J. A. Benediktsson, and J. Chanussot, “Spectral & spatial classification of hyperspectral imagery based on partitioning clustering techniques,” *IEEE Transactions on Geoscience and Remote Sensing*, vol. 47, no. 8, pp. 2973–2987, 2009.

- [66] Y. Tarabalka, J. Chanussot, and J. A. Benediktsson, "Segmentation and classification of hyperspectral images using minimum spanning forest grown from automatically selected markers," *Systems, Man, and Cybernetics, Part B: Cybernetics, IEEE Transactions on*, vol. PP, no. 99, pp. 1–13, 2010.
- [67] Y. Tarabalka, J. Chanussot, J. A. Benediktsson, J. Angulo, and M. Fauvel, "Segmentation and classification of hyperspectral data using watershed," in *Proc. IEEE International Geoscience and Remote Sensing Symposium 2008, IGARSS '08*, vol. 3, Jul. 7–11, 2008, pp. III-652–III-655.
- [68] R. Gaetano, G. Scarpa, and G. Poggi, "Hierarchical texture-based segmentation of multiresolution remote-sensing images," *IEEE Transactions on Geoscience and Remote Sensing*, vol. 47, no. 7, pp. 2129–2141, 2009.
- [69] M. Bouziani, K. Goita, and D.-C. He, "Rule-based classification of a very high resolution image in an urban environment using multispectral segmentation guided by cartographic data," *IEEE Transactions on Geoscience and Remote Sensing*, vol. 48, no. 8, pp. 3198–3211, 2010.
- [70] L.-K. Soh and C. Tsatsoulis, "Segmentation of satellite imagery of natural scenes using data mining," *IEEE Transactions on Geoscience and Remote Sensing*, vol. 37, no. 2, pp. 1086–1099, Mar. 1999.
- [71] L. Bruzzone and L. Carlin, "A multilevel context-based system for classification of very high spatial resolution images," *IEEE Transactions on Geoscience and Remote Sensing*, vol. 44, pp. 2587–2600, Sept. 2006.
- [72] M. Pesaresi and J. A. Benediktsson, "A new approach for the morphological segmentation of high-resolution satellite imagery," *IEEE Transactions on Geoscience and Remote Sensing*, vol. 39, no. 2, pp. 309–320, 2001.
- [73] X. Huang and L. Zhang, "An adaptive mean-shift analysis approach for object extraction and classification from urban hyperspectral imagery," *IEEE Transactions on Geoscience and Remote Sensing*, vol. 46, no. 12, p. 4173–4185, 2008.
- [74] L. Sanders, *Models in spatial analysis*, ser. The GIS sourcebook. ISTE, 2007.
- [75] B. Nicolin and R. Gabler, "A knowledge-based system for the analysis of aerial images," *IEEE Transactions on Geoscience and Remote Sensing*, vol. GE-25, no. 3, pp. 317–329, May 1987.

- [76] G. J. Hay, T. Blaschke, D. J. Marceau, and A. Bouchard, "A comparison of three image-object methods for the multiscale analysis of landscape structure," *ISPRS Journal of Photogrammetry and Remote Sensing*, vol. 57, no. 5-6, p. 327-345, 2003.
- [77] S. Aksoy, K. Koperski, C. Tusk, G. Marchisio, and J. Tilton, "Learning bayesian classifiers for scene classification with a visual grammar," *IEEE Transactions on Geoscience and Remote Sensing*, vol. 43, no. 3, pp. 581 - 589, 2005.
- [78] C.-R. Shyu, M. Klaric, G. Scott, A. Barb, C. Davis, and K. Palaniappan, "Geoiris: Geospatial information retrieval and indexing system mdash;content mining, semantics modeling, and complex queries," *IEEE Transactions on Geoscience and Remote Sensing*, vol. 45, no. 4, pp. 839 -852, 2007.
- [79] S. Aksoy and R. Cinbis, "Image mining using directional spatial constraints," *IEEE Geoscience and Remote Sensing Letters*, vol. 7, no. 1, pp. 33 -37, 2010.
- [80] J. Serra, *Image Analysis and Mathematical Morphology, Theoretical Advances, Vol. 2*. New York: Academic Press, 1988.
- [81] ———, *Image Analysis and Mathematical Morphology*. Academic Press, 1983.
- [82] P. Soille, *Morphological Image Analysis, Principles and Applications*, 2nd ed. Berlin, Germany: Springer Verlag, 2003.
- [83] L. Najman and H. Talbot, *Mathematical Morphology*. Wiley-ISTE, Aug. 2010.
- [84] P. Soille and M. Pesaresi, "Advances in mathematical morphology applied to geosciences and remote sensing," *IEEE Transactions on Geoscience and Remote Sensing*, vol. 40, pp. 2042-2055, 2002.
- [85] P. Soille, "Recent developments in morphological image processing for remote sensing," in *Proceedings of SPIE*, Berlin, Germany, 2009, pp. 747 702-747 702-11.
- [86] P. Salembier and J. Serra, "Flat zones filtering, connected operators, and filters by reconstruction," *IEEE Transactions on Image Processing*, vol. 4, no. 8, pp. 1153 -1160, Aug. 1995.
- [87] P. Salembier, "Connected operators based on region-trees," in *Proc. 15th IEEE International Conference on Image Processing ICIP 2008*, 2008, pp. 2176-2179.

- [88] M. Dalla Mura, J. A. Benediktsson, B. Waske, and L. Bruzzone, "Morphological attribute filters for the analysis of very high resolution remote sensing images," in *Proc. IEEE International Geoscience and Remote Sensing Symposium 2009, IGARSS '09*, vol. 3, July 2009, pp. III-97 -III-100.
- [89] E. J. Breen and R. Jones, "Attribute openings, thinnings, and granulometries," *Comput. Vis. Image Underst.*, vol. 64, no. 3, pp. 377-389, 1996.
- [90] P. Salembier, A. Oliveras, and L. Garrido, "Antiextensive connected operators for image and sequence processing," *IEEE Transactions on Image Processing*, vol. 7, no. 4, pp. 555-570, 1998.
- [91] M. Dalla Mura, J. A. Benediktsson, B. Waske, and L. Bruzzone, "Morphological attribute profiles for the analysis of very high resolution images," *IEEE Transactions on Geoscience and Remote Sensing*, vol. 48, no. 10, pp. 3747 - 3762, Oct. 2010.
- [92] —, "Extended profiles with morphological attribute filters for the analysis of hyperspectral data," *International Journal of Remote Sensing*, vol. 31, no. 22, pp. 5975-5991, Nov. 2010.
- [93] M. Dalla Mura, J. A. Benediktsson, and L. Bruzzone, "Alternating sequential filters with morphological attribute operators for the analysis of remote sensing images," in *Image and Signal Processing for Remote Sensing XVI - SPIE Proceeding*, vol. 7830. Toulouse, France: SPIE Publications, Bellingham, WA, 2010, pp. 783 006-1-783 006-8.
- [94] —, "Self-dual attribute profiles for the analysis of remote sensing images," in *Proc. of 10th Int. Symp. on Mathematical Morphology (ISMM 2011)*, P. Soille, G. K. Ouzounis, and M. Pesaresi, Eds., Intra, Lake Maggiore, Italy, 6th-8th July 2011.
- [95] —, "A general approach to the spatial simplification of remote sensing images based on morphological connected filters," in *2011 IEEE International Geoscience and Remote Sensing Symposium (IGARSS)*, 2011, accepted.
- [96] M. Dalla Mura, A. Villa, J. A. Benediktsson, J. Chanussot, and L. Bruzzone, "Classification of hyperspectral images by using extended morphological attribute profiles and independent component analysis," *IEEE Geoscience and Remote Sensing Letters*, vol. 8, no. 3, pp. 541 -545, 2010.

- [97] —, “Classification of hyperspectral images by using morphological attribute filters and independent component analysis,” in *Proc. 2nd Workshop on Hyperspectral Image and Signal Processing: Evolution in Remote Sensing*, Reykjavik, Iceland, 14–16 June 2010.
- [98] M. Dalla Mura, J. Benediktsson, and L. Bruzzone, “Classification of hyperspectral images with extended attribute profiles and feature extraction techniques,” in *2010 IEEE International Geoscience and Remote Sensing Symposium (IGARSS)*, 2010, pp. 76–79.
- [99] M. Dalla Mura, J. A. Benediktsson, F. Bovolo, and L. Bruzzone, “An unsupervised technique based on morphological filters for change detection in very high resolution images,” *IEEE Geoscience and Remote Sensing Letters*, vol. 5, no. 3, pp. 433–437, July 2008.
- [100] N. Falco, M. Dalla Mura, F. Bovolo, J. A. Benediktsson, and L. Bruzzone, “Study on the capabilities of morphological attribute profiles in change detection on VHR images,” in *Image and Signal Processing for Remote Sensing XVI - Proceedings of SPIE*, vol. 7830. Toulouse, France: SPIE, Bellingham, WA, 2010, pp. 783 016–1–783 016–10.
- [101] M. Dalla Mura, J. A. Benediktsson, and L. Bruzzone, “Modeling structural information for building extraction with morphological attribute filters,” in *Image and Signal Processing for Remote Sensing XV - SPIE Proceeding*, vol. 7477. Berlin, Germany: SPIE, Bellingham, WA, 2009, pp. 747 703–1–747 703–9.
- [102] J. Serra, “Connectivity on complete lattices,” *Journal of Mathematical Imaging and Vision*, vol. 9, no. 3, pp. 231–251, 1998.
- [103] L. Vincent, “Morphological grayscale reconstruction in image analysis: Applications and efficient algorithms,” *IEEE Transactions on Image Processing*, vol. 2, no. 2, pp. 176–201, 1993.
- [104] P. Maragos and R. Ziff, “Threshold superposition in morphological image analysis systems,” *IEEE Transactions on Pattern Analysis and Machine Intelligence*, vol. 12, no. 5, pp. 498–504, 1990.
- [105] E. R. Urbach, J. B. T. M. Roerdink, and M. H. F. Wilkinson, “Connected shape-size pattern spectra for rotation and scale-invariant classification of gray-scale images,” *IEEE Transactions on Pattern Analysis and Machine Intelligence*, vol. 29, no. 2, pp. 272–285, 2007.
- [106] V. Caselles and P. Monasse, *Geometric Description of Images as Topographic Maps*. Springer, 2010.

- [107] P. Monasse and F. Guichard, "Fast computation of a contrast-invariant image representation," *IEEE Transactions on Image Processing*, vol. 9, no. 5, pp. 860–872, May 2000.
- [108] P. Salembier and L. Garrido, "Binary partition tree as an efficient representation for image processing, segmentation, and information retrieval," *IEEE Transactions on Image Processing*, vol. 9, no. 4, pp. 561–576, Apr. 2000.
- [109] P. Salembier and M. Wilkinson, "Connected operators," *IEEE Signal Processing Magazine*, vol. 26, no. 6, pp. 136–157, 2009.
- [110] A. Plaza, J. A. Benediktsson, J. W. Boardman, J. Brazile, L. Bruzzone, G. Camps-Valls, J. Chanussot, M. Fauvel, P. Gamba, A. Gualtieri, M. Marconcini, J. C. Tilton, and G. Trianni, "Recent advances in techniques for hyperspectral image processing," *Remote Sensing of Environment*, vol. 113, no. Supplement 1, pp. 110–122, Sep. 2009.
- [111] J. A. Benediktsson, M. Pesaresi, and K. Amason, "Classification and feature extraction for remote sensing images from urban areas based on morphological transformations," *IEEE Transactions on Geoscience and Remote Sensing*, vol. 41, no. 9, pp. 1940–1949, 2003.
- [112] J. Chanussot, J. A. Benediktsson, and M. Pesaresi, "On the use of morphological alternated sequential filters for the classification of remote sensing images from urban areas," in *Proc. IEEE International Geoscience and Remote Sensing Symposium 2003, IGARSS '03*, vol. 1, Jul. 21–25, 2003, pp. 473–475.
- [113] J. Chanussot, J. A. Benediktsson, and M. Fauvel, "Classification of remote sensing images from urban areas using a fuzzy possibilistic model," *IEEE Geoscience and Remote Sensing Letters*, vol. 3, no. 1, pp. 40–44, 2006.
- [114] R. Bellens, S. Gautama, L. Martinez-Fonte, W. Philips, J.-W. Chan, and F. Canters, "Improved classification of VHR images of urban areas using directional morphological profiles," *IEEE Transactions on Geoscience and Remote Sensing*, vol. 46, no. 10, pp. 2803–2813, Oct. 2008.
- [115] J. A. Benediktsson, J. A. Palmason, and J. R. Sveinsson, "Classification of hyperspectral data from urban areas based on extended morphological profiles," *IEEE Transactions on Geoscience and Remote Sensing*, vol. 43, no. 3, pp. 480–491, 2005.

- [116] R. Duda, P. Hart, and D. Stork, *Pattern Classification*. J. Wiley & Sons, Inc., U.S.A., 2000.
- [117] K. Fukunaga, *Introduction to Statistical Pattern Recognition*. 2nd ed. London: Academic Press, 1990.
- [118] A. Plaza, P. Martinez, J. Plaza, and R. Perez, "Dimensionality reduction and classification of hyperspectral image data using sequences of extended morphological transformations," *IEEE Transactions on Geoscience and Remote Sensing*, vol. 43, no. 3, pp. 466–479, 2005.
- [119] F. Dell'Acqua, P. Gamba, A. Ferrari, J. A. Palmason, J. A. Benediktsson, and K. Arnason, "Exploiting spectral and spatial information in hyperspectral urban data with high resolution," *IEEE Geoscience and Remote Sensing Letters*, vol. 1, no. 4, pp. 322–326, 2004.
- [120] J. A. Palmason, J. A. Benediktsson, J. R. Sveinsson, and J. Chanussot, "Classification of hyperspectral data from urban areas using morphological preprocessing and independent component analysis," in *Proc. IEEE International Geoscience and Remote Sensing Symposium 2005, IGARSS '05*, vol. 1, Jul. 25–29, 2005, pp. 176–179.
- [121] M. Fauvel, J. Chanussot, and J. A. Benediktsson, "Kernel principal component analysis for feature reduction in hyperspectral images analysis," in *Proc. 7th Nordic Signal Processing Symposium NORSIG 2006*, Jun. 2006, pp. 238–241.
- [122] M. Fauvel, J. A. Benediktsson, J. Chanussot, and J. R. Sveinsson, "Spectral and spatial classification of hyperspectral data using SVMs and morphological profiles," *IEEE Transactions on Geoscience and Remote Sensing*, vol. 46, no. 11, pp. 3804–3814, 2008.
- [123] H. Akcay and S. Aksoy, "Automatic detection of geospatial objects using multiple hierarchical segmentations," *IEEE Transactions on Geoscience and Remote Sensing*, vol. 46, no. 7, pp. 2097–2111, July 2008.
- [124] L. Vincent, "Morphological area openings and closings for greyscale images," *Proc. NATO Shape in Picture Workshop*, pp. 197–208, 1992.
- [125] A. Meijster and M. H. F. Wilkinson, "A comparison of algorithms for connected set openings and closings," *IEEE Transactions on Pattern Analysis and Machine Intelligence*, vol. 24, no. 4, pp. 484–494, 2002.

- [126] M. H. F. Wilkinson, H. Gao, W. H. Hesselink, J.-E. Jonker, and A. Meijster, "Concurrent computation of attribute filters on shared memory parallel machines," *IEEE Transactions on Pattern Analysis and Machine Intelligence*, vol. 30, no. 10, pp. 1800–1813, 2008.
- [127] C. Persello and L. Bruzzone, "A novel approach to the selection of spatially invariant features for classification of hyperspectral images," in *Proc. IEEE International Geoscience and Remote Sensing Symposium 2009, IGARSS '09*, vol. 2, July 2009, pp. II-61 –II-64.
- [128] —, "A novel protocol for accuracy assessment in classification of very high resolution images," *IEEE Transactions on Geoscience and Remote Sensing*, vol. 48, no. 3, pp. 1232 –1244, 2010.
- [129] L. Breiman, "Random forests," *Mach. Learn.*, vol. 45, no. 1, pp. 5–32, 2001.
- [130] R. G. Congalton and K. Green, *Assessing the Accuracy of Remotely Sensed Data*. CRC Press, Dec. 2008.
- [131] J. Chanussot and P. Lambert, "Total ordering based on space filling curves for multivalued morphology," in *4th International Symposium on Mathematical Morphology and its Applications*, 6 1998, pp. 51–58.
- [132] L. Garrido, P. Salembier, and D. Garcia, "Extensive operators in partition lattices for image sequence analysis," *Signal Processing*, vol. 66, no. 2, pp. 157–180, 1998.
- [133] P. Lambert and J. Chanussot, "Extending mathematical morphology to color image processing," in *CGIP-1st Internat. Conf. on Color in Graphics and Image Processing*, Saint-Etienne, France, 2000, pp. 158–163.
- [134] E. Aptoula and S. Lefavre, "A comparative study on multivariate mathematical morphology," *Pattern Recognition*, vol. 40, no. 11, pp. 2914–2929, 2007.
- [135] M. Fauvel, J. Chanussot, and J. A. Benediktsson, "Kernel principal component analysis for the classification of hyperspectral remote sensing data over urban areas," *EURASIP Journal on Advances in Signal Processing*, vol. 2009, 14 pages, 2009.
- [136] T. Castangs, B. Waske, J. A. Benediktsson, and J. Chanussot, "On the influence of feature reduction for the classification of hyperspectral images based on the extended morphological profile," *International Journal of Remote Sensing*, vol. 31, no. 22, pp. 5921–5939, Nov. 2010.

- [137] X. Huang and L. Zhang, "A comparative study of spatial approaches for urban mapping using hyperspectral ROSIS - images over pavia city, northern italy," *International Journal of Remote Sensing*, vol. 30, no. 12, p. 3205, 2009.
- [138] M. Hu, "Visual pattern recognition by moment invariants," *IRE Transactions on Information Theory*, vol. 8, no. 2, pp. 179–187, 1962.
- [139] A. Villa, J. Chanussot, C. Jutten, J. A. Benediktsson, and S. Mossaoui, "On the use of ICA for hyperspectral image analysis," in *Proc. IEEE International Geoscience and Remote Sensing Symposium 2009, IGARSS '09*, vol. 4, Jul.12-17 2009, pp. IV–97–IV–100.
- [140] A. Hyvarinen, J. Karhunen, and E. Oja, *Independent Component Analysis*. Wiley, New York, 2001.
- [141] A. Villa, M. Fauvel, J. Chanussot, P. Gamba, and J. A. Benediktsson, "Gradient optimization for multiple kernel's parameters in support vector machines classification," in *Proc. IEEE International Geoscience and Remote Sensing Symposium 2008, IGARSS '08*, vol. 4, Jul. 7–11, 2008, pp. IV–224–IV–227.
- [142] R. Levillain, T. Géraud, and L. Najman, "Milena: Write generic morphological algorithms once, run on many kinds of images," in *Proc. ISMM 2009*, ser. Lecture Notes in Computer Science, M. Wilkinson and J. Roerdink, Eds., vol. 5720, 2009, pp. 295–306.
- [143] X. Jin and C. H. Davis, "Automated building extraction from high-resolution satellite imagery in urban areas using structural, contextual, and spectral information," *EURASIP Journal on Applied Signal Processing*, pp. 2196–2206, 2005.
- [144] E.-G. Talbi, *Metaheuristics: from design to implementation*. John Wiley & Sons, 2009.
- [145] A. Singh, "Digital change detection techniques using remotely-sensed data," *Int. J. Remote Sensing*, vol. 10, pp. 989–1003, 1989.
- [146] F. Bovolo, L. Bruzzone, and S. Marchesi, "A multiscale technique for reducing registration noise in change detection on multitemporal VHR images," 2007.
- [147] P. Coppin, I. Jonckheere, K. Nackaerts, and B. Muys, "Digital change detection methods in ecosystem monitoring: a review," *Int. J. Remote Sensing*, vol. 25, pp. 1565–1596, 2004.

- [148] F. Bovolo and L. Bruzzone, "A detail-preserving scale-driven approach to unsupervised change detection in multitemporal sar images," *IEEE transactions on geoscience and remote sensing*, vol. 43, pp. 2963–2972, 2005.
- [149] J. Crespo, J. Serra, and R. Schafer, "Theoretical aspects of morphological filters by reconstruction," *Signal Process.*, vol. 47, pp. 201–225, 1995.
- [150] Envi user manual. Boulder, CO: RSI, 2003. [Online]. Available: <http://www.RSInc.com/envi>
- [151] J. Kittler and J. Illingworth, "Minimum error thresholding," *Pattern Recognition*, vol. 19, pp. 41–47, 1986.
- [152] L. Bruzzone and R. Cossu, "Analysis of multitemporal remote-sensing images for change detection: bayesian thresholding approaches," *Geospatial Pattern Recognition*, 2002.

This thesis was typeset with $\text{\LaTeX} 2_{\epsilon}$ using André Miede's `classicthesis.sty`.

(MS) Word is for secretaries.

— Allan Aasbjerg Nielsen